

Final Report On

DIFFUSION OF GASES IN SOLIDS

- Rare Gas Diffusion in Solids
- Tritium Diffusion in Fission
and Fusion Reactor Metals

P. M. Abraham
D. Chandra
J. M. Mintz
T. S. Elleman (Principal Investigator)
K. Verghese

Department of Nuclear Engineering
North Carolina State University
Raleigh, North Carolina 27607

NOTICE
This report was prepared as an account of work sponsored by the United States Government. Neither the United States nor the United States Energy Research and Development Administration, nor any of their employees, nor any of their contractors, subcontractors, or their employees, makes any warranty, express or implied, or assumes any legal liability or responsibility for the accuracy, completeness or usefulness of any information, apparatus, product or process disclosed, or represents that its use would not infringe privately owned rights.

Prepared for the Energy Research and Development Agency
under Contract No. AT-(40-1)3508

Contract Period: November 1, 1970 - June 30, 1975

This document is
PUBLICLY RELEASABLE

Larry E. Williams
Authorizing Official

Date: 12/14/2005

MASTER

DISTRIBUTION OF THIS DOCUMENT IS UNLIMITED

fly

DISCLAIMER

This report was prepared as an account of work sponsored by an agency of the United States Government. Neither the United States Government nor any agency Thereof, nor any of their employees, makes any warranty, express or implied, or assumes any legal liability or responsibility for the accuracy, completeness, or usefulness of any information, apparatus, product, or process disclosed, or represents that its use would not infringe privately owned rights. Reference herein to any specific commercial product, process, or service by trade name, trademark, manufacturer, or otherwise does not necessarily constitute or imply its endorsement, recommendation, or favoring by the United States Government or any agency thereof. The views and opinions of authors expressed herein do not necessarily state or reflect those of the United States Government or any agency thereof.

DISCLAIMER

Portions of this document may be illegible in electronic image products. Images are produced from the best available original document.

TABLE OF CONTENTS

	Page
ABSTRACT	1
INTRODUCTION	3
RESULTS	5
1. RARE GAS DIFFUSION IN SOLIDS	5
1.1. Classical Rare Gas Diffusion	5
1.2. Gas Atom Trapping in "Growth-Induced" Defects	7
1.3. Gas Atom Trapping at High Gas Concentrations	7
1.4. Gas Atom Trapping at Radiation-Induced Defects	9
1.5. Mechanism of Gas Diffusion	10
1.6. Diffusion and Trapping in UO ₂ Single Crystals	11
2. TRITIUM DIFFUSION IN FISSION REACTOR CLADDING	13
2.1. Tritium Transport in Stainless Steels	13
2.1.1. Summary of Prior Year's Work	13
2.1.2. Grainboundary Diffusion in 304L Stainless Steel-Predicted Permeation Rates	15
2.1.2.1. Grainboundary Diffusion Model	15
2.1.2.2. Bulk Diffusion Model	19
2.1.2.3. Computational Results	20
2.1.2.4. Autoradiography	21
2.1.2.4.1. Techniques	21
2.1.2.4.2. Tritium Segregation at Defects	22
2.1.2.4.3. Grainboundary Diffusion	23
2.1.2.5. Discussion and Conclusions	25
2.2. Tritium Transport in Zircaloy-2	27
2.2.1. Summary of Prior Year's Work	27

TABLE OF CONTENTS (CONT.)

	Page
2.3. Tritium in Light Water Reactors	29
2.3.1. Summary of Prior Year's Work	30
2.3.2. Work in Progress - A Computer Code for Tritium Calculations in PWR's	31
3. TRITIUM DIFFUSION IN FUSION REACTORS	33
3.1. Tritium Transport in Niobium	33
3.1.1. Summary of Prior Year's Work	33
3.1.2. Tritium Diffusion Through Oxide Films on Nb	34
3.1.2.1. Techniques	34
3.1.2.2. Results and Discussion	35
3.1.2.2.1. Diffusion in Bulk Niobium	35
3.1.2.2.2. Tritium Release Results	37
3.1.2.2.3. Tritium Release Model	38
3.1.2.2.4. Temperature Cycling	44
3.1.2.2.5. Film Thickness Effects	45
3.1.2.2.6. Effects of Reducing Atmospheres	50
3.1.2.3. Conclusions	53
3.2. Tritium in Fusion Reactor Blankets	55
3.2.1. The Model	56
3.2.1.1. Equilibrium Diffusion	56
3.2.1.2. Equilibration Times	61
3.2.2. Results	62
3.2.2.1. Insulator Effects	63
3.2.2.2. Effect of Oxide Films	64
3.2.2.3. Tritium Inventories	65

TABLE OF CONTENTS (CONT.)

	Page
3.2.2.4. Lag Times	68
3.2.2.5. General	71
3.2.3. Conclusions	73
REFERENCES	74

FIGURES

ATTACHMENTS

- I. SUGGESTIONS FOR FUTURE WORK
- II. LIST OF STUDENTS SUPPORTED
- III. PUBLICATIONS RESULTING FROM CONTRACT
- IV. PRACTICAL BENEFITS

ABSTRACT

Major results of tritium and rare gas diffusion research conducted under the contract are summarized. The rare gas diffusion studies were concerned with an investigation of trapping effects on xenon transport in solids. The more recent work has been on generation of basic diffusion data for tritium in fission and fusion reactor structural materials. These basic data have been applied in mathematical models to predict tritium transport rates in pressurized water reactors and in the blanket regions of the Reference Theta Pinch Fusion Reactor design. The materials studied were austenitic stainless steels, Zircaloy, and niobium.

In all three of the metal systems investigated, tritium release rates were found to be inhibited by surface oxide films. The effective diffusion coefficients that control tritium release from surface films on Zircaloy and niobium were determined to be eight to ten orders of magnitude lower than the bulk diffusion coefficients. A rapid component of diffusion due to grainboundaries was identified in stainless steels. The grainboundary diffusion coefficient was determined to be about six orders of magnitude greater than the bulk diffusion coefficient for tritium in stainless steel.

Calculations based on models that considered different diffusion coefficients in bulk and surface regions on fission reactor cladding materials showed that the basic tritium diffusion data for stainless steels and Zircaloy were consistent with the tritium distributions in reactor fuel pins reported by other investigators. In Zircaloy clad fuel pins, the permeation rate of tritium through the cladding is rate-limited by the extremely slow diffusion rate in the surface films.

Tritium diffusion rates through surface oxide films on niobium appear to be controlled by cracks in the surface films at temperatures up to 600°C. Beyond

600°C, the cracks appear to heal, thereby increasing the activation energy for diffusion through the oxide film. Reducing atmospheres such as hydrogen and lithium appear to be able to reduce the oxide layers above 600°C resulting in tritium release rates that are controlled only by bulk diffusion coefficients.

The steady-state diffusion of tritium in a fusion reactor blanket has been evaluated using the Los Alamos Theta Pinch reactor as a reference system. The purpose was to calculate the equilibrium tritium transport rate, approximate time to equilibrium, and tritium inventory in various regions of the reactor blanket as a function of selected blanket parameters. Values for these quantities have been tabulated for blanket conditions which appear reasonable for the reference system.

INTRODUCTION

This report summarizes the work performed from February 1966 until June 1975 under Contract #AT-(40-1)3508 on diffusion of rare gases and tritium in nuclear reactor materials. Until November 1970, the primary emphasis was on understanding the mechanisms of rare gas diffusion in uranium dioxide and other compounds which could simulate reactor fuels. Since then, the major effort has been to obtain basic diffusion data for tritium in fission and fusion reactor structural materials. All of the work which has been described in earlier annual reports is briefly summarized in this final report. The investigations which were carried out over the last contract period of sixteen months and which are as yet unpublished are described in greater detail.

Fission product transport in reactor materials has been a subject of considerable interest from the very beginning of nuclear power programs throughout the world. Inert gas diffusion in uranium dioxide is an important consideration in the design of nuclear fuel from the standpoint of both safety and fuel performance. The first section of this report summarizes the major findings of the research carried out to investigate trapping effects on the transport mechanisms for fission product xenon in UO_2 and other nonmetallic solids.

The rest of this report deals with tritium diffusion in reactor structural materials. Nuclear energy generating systems such as light water reactors and high temperature gas-cooled fission reactors of the type in use currently, as well as advanced systems of the future such as liquid-metal cooled fast breeder reactors (LMFBR) and controlled thermonuclear reactors (CTR), all produce tritium in abundant quantities. As an example, a 3600 MWth LMFBR would produce about 15,000-20,000 Ci/year of tritium and a CTR of comparable power is expected to breed about 10^9 Ci/year. The allowable tritium release from these facilities to the environment is an extremely small fraction of the tritium generated. Basic to the problem of tritium containment is the need to understand tritium transport

characteristics of materials used in these systems.

The work on tritium diffusion was initiated with bulk diffusion coefficient measurements in austenitic stainless steels and in Zircaloy-2 because of the widespread use of these alloys as cladding materials in existing light water reactors. The rate-controlling mechanism for the release of tritium from these materials was identified to be permeation through thin oxide films on the surfaces. These studies yielded bulk diffusion coefficients as well as surface film diffusion coefficients which, when used in classical multi-region diffusion models for reactor cladding, gave tritium release rates that agreed well with literature data obtained by reactor fuel pin irradiations. This work was later extended to niobium because of its potential use as a structural material in fusion reactors. The results again showed that the surface oxide film effects control the release rate of tritium at low concentrations. The oxide film characteristics were studied, and the results are reported in detail in this report. The diffusion data generated from this work as well as data reported in literature for other systems were used to compute the steady-state tritium concentration and fluxes in the torus of the Reference Theta Pinch Reactor which is one of the current concepts for a fusion reactor power plant. This work is also discussed in detail in this report.

Each of the following major sections is essentially self-contained and presents results of prior work, experimental findings, mathematical models, discussion of results, and conclusions.

RESULTS

1. RARE GAS DIFFUSION IN SOLIDS

The principal activity from January 1966 until November 1970 was to better define the relationship between trapping of rare gases in solids and post-irradiation gas release experiments with reactor fuel materials. Alkali metal halide and calcium fluoride single crystals were used as substitutes for fissionable materials in order to allow delineation of specific effects. Rare gas retention in surface films, trapping at radiation-induced defects, and gas concentration effects were identified and studied.

Diffusion coefficients of xenon in these two materials at low defect concentrations have been measured. Trap concentration and xenon retention time in traps in CaF_2 and UO_2 single crystals also have been determined. These trapping parameters, when applied to appropriate trapping models, appear to give effective diffusion coefficients for UO_2 which are in agreement with a number of literature values.

1.1. Classical Rare Gas Diffusion

The early literature on rare gas diffusion in solids contains surprisingly few examples of classical diffusion behavior. The term, "classical diffusion," is used here to imply a condition where:

1. The time rate of gas release is consistent with solutions to Fick's diffusion equations with constant diffusion coefficient D .
2. The temperature dependence of D is of the general form:

$$D = D_0 e^{-\Delta H/kT}$$

3. Gas diffusion is controlled by thermally generated defects.

Gas diffusion experiments were carried out for the purpose of establishing whether classical diffusion of a rare gas could be obtained when radiation damage

and gas concentration effects were minimized. Single crystals of CsI, RbI, and KI were grown from a melt doped with ^{133}I which is the precursor of radioactive ^{133}Xe . The resulting crystals contained a homogeneous distribution of radioactive rare gas at low concentration with negligible radiation damage to the lattice. Diffusion experiments were performed by isothermally annealing the crystals and radioassaying the released ^{133}Xe as a function of time. The measured gas diffusion coefficients were reproducible and met criteria (1) and (2) for classical diffusion.

Experiments in which ^{133}Xe was recoiled into the surface layers of crystals through fission of an external uranium foil were also employed to study rare gas diffusion. The diffusion coefficients calculated from the back-diffusion of ^{133}Xe from the surface layers of the recoil doped specimens agreed with the values determined from ^{133}I doping as long as fission recoil fluences were kept below approximately 10^{12} fission fragments cm^{-2} . The two experiments were so greatly different that identical results appear justified only if the Xe diffusion is controlled by thermally generated defects in both cases.

The experiments indicate that it is possible to obtain classical diffusion kinetics for rare gas diffusion if radiation damage levels and gas concentrations are low. Table 1.1 summarizes the characteristic diffusion coefficients and enthalpies measured for ^{133}Xe diffusion in four solids.

Table 1.1. Measured Diffusion Constants for ^{133}Xe Diffusion in Alkali Metal Iodides and Calcium Fluoride.

Solid	D_0 (cm^2/sec)	ΔH (eV)	Temperature Range
KI	1.40 $\begin{matrix} +3.44 \\ -0.84 \end{matrix}$	1.03 ± 0.05	150 C - 500 C
RbI	0.082 $\begin{matrix} +3.11 \\ -0.03 \end{matrix}$	0.93 ± 0.05	150 C - 500 C
CsI	0.57 $\begin{matrix} +2.30 \\ -0.43 \end{matrix}$	1.00 ± 0.04	150 C - 500 C
CaF_2	9.5×10^6	4.42	750 C - 1000 C

1.2. Gas Atom Trapping in "Growth Induced" Defects

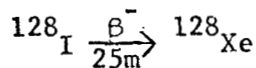
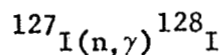
It was found that alkali halide single crystals could be grown which contained considerable strain as the result of defects introduced during the growth process. These crystals were cloudy in appearance and gave indistinct X-ray diffraction patterns, indicative of strain. The defects were presumably small voids and low angle tilt boundaries but no direct observations of the defects were made.

Xenon diffusion measurements on cloudy CsI single crystals gave values for the diffusion coefficient which appeared to decrease with heating time, which was consistent with a trapping process in which gas atoms were being immobilized at defects while they diffused. Application of the trapping model developed by Hurst⁽¹⁾ showed that the experimental results were consistent with a trap concentration of approximately 1.2×10^{11} traps cm^{-3} and a long retention time in the traps. It was possible to eliminate the traps by annealing the crystals before the ^{133}I decayed to ^{133}Xe and the higher the annealing temperature, the greater the fraction of traps annealed. After the gas atoms become immobilized at the traps, they apparently stabilized the traps as heating at this stage did not result in trap annealing.

1.3. Gas Atom Trapping at High Gas Concentrations

A series of experiments were carried out to show the effect of gas concentration on rare gas diffusion kinetics. Three types of experiments were performed:

1. Total Xe concentrations were varied by growing alkali halide crystals in a Xe atmosphere with differing Xe partial pressures. The gas tag was introduced through incorporation of ^{133}I into the melt.
2. Total Xe was varied by irradiating alkali halide crystals with different thermal neutron fluences to generate stable ^{128}Xe through the reaction:



The gas tag was again introduced through incorporation of ^{133}I into the melt.

3. Total Xe was controlled by varying the amount of ^{133}I tag added to the alkali halide melt.

The first technique permitted a wide range of Xe concentrations, but it was not possible to insure uniform gas distribution in the solid. Transmission electron microscopy was used to show that at least some of the Xe was inhomogeneously distributed as bubbles. Methods (2) and (3) produced an initially homogeneous gas distribution but they did not permit as wide a range of possible gas concentrations as method (1). Also, some fast neutron radiation damage was produced by (2) even though this was kept to a minimum by irradiating specimens in the reactor thermal column.

Crystals with relatively high rare gas concentrations (10^{14} - 10^{16} atoms cm^{-3}) exhibited lower diffusion coefficients than the crystals with low rare gas concentrations (10^{10} - 10^{13} atoms cm^{-3}), apparently reflecting trapping of gas atoms in small gas clusters or bubbles. Values of D were lowered at all of the studied temperatures for the high concentration cases and the observed D was constant for the gas release at any given temperature.

Flux limitations on our reactor prevented a study of concentration effects over wide concentration limits. However, the experiments do show that rather pronounced effects (an order of magnitude reduction in the observed diffusion coefficient) occurs when gas concentrations are as high as 10 ppm. Experiments with KI single crystals show effects on the diffusion coefficient which appear to result from gas concentration effects at gas concentrations as low as 0.004 ppm.

In any event, effects due to gas atom clustering clearly occur in alkali halides in the concentration ranges frequently employed for rare gas diffusion experiments.

1.4. Gas Atom Trapping at Radiation-Induced Defects

It was found that radiation produces defects that trap diffusing gas atoms. Radiation damage was produced by doping alkali halide and calcium fluoride crystals through the fission recoil technique at moderately high fission recoil concentrations ($> 10^{12}$ fission fragments cm^{-2}). Each fission fragment deposited an average of 30 MeV, of which approximately 5% was dissipated in displacement type interactions, so a relatively large fraction of the atoms were displaced. The trapping behavior observed in these crystals differed significantly from the trapping defects produced by high gas concentrations or grown-in defects. The radiation-induced effects annealed at high temperatures, and the best fit of the trapping model to the experimental data showed that the trap concentrations were considerably higher and the mean gas retention time in traps considerably lower than was observed with the crystals containing growth-generated defects. The radiation-induced traps had a concentration of at least 10^6 higher than the traps produced by growing defective crystals. Annealing of the radiation-induced defects was not affected by gas stabilization of the traps since the trap concentrations exceeded the gas concentrations.

A detailed analysis was carried out of the trap concentrations and retention times in traps for fission doped CaF_2 single crystals. The model proposed by Hurst⁽¹⁾ was modified for use with fission recoil gas concentration profiles, and trap concentrations and gas retention times were calculated from gas release experiments conducted at two concentrations and four temperatures. The trap concentrations were found to be too high to be explained in terms of gas atom clustering and must have resulted from radiation damage. Semi-log plots of trap concentrations and trap retention times versus $(\text{temperature})^{-1}$ gave straight lines,

implying that these quantities were adequately represented by single values for the activation energies over the temperature range studied.

The experiments summarized in Sections 1.2, 1.3, and 1.4 indicate three distinct gas atom trapping processes which can occur in solids — trapping at small voids and other defects produced during crystal growth, trapping through gas atom clustering at high gas concentrations, and trapping at radiation-induced defects. Each trapping process led to somewhat different gas release kinetics and a different temperature dependence for diffusion.

1.5. Mechanism of Gas Diffusion

The classical diffusion results were interpreted in terms of possible gas diffusion mechanisms. The two most well-established diffusion processes, interstitial diffusion and vacancy diffusion, are incompatible with much of the available data on rare gas migration, including the results of the present study. The principal objection to an interstitial mechanism is the wide discrepancy between calculated and observed diffusion activation energies with the observed values greatly exceeding the calculated values. This discrepancy was supported by the present study where the measured diffusion activation energies for Xe diffusion in KI, RbI, and CsI were observed to be approximately three times the calculated migration energies for interstitial diffusion.⁽²⁾

Objections to simple vacancy diffusion are based upon the absence of an impurity effect on the observed diffusion coefficient,⁽³⁻⁶⁾ channeling results with alpha-emitting rare gases,^(7,8) and the wide discrepancy between rare gas diffusion results and self-diffusion results where self-diffusion is known to occur by a vacancy mechanism.⁽⁹⁾ The present work has noted the absence of an impurity effect for Xe diffusion in Cu_2O and BaI_2 doped crystals and the large difference between the Xe and self-diffusion coefficients.

The two mechanisms that are most frequently discussed as applicable to rare gas diffusion are the trapped-interstitial model proposed by Norgett and Lidiard⁽¹⁰⁾

and the mobile defect cluster model first suggested by Matzke.⁽¹¹⁾ The trapped-interstitial model assumes that rare gas atoms diffuse interstitially but that they also become trapped at defects such as vacancies. The release rate from the vacancy traps can be the rate-determining step in gas diffusion under certain conditions and the measured diffusion activation energy will therefore be higher than that predicted for interstitial migration. The mobile defect cluster model assumes that gas atoms associate with mobile defect clusters in the lattice and move with these clusters through the lattice.

The principal inconsistency between the trapped-interstitial diffusion model and the present work lies in the fact that unusually high defect concentrations are required to explain the low temperature, fission recoil diffusion results where the gas atoms move extremely short distances before release at a surface. The mobile cluster model appears qualitatively consistent with the experimental results, and it appears to be the better choice of the two to explain rare gas diffusion in alkali halides.

1.6. Diffusion and Trapping in UO₂ Single Crystals

Diffusion studies were performed with UO₂ single crystals using fission-recoil doping and radioassay of the released ¹³³Xe. It was observed that below a fission fragment dose of 3×10^{11} ff cm⁻², classical diffusion solutions would fit the gas release, implying that radiation-induced defects did not affect the diffusion process. The classical diffusion coefficient could be represented by

$$D = 2.88 \times 10^3 \exp(-110 \text{ kcal/RT}) \text{ cm}^2 \text{ sec}^{-1} \quad (1)$$

over the temperature range 1065°C to 1300°C. Increasing the recoil concentration to 3×10^{12} fission fragments/cm² (3×10^{-8} fission atom fraction) produced anomalies in the gas release curves which probably resulted from gas atom trapping. The gas release curves at this fission fragment dose were consistent with the

trapping model of Ong and Elleman.⁽¹²⁾ The trap concentrations and retention time in the traps could be determined at 3×10^{12} fission fragments/cm² at three different temperatures.

2. TRITIUM DIFFUSION IN FISSION REACTOR CLADDING

This section summarizes the previous years' work on tritium diffusion studies in reactor cladding materials (stainless steels and Zircaloy) and discusses in detail this year's work on grainboundary diffusion in stainless steel.

2.1. Tritium Transport in Stainless Steels

2.1.1. Summary of Prior Years' Work

Stainless steel was a fairly common cladding material in nuclear power reactors of the late 1960's and is used in current reactors as the cladding material for burnable poison rods in light water reactors. It is also proposed for use as the first wall material in at least two of the current designs for controlled thermonuclear reactors. Previous hydrogen diffusion measurements in stainless steels were obtained by either permeation studies or by exposing the specimens to hydrogen gas and measuring the concentration profile. In both types of studies, the results will be influenced by various interferences such as surface effects.

In order to measure diffusion coefficients uninfluenced by these effects and to understand the rate-controlling steps in tritium release from stainless steel, tritium was introduced into cylindrical specimens by recoil-injection from a ${}^6\text{LiF}$ surface blanket irradiated with thermal neutrons to produce ${}^6\text{Li}(n,\beta){}^3\text{H}$ reaction. The irradiated samples were electropolished to remove thin layers which were assayed for tritium to ascertain that the recoil injection produced a linearly decreasing concentration profile as expected. ⁽¹³⁾ Other irradiated samples were diffusion-annealed at known constant temperatures and subsequently electropolished to generate tritium concentration profiles. The kinetics of tritium release during diffusion anneals were also monitored. The experimental methods used and the results are described by Austin and Elleman. ⁽¹⁴⁾

The concentration profiles showed three components of diffusion which were identified as a surface trapping region with high concentration in 2-5 μm at the surface, a bulk diffusion region and a long-range grainboundary component. The bulk diffusion components in 304- and 316-stainless steels were consistent with classical diffusion solutions⁽¹³⁾ from which diffusion coefficients in the bulk region could be determined. These are represented by

$$D = 0.018 \exp(-14 \text{ kcal/RT}) \text{cm}^2 \text{-sec}^{-1} \quad (2)$$

in the temperature range 25°C to 222°C. There was no apparent difference between 304- and 316-stainless steels.

The grainboundary diffusion components were determined up to depths of 2000 μm into the sample by sectioning using a combination of lathe and electropolishing. These concentration profiles were fitted to Fisher's⁽¹⁵⁾ and Suzouka's⁽¹⁶⁾ models to obtain grainboundary diffusion coefficients. The values obtained from the two models agreed to within a factor of 1.4. Fisher's model gave values represented by the Arrhenius expression

$$D_G = \exp(8.85 \pm 1.2) \exp(-10.3 \pm 0.7 \text{ kcal/RT}) \text{cm}^2 \text{-sec} \quad (3)$$

over the temperature range -78°C to 185°C. Only a relatively small fraction (about 1-4%) of the injected tritium was found in the grainboundary diffusion component during the relatively short annealing times used in the experiment. These grainboundary diffusion coefficients are about eight orders of magnitude greater than the bulk diffusion coefficient represented by equation (2). The grainboundary diffusion results are discussed by Calder, et al.⁽¹⁷⁾

The near-surface trapping in stainless steel was studied by following the kinetics of tritium release at constant temperature. A two-region classical diffusion model which assumes different diffusion coefficients in the surface region and in the bulk region could fit the surface release results although the

model did not explicitly take into account tritium trapping and the build-up of tritium in the surface layer. The apparent diffusion coefficients for the surface region determined by this model gave the Arrhenius expression

$$D = 3.0 \times 10^{-4} \exp(-15.4 \text{ kcal/RT}) \text{ cm}^2 \text{ -sec}^{-1} \quad (4)$$

in the temperature range 25°C to 184°C. These surface-layer diffusion coefficients are lower than the bulk diffusion coefficients quoted in equation (2) by about 2 to 3 orders of magnitude. The possibility was considered that the near-surface trapping was caused by the recoil-injection process in which helium (α -particles) were injected to a depth of 3 μm and possibly produced helium stabilized vacancy clusters. To check this, concentration profiles were measured in stainless steel foils which were implanted with monoenergetic helium ions from a tandem Van de Graaf accelerator prior to tritium injection and diffusion anneal at sufficiently large Dt to allow the tritium to diffuse past the helium region. They showed no discernible evidence of tritium trapping by the helium layer. It is believed that the surface trapping is caused by a thin layer of oxide region on the sample surface. These surface effects results are discussed in a paper by Austin, et al. (18)

2.1.2. Grainboundary Diffusion in 304L-Stainless Steel-Predicted Permeation Rates.

Based on the bulk and grainboundary diffusion coefficients, we have investigated the question of by how much the tritium permeation rate would be influenced by grainboundary diffusion. This section discusses the results of these computations. This information has not been presented in prior annual reports and is therefore treated in some detail.

2.1.2.1 Grainboundary Diffusion Model

Permeation rates through grainboundaries in a finite slab can be computed by adapting the mathematical model developed by Levine and MacCallum. (19) This

model assumes a uniform, time-independent concentration of tritium on one side of the specimen. It is assumed that diffusion takes place through the boundaries into the grains and not vice versa. The grains merely act as infinite sinks. Following the arguments of Levine and MacCallum, tritium concentration $C'(y, t)$ in the grainboundaries at a distance y from the surface is given by the balance equation,

$$\frac{\partial C'}{\partial t} = \frac{2}{3} D' \frac{\partial^2 C'}{\partial y^2} - \frac{\sigma}{\epsilon} \int_0^t G(t - v) dv \quad (5)$$

where

D' = the grainboundary diffusion coefficient,

σ = total surface area of the grains,

ϵ = the volume fraction of grainboundaries
in the specimen,

and

$G(t)$ = The Green's function for the flux into a grain from the surrounding grainboundary.

For a grain of diffusivity D , $G(t)$ is given by

$$G(t) = (D/\pi t)^{\frac{1}{2}} \exp(-4\epsilon^2 D t / \delta^2) \quad (6)$$

δ = the width of the grainboundary

Consider a finite slab of thickness L , through which the diffusant is permeating.

The boundary conditions are

$$\begin{aligned} C'(L, t) &= 0 \\ C'(0, t) &= 1 \end{aligned} \quad \text{for all } t \geq 0 \quad (7)$$

For convenience, we assume the surface concentration to be unity at the inlet side. The initial condition is given by

$$C'(y, t) = 0 \quad \text{for } y > 0 \quad \text{and} \quad t \leq 0 \quad (8)$$

Taking Laplace Transforms of equations (5) and (6) and of the initial and boundary conditions, it can be shown that

$$\mathfrak{L}\{C'(y, t)\} = \bar{C}'(y, s) = \frac{1}{s} \left[\frac{e^{-\alpha y}}{1 - e^{-2\alpha L}} + \frac{e^{\alpha y}}{1 - e^{2\alpha L}} \right] \quad (9)$$

where

$$\alpha = \left\{ \frac{3s}{2D'} \left[1 + \left(\epsilon^2 + \frac{\delta^2 s}{4D} \right)^{-\frac{1}{2}} \right] \right\}^{\frac{1}{2}} \quad (10)$$

The concentration $\phi(y, t)$ averaged over the grains and the grainboundaries on any plane at a distance y from the entry side can be written as

$$\phi(y, t) = \epsilon C'(y, t) + \sigma \int_0^t C'(y, v) G(t - v) dv \quad (11)$$

It follows that

$$\mathfrak{L}\{\phi(y, t)\} = \bar{\phi}(y, s) = \epsilon \left[1 + \left(\epsilon^2 + \frac{\delta^2 s}{4D} \right)^{\frac{1}{2}} \right] \bar{C}'(y, s) \quad (12)$$

The release rate per unit area $R(t)$ from the surface $y = L$ may be written as

$$R(t) = -D \left. \frac{\partial \phi(y, t)}{\partial y} \right|_{y=L} \quad (13)$$

where D is the bulk diffusion coefficient. Therefore

$$\begin{aligned} \mathfrak{L}\{R(t)\} &= -D \left. \frac{\partial \bar{\phi}(y, s)}{\partial y} \right|_{y=L} \\ &= \frac{\epsilon \alpha D}{s} \left[1 + \left(\epsilon^2 + \frac{\delta^2 s}{4D} \right)^{-\frac{1}{2}} \right] \frac{1}{\text{Sinh}(\alpha L)} \end{aligned} \quad (14)$$

The release rate per unit area through the grainboundaries that are exposed to the exit side is given by

$$R'(t) = -\frac{8}{3\pi} \delta \lambda D' \left. \frac{\partial D'}{\partial y} (y, t) \right|_{y=L} \quad (15)$$

where λ = the total length of all grainboundary trace exposed per unit area.

Therefore,

$$\begin{aligned} \mathcal{L}\{R'(t)\} = \bar{R}'(s) &= -\frac{8}{3\pi} \delta \lambda D' \frac{\partial \bar{C}'(y, s)}{\partial y} \Big|_{y=L} \\ &= \frac{8}{3\pi} \delta \lambda D' \frac{\alpha}{s} \frac{1}{\text{Sinh}(\alpha L)} \end{aligned} \quad (16)$$

Inverse transformation of equations (9), (12), (14), and (16) would give the concentration in the grainboundary, the average concentration along any plane parallel to the faces of the slab, the release rate from the exit face and the release rate from the grainboundaries exposed at the exit face, respectively. Analytical inversion of these equations is not possible because of the complicated nature of $\alpha(s)$ defined by equation (10). Here, we resort to the numerical inversion method described by Bellman and Kalaba.⁽²⁰⁾ They have shown that the Laplace Transform equation

$$\bar{f}(s) = \int_0^{\infty} e^{-st} f(t) dt \quad (17)$$

may be solved for $f(t)$ by defining a variable $x = e^{-t}$, such that $f(t)$ becomes $f(-\ln x)$, hereafter called $g(x)$ and given by

$$f(s) = \int_0^1 x^{s-1} g(x) dx \quad (18)$$

Applying numerical quadrature to the integral term and letting s assume N different values results in a linear system of N equations

$$\bar{f}(k+1) = \sum_{i=1}^N \omega_i x_i^k g(x_i), \quad k = 0, 1, 2, \dots, (N-1) \quad (19)$$

Bellman and Kalaba have shown that $x_i = \frac{1+r_i}{2}$ and $\omega_i = \frac{a_i}{2}$ where r_i are roots of Legendre polynomials of order N and a_i are Christoffel weights. r_i

and a_i are tabulated. (21) From equation (17),

$$g(x_i) = \sum_{k=0}^{N-1} B_{ik} \bar{f}(k+1) \quad (20)$$

where B_{ik} are the elements of the inverse of the matrix with elements $A_{ik} = \omega_i x_i^k$. B_{ik} are tabulated by Bellman and Kalaba for values of N upto 15.

Equation (18) gives the approximate inverse transform of $\bar{f}(s)$ at time $t_i = \ln x_i$. To obtain the values of the function at other values of t , one may use the relationship

$$f(-a \ln x_i) = \sum_{k=0}^{N-1} \frac{B_{ik} \bar{f}\left(\frac{k+1}{a}\right)}{a} \quad (21)$$

The inverse transforms of $\bar{C}'(y,s)$, $\bar{\theta}(y,s)$, $\bar{R}(s)$ and $\bar{R}'(s)$ could be computed by the above numerical scheme. The following topological relationships given by Levine and MacCallum were used to calculate σ , λ and ϵ from the mean grain size, ℓ and the grainboundary width, δ .

$$\sigma = \frac{4}{\ell}, \quad \lambda = \frac{\pi}{2\ell} \quad \text{and} \quad \epsilon = \frac{2\delta}{\ell}$$

The grainboundary diffusivities were taken from the measurements of Calder, et al. (17) and the bulk diffusivities from Austin and Elleman. (14)

2.1.2.2. Bulk Diffusion Model

One-dimensional bulk diffusion in a slab satisfying the initial and boundary conditions given by equations (7) and (8) results in a concentration profile $C(y,t)$ given by,

$$C(y,t) = 1 - \frac{y}{L} - \frac{2}{\pi} \sum_{n=1}^{\infty} \sin\left(\frac{n\pi y}{L}\right) \exp\left(-\frac{n^2 \pi^2 D t}{L^2}\right) \quad (22)$$

The release rate from the exit face at $y = L$ is given by

$$R(t) = \frac{D}{L} \left[1 + 2 \sum_{n=1}^{\infty} (-1)^n \exp\left(-\frac{n^2 \pi^2 D t}{L^2}\right) \right] \quad (23)$$

2.1.2.3. Computational Results

Using the models presented in the previous sections, tritium concentration and release rates due to grainboundary and classical bulk diffusion in thin stainless steel slabs at various temperatures were computed. The bulk diffusion coefficient and the grainboundary diffusion coefficient were calculated from the rate equations given by Austin and Elleman⁽¹⁴⁾ and by Calder, et al.,⁽¹⁷⁾ respectively. Calculations were made for slab thicknesses of 0.0254 cm and 0.0445 cm (cladding thickness of the Fast Flux Test Facility). An average grain size of 50 μm and a grainboundary width of 5 $^{\circ}\text{A}$ were assumed.

Figure 1 shows the tritium concentration profiles in a stainless steel slab of thickness 0.0445 cm at 500 $^{\circ}\text{C}$ (typical cladding temperature of LMFBR fuel pins). The solid lines were the results of computations using equations (9) and (12) and the dashed curves were computed from equation (22). The grainboundary diffusion model predicts a much quicker buildup of tritium in the slab than does the bulk diffusion model. The first term in equation (12) represents the total concentration of tritium in the grainboundaries and the second term represents the concentration accumulated in the grains. Separate computation of these two terms revealed that the amount of tritium retained in the grainboundaries is about five orders of magnitude smaller than the amount in the grains. This implies that even though the grainboundaries act as rapid diffusion paths, net concentration in the solid is controlled by the tritium in the grains.

Figure 2 shows the release rates per unit area at the outer surface of the slab. Curve a is the release rate through the grainboundaries as calculated by equation (16). Curve b is the release rate through the lattice due to grainboundaries rapidly transporting the tritium through the specimens and feeding into the grains using equation (14). Curve c represents the release rate predicted by the bulk diffusion model equation (23). The equilibrium release rate through the lattice from the grainboundary diffusion model is the same as that from the

classical bulk diffusion model. However, the release rate through the grain-boundaries is about 55 times greater than through the lattice. Furthermore, the grainboundary model predicts extremely rapid equilibration of the tritium permeation in the slab. However, the permeation experiments reported in the literature are consistent with the lower bulk diffusion coefficients and do not show the short equilibration times predicted by the grainboundary model.

Thus, the question arises as to why one is able to observe fast diffusion through grainboundaries in sectioning experiments but at the same time, not be able to observe grainboundary effects in permeation studies. Several reasons may be postulated for this discrepancy. For example, it is possible that the solubility limit for hydrogen in grainboundaries is much less than that in the lattice, so that precipitation may occur in the grainboundaries and impede the transport via grainboundaries. Furthermore, if surface effects control the desorption of hydrogen near the surface, the release rate could be significantly reduced. In order to gain insight into possible mechanisms that inhibit grainboundary transport, autoradiographic examination was carried out in stainless steel specimens which had been charged with tritium. These experiments are discussed in the following section.

2.1.2.4. Autoradiography

2.1.2.4.1. Techniques

Type 304L stainless steel foils (supplied by Hamilton Precision Metals) 5 mils thick and cut to $\frac{1}{2}$ " x $\frac{1}{2}$ " size were strain annealed for two hours at 1050°C at a pressure of 4×10^{-5} Torr. The average grain size of the heat treated samples was 50 μ m. Samples with three different (unpolished) surface characteristics were studied: unpolished, electropolished and electropolished and etched. Electropolishing was carried out in a 60% H₃PO₄ - 40% H₂SO₄ solution at 50°C and at 3 volts for 3 minutes. Etching was performed electrolytically in

a 50% HNO_3 - 50% H_2O at ambient room temperature using 1-5 volts for 10-15 seconds. All samples were washed well in deionized water and ethyl alcohol.

Tritium charging was carried out by either exposing the samples at room temperature for about 10 days in a glass chamber containing about 0.5 Ci of ^3H gas or by recoil injection through neutron transmutation of ^6Li in a $^6\text{Li}_2\text{CO}_3$ blanket placed on contact with one side of the foil sample. The concentration of the tritium at the surface of the recoil injected samples was estimated to be 3×10^{16} atoms/cm³.

The tritiated specimens were washed, dried and mounted on microscope slides. Kodak AR-10 stripping film which has a 5 μm layer of emulsion in a 10 μm gelatin base was used for autoradiography. The mean diameter of the AgBr grains was 0.2 μm which could give an overall resolution of 2.5 μm . Small sections of the emulsion were floated on water with the emulsion side downward and then picked up carefully on the stainless steel sample in a manner to assure good emulsion contact with the specimen. Exposure times ranging from 0.5 to 10 hours were used for the absorption charged samples, while for recoil injected samples, the exposure time was 100 hours.

After development, the emulsions were stripped from the specimen, floated on water and picked up on glass slides for microscopic observations.

2.1.2.4.2. Tritium Segregation at Defects

Tritium distributions on the surfaces of the specimens were highly non-uniform; tritium appeared to segregate at crystallographic defect structures such as second phases, twin and grainboundaries and at non-metallic inclusions. Typical results are shown in Figures 3, 4, and 5. Figure 3 is a stripped autoradiograph from an unpolished specimen while the corresponding micrograph of approximately the same region of the metal surface is shown in Figure 4. The tritium is observed to segregate at defect structures visible in the radiographs. The martensitic bands and other second phases probably were formed from storing the tritium charged

specimens in liquid nitrogen. Such spontaneous phase transformations have been reported by Reed.⁽²²⁾ The randomly distributed dark spots seen in Figure 3 are presumably due to tritium concentration at non-metallic inclusions in stainless steel. Figure 5 is a stripped autoradiograph from an electropolished and etched specimen showing tritium segregation at twin boundaries. The twinned regions generally contained a higher concentration of tritium than the grains surrounding them.

In samples with absorption charged tritium, large concentrations of tritium in irregular patterns covering many grains were visible on autoradiographs. Figure 6 shows one such patch on an electropolished and etched specimen. Repeated heat treatments of the sample at up to 185°C did not remove this feature and electron microprobe analysis of this region did not show any significant differences in composition. It is presumed to be highly oxidized regions which trap tritium. Such regions have been observed by Roy⁽²³⁾ on the surface of oxidized Zircaloy specimens.

Recoil injected specimens showed autoradiographs with uniform distributions except at second phase formations until heat treatment or long duration anneal at room temperature when grainboundaries were visible. This is to be expected since the recoiled tritium enters the lattice uniformly and therefore grain-boundary-lattice contrast on radiographs will be visible only after some diffusion of the tritium has occurred.

All of the above features demonstrate trapping of tritium at surface or bulk defects and may account for the retarded release of tritium from stainless steel surfaces as observed by Austin, et al.⁽¹⁸⁾

2.1.2.4.3. Grainboundary Diffusion

Autoradiographs of specimens from which a surface layer of approximately 1-2 μm was removed electrolytically following diffusion anneal showed that tritium was essentially confined to the grainboundaries. A typical case is shown in

Figure 7. The tritium presumably moved rapidly along the grainboundaries and became trapped at the grainboundary sites by bulk diffusion. Repeated autoradiographs of the same surface taken over a span of several weeks showed the same distribution of tritium at the grainboundaries.

Tritium was recoiled into only one side of the specimens in the recoil injection experiments. However, autoradiographs of the back faces following heating at 185°C for two hours showed considerable tritium trapping on the back face. Figure 8 shows one such autoradiograph from an electropolished and etched specimen. The precipitation at the grainboundaries on the surface even at low concentrations may be explained by near-surface trapping. The required rate of transport for tritium to appear at the back face exceeded the values predicted by the bulk diffusion coefficients and implied rapid diffusion along grainboundaries.

Heat treatment and subsequent cooling increased the precipitation of tritium along grainboundaries. Figure 9 shows a stripped autoradiograph from a polished and etched specimen. The grainboundaries are not clearly discernible. Figure 10 is a radiograph of the same region of the specimen after it had been heated at 185°C for two hours. The grainboundaries are now clearly visible.

Grainboundaries near the surface therefore apparently act as tritium sinks rather than rapid diffusion paths. This effect may be due to trapping of tritium in the oxide films which occur at the surface since the earlier observations in this section imply rapid diffusion along the grainboundaries in bulk.

Grainboundaries denuded of tritium could be observed under certain conditions. Figure 11 is an autoradiograph of a specimen which had been etched prior to tritium exposure and shows low tritium concentrations at grainboundaries. This behavior was consistently observed with specimens treated in this fashion. The absence of tritium is consistent with rapid diffusion along grainboundaries but it is not clear why the etched specimens exhibited little surface trapping at

grainboundaries while the unetched specimens showed high grainboundary concentrations.

Autoradiographs of specimens which had been electropolished but not etched gave no indication of grainboundaries. The surface concentration of tritium as observed from autoradiographs was generally much lower on unetched samples than on etched samples. The reason for this behavior is not clear.

In presenting the above results, it has been assumed that localized darkening on the autoradiographs represented high local concentrations of tritium. Louthan, et al.⁽²⁴⁾ have pointed out that such variations in darkening could also be due to high local diffusivities and resulting tritium release. In our study we have seen the same relative darkening between regions when autoradiography was repeated on the same specimens after as long as three months following tritium charging. This makes it unlikely that the observed local variations in optical density were due to high diffusivities.

2.1.2.5. Discussion and Conclusions

Results of the computations using the grainboundary diffusion model of Levine and MacCallum⁽¹⁹⁾ along with experimentally measured tritium diffusion coefficients in stainless steel for volume diffusion⁽¹⁴⁾ and for grainboundary diffusion⁽¹⁷⁾ show that permeation rates should be controlled by transport along grainboundaries. However, the published literature on hydrogen permeability measurements in austenitic stainless steels show little contribution from fast diffusion along grainboundaries. There are several possible explanations for this anomaly which appear consistent with the autoradiography experiments.

The permeation of tritium through stainless steel could be controlled by trapping on the surfaces of the specimen. There is some evidence for surface trapping in the autoradiographs and in the earlier work of Austin, et al.⁽¹⁸⁾ The persistence of high concentrations of tritium at grainboundaries on the surface

even after repeated heat treatments indicates that the tritium at the surface was trapped. Furthermore, for the absorption charged specimens, the electropolished foils had to be etched prior to charging to make grainboundaries visible on autoradiographs which implies that a surface layer at the grainboundaries had to be removed before gaseous tritium would enter the boundaries in sufficiently high concentrations to be observed. In the case of recoil injected specimens, surface trapping was observed both at the front and the back faces within the grainboundaries.

Another explanation for the discrepancy may be that in permeation experiments, the source term for the exposed grainboundaries is less than that at the exposed grains, possibly because of lower hydrogen solubility in the grainboundaries as compared to that in the grains. The model of Levine and MacCallum assumes a constant uniform concentration everywhere on the front face and therefore it would show large contributions to permeation from rapid grainboundary transport. The grainboundary diffusion experiments by Calder, et al.⁽¹⁷⁾ showed that about 3.6% of the total tritium was associated with grainboundary diffusion. Therefore, an upper limit of the ratio of equilibrium grainboundary concentration to the equilibrium lattice concentration may be obtained from Calder's data and from the calculated concentration profiles in the grainboundary and bulk diffusion models. The amount of tritium in the grainboundary diffusion component is $\gamma \int_0^L \phi(y,t) dy$, where γ = the ratio of equilibrium concentration in the boundary to that in the lattice and $\phi(y,t)$ is the average concentration at depth y in the grainboundary model. The total tritium in the sample is $\int_0^L c(y,t) dt + \gamma \int_0^L \phi(y,t) dt$, where $c(y,t)$ is the concentration in the bulk model. Equating the calculated fraction to the measured fraction, γ was determined to be 0.037 which is considerably below the value of 1.0 expected for equal tritium solubility in grains and grainboundaries. If one uses this reduced grainboundary concentration, the

ratio of equilibrium release rate through the boundaries to that through the lattice at 500°C, 570°C and 698°C is found to be 2.05, 1.7 and 1.2 respectively. The corresponding values assuming no difference in equilibrium concentration between the grainboundaries and the lattice are 55, 42, and 32. Thus it appears that low solubility of tritium in the grainboundaries could explain the absence of a significant grainboundary contribution to hydrogen permeation of stainless steel.

The following conclusions are drawn from the grainboundary diffusion work:

1. The idealized model of grainboundary diffusion used in this study overestimates the actual movement of tritium along grainboundaries. The grainboundary diffusion model predicts a much earlier release of tritium from the back face than the predicted by bulk diffusion model. It also predicts equilibrium release rates through grainboundaries that are 30-60 times greater than that predicted by bulk diffusion between 500°C and 700°C.
2. While autoradiography of tritium tagged stainless steel foils show that grainboundaries are indeed rapid diffusion paths, their contribution to the overall permeation rate appears to be minimized by surface trapping and possibly by low solubility of tritium within the grainboundaries.
3. Tritium segregates at various crystallographic defects such as second phases, twin boundaries and stacking faults as well as around slip bands on cold-worked specimens. It also concentrates on the specimen surface in large patches which are believed to correspond with oxide layers.

2.2. Tritium Transport in Zircaloy-2.

2.2.1. Summary of Prior Year's Work

No new studies on Zircaloy were undertaken during the last renewal period of this contract.

Literature data for bulk diffusion coefficients of hydrogen in Zircaloy differed over 4-10 orders of magnitude in the temperature range 50°C-400°C. It was believed that a reason for this disagreement between the results of various methods of measurement might have been surface effects which could inhibit both the absorption of hydrogen into the bulk and the release of hydrogen from the bulk. Recoil-injection, as in the case of stainless steel studies, appeared to be a possible way to introduce tritium into the bulk region without being affected by surface effects.

The Zircaloy-2 samples were prepared in a similar manner to the stainless steel samples described earlier. It was found that reproducible measurements of tritium concentration profiles could be made by removing thin sections by chemical polishing and assaying the polish solution for tritium after distillation. Diffusion anneals were performed either using an oil bath or using a molten tin bath. During the annealing, it was possible to monitor the release rate of tritium from the samples by flowing P-10 gas around the specimen and then through a proportional counter. The experimental methods and the results are discussed by Austin, et al.⁽¹⁸⁾

The concentration profiles of diffusion-annealed specimens consisted of two components: a high concentration on the surface within a 1-3 μm region followed by a bulk diffusion region. No significant grainboundary component was observed. The bulk diffusion component was consistent with classical one-region diffusion model and yielded bulk diffusion coefficients given by the expression

$$D(\text{cm}^2 - \text{sec}^{-1}) = 0.00021 \exp(-8.5 \text{ KCal}/RT) \quad (24)$$

in the temperature range -78°C to 204°C. These values are in close agreement with the measurements reported by Kearns⁽²⁵⁾ and are well above the values obtained from experiments where surface effects could have been significant.

The surface region diffusion coefficients were obtained by analysis of the tritium release kinetics data using the two-region diffusion model⁽¹⁸⁾ as in the case of stainless steel data. The resulting apparent diffusion coefficients gave the Arrhenius relation

$$D(\text{cm}^2 - \text{sec}^{-1}) = 0.12 \times 10^{-13} \exp(-5.5 \text{ kcal/RT}) \quad (25)$$

in the temperature range 25°C to 411°C. These values are lower than the bulk diffusion coefficients by seven to eight orders of magnitude and were found to be the rate-limiting parameters for tritium evolution from the specimens. It is believed that the low release rate from the surface layers of Zircaloy is due to oxides of zirconium that form readily upon exposure to air.

Tritium transport through ZrO_2 surface films was studied further by forming oxide layers on Zircaloy-2 specimens by controlled oxidation in oxygen at 200 Torr and studying the kinetics of release of recoil-injected tritium from these specimens. In spite of long-term diffusion anneals at up to 600°C, there was little breakthrough release from the bulk region through the oxide layer (although based on the surface layer diffusion coefficients given by equation (25) breakthrough release would have been expected). The total tritium released in these experiments came from what had been originally recoiled into the oxide layer. Thus it appears that the diffusion coefficients given by equation (25) may be upper limits for the values that control tritium permeation through oxide films on Zircaloy.

2.3. Tritium in Light Water Reactors

It is of interest to consider the implications of the diffusion results discussed to nuclear power reactors. From the standpoint of environmental safety, the quantity of interest is the amount of tritium in the primary coolant. Light water reactor plants keep this concentration within reasonable limits by frequently replacing a portion of the primary system water with fresh water. There have

been efforts by reactor manufacturers⁽²⁶⁾ to correlate the observed primary system tritium activity to the activity due to boron and lithium reactions in the primary water and assign the difference between these to release of tritium from fuel pins and burnable poison pins. In general, the results show that most of the tritium in stainless steel clad pins is released. Such programs for following tritium in power reactors do not, however, predict the time-dependent release rate from the pins.

2.3.1. Summary of Prior Year's Work

A tritium release model that included surface effects in cladding was formulated in order to check whether the basic tritium diffusion data would predict release rates from fuel pins which are consistent with observations in pressurized water reactors. The model assumed a cylindrical fuel rod generating a constant power with all of the tritium diffusing classically within the fuel; the tritium atoms released from the fuel were assumed to dissolve into the cladding surface and diffuse classically through an inner surface layer and a bulk region and an outer surface layer with diffusion coefficients in each region given by equations (24) and (25) was assumed. The model and the predicted release rates for fuels pins of PWR and BWR types are discussed by Abraham, et al.⁽²⁷⁾

The results showed that in a year of irradiation, about 80% of the tritium generated in the UO_2 fuel would be expected to diffuse out of the fuel and in stainless steel clad fuel pins, almost all of this tritium would permeate through the cladding into the coolant water. However, in Zircaloy clad pins less than 1% of the tritium generated in a year would be expected to enter the coolant if the Zircaloy has outside layers on either side which are 2 μm thick. This difference between stainless steel and Zircaloy cladding occurs because of the dramatic difference in tritium surface layer diffusion coefficients. In stainless steel the surface region diffusion coefficient is only about 200 times smaller

than the bulk diffusion coefficient, whereas in Zircaloy the corresponding difference is a factor of about 10^8 . Since an 1150 Mw light water reactor would generate about 15,000 Ci of tritium/year in the fuel, even 1% of it if released into the coolant would result in about the same amount of tritium in the PWR reactor coolant as is produced through boron reactions. This result indicates that even though surface films on Zircaloy are nearly perfect barriers to tritium diffusion, release of ternary fission tritium from stainless steel clad elements should be considered on an equal basis with other sources of tritium in light water reactors. These conclusions are generally in agreement with reports in literature of measurements on irradiated fuel pins.⁽²⁸⁻³¹⁾ They are also consistent with the general observation that reactors with stainless steel clad cores have shown about 50 times higher tritium activity in the coolant than those with Zircaloy clad cores.

In order to compare plant data with model predictions, the tritium activity in coolant water resulting from $^{10}\text{B}(n,2\alpha)^3\text{H}$ and from $^7\text{Li}(n,\alpha n)^3\text{H}$ reactions were calculated for Carolina Power and Light Company's H. B. Robinson Plant for an 80-day period in the middle of the first cycle. Actual boron and lithium concentrations and time-dependent let-down rates from plant records were used. The results were compared to plant data on ^3H activities in the primary system water. The comparison showed that about 50% of the observed activity resulted from the boron and lithium reactions, thus implying that the rest must have been the result of tritium release from fuel pins and burnable poisons. Release of about 0.5% of the tritium from the fuel pins alone would be sufficient to account for this difference.

2.3.2. Work in Progress - A Computer Code for Tritium in PWR's

Based on a request from a utility company, a computer code to calculate tritium activity in the primary system of pressurized water reactors is being compiled currently. The code calculates production rates of tritium in all types

of sources within a PWR and computes release rates from the various sources into the primary coolant. Based on these release rates and the coolant let-down and make-up rates, it calculates the time-dependent tritium activity in the coolant.

The predictions from this code will be compared against extensive data from the H. B. Robinson #2 nuclear plant and parametric studies will be conducted to establish the sensitivity of the results to parameters that are most uncertain in the model. It is expected that this code can be made available from the Argonne Code Center for general use.

3. TRITIUM DIFFUSION IN FUSION REACTORS

3.1. Tritium Transport in Niobium

Niobium and niobium alloys are prime candidates for use as a structural material in CTR's. Measurements of hydrogen diffusion coefficients in niobium by a variety of methods⁽³²⁾ indicate that in the temperature range of operating CTR's (500°C - 1000°C), these diffusion coefficients are nearly as high as for liquids. Because of the possible problems this might introduce in CTR blankets, it was felt that an investigation of rate-limiting steps in the release of tritium from niobium is important.

3.1.1. Summary of Prior Year's Work

Cylindrical specimens of niobium were recoil-doped with tritium up to a maximum tritium concentration of 0.005 ppm by weight. It was verified by electro-polishing 1-2 μm sections that the concentration profiles in the bulk region at room temperature was consistent with tritium diffusion coefficients quoted by Hickman.⁽³³⁾ Large concentration of tritium was observed in a 1-2 μm surface layer of the samples, indicating that surface trapping of tritium.

Release rate of tritium from the recoil-injected specimens was monitored. Below 600°C the total release of tritium over a 4- to 5-day period was no more than about 3% of the total tritium in the sample. The apparent diffusion coefficients for release of tritium from surface layer as determined from this data were seven to ten orders of magnitude lower than the bulk diffusion coefficients in the temperature range 600°C to 900°C.

Above 600°C, it was possible to observe tritium from the bulk region permeating through the surface layers. This release through the surface film could be analyzed according to two different models. If one hypothesized that this release was occurring freely only through cracks in the surface film, based on the model of Inthoff and Zimen,⁽³⁴⁾ one could calculate the effective fractional

surface areas through which the tritium release occurred. These fractional surface areas ranged from 10^{-3} at 600°C to 10^{-1} at 900°C . It was also possible to analyze the tritium release data using mass-transfer model in which case one assumes that the flux at the surface is proportional to the surface concentration of tritium. From such a model, the mass-transfer coefficient could be determined at various temperatures. While the mass-transfer model could fit the experimental results reasonably well, it was not consistent with the observation that the build up of tritium at the surface occurs over a depth of 1-3 μm and is not strictly a surface effect.

All of these results for niobium are discussed by Pennington, et al. (35)

It was clear that the surface layers on niobium act as very strong barriers to release of tritium and that release rates calculated using only bulk diffusion coefficients would grossly overestimate the true release. However, the surface film characteristics, their stability in a strongly reducing environment (such as in contact with lithium in CTR's) and the model that appropriately describes diffusion through these films were unclear from this work. Therefore, it was decided to pursue further investigation on tritium diffusion through niobium surface films.

3.1.2. Tritium Diffusion Through Oxide Films on Nb

3.1.2.1. Techniques

Cylindrical niobium specimens, strain-annealed at 800°C in high vacuum, were either electropolished to remove any surface films or electropolished and heated in air to obtain oxide films of different thicknesses and adherence. Following recoil implantation of tritium into these specimens, the tritium release rate from the surface was measured as a function of time by mixing the tritium with P-10 counting gas and flowing through a proportional counter. Some specimens were heated through a series of temperatures to establish release rates at each temperature while other samples were heated only at a single temperature (denoted as a "fresh" sample in the text). The maximum initial tritium concentration in the specimens was approximately 0.005 ppm H^3 by weight.

Direct measurements of tritium profiles were made in some specimens through removal of surface layers by electropolishing followed by measurement of the contained tritium. Details of this experimental technique have been described earlier. (35)

Oxide film thicknesses were measured by direct observation with an optical microscope, Auger spectroscopy, or indirectly through anomalies in tritium release kinetics. For direct observation, niobium foil samples were coated with nickel layers approximately 0.001 inch thick following a standard procedure described by the Buehler Corporation. (36) The foils were mounted in lucite with one edge exposed and polished or polished and etched for observation. The method was not particularly successful and often yielded oxide film thicknesses which were at variance with the other techniques. The Auger spectroscopy studies were performed at NASA Langley and at the Physical Electronic Industries, Inc., Minneapolis, Minnesota. Compositional depth profiles of various elements present on the surface were obtained by "sputtering" away the surface at a predetermined rate and determining concentration progressively.

In order to determine if surface oxide films on niobium can be maintained in the presence of lithium on the surface, release experiments were run by wrapping specimens with lithium ribbon and heating. A P-10-hydrogen gas purge was used to sweep release tritium into the proportional counter. Some oxidation of lithium occurred during heating but the ribbon remained in contact with the niobium surface. Tritium in the lithium was determined by dissolution of the lithium in water followed by liquid scintillation counting of the neutralized solution.

3.1.2.2. Results and Discussion

3.1.2.2.1. Diffusion in Bulk Niobium

An estimate of the tritium diffusion coefficient within niobium at room temperature was obtained by three techniques.

Tritium profiles were measured to a depth of approximately 50 μ in three niobium specimens by electropolishing layers from the injection face soon after tritium injection. Following a high tritium concentration in the first 1-2 μm , the concentration profiles appeared to be nearly flat even though diffusion times were only 1 to 2 hours at 20-40°C. These profiles were found to be in general agreement with the profile predicted by Hickman's equation (Figure 13) but not the expression proposed by Ogurtani (Figure 13). The diffusion solutions for an initial recoil concentration distribution have been presented by DiCola and Matzke⁽¹³⁾ and profiles for specific values of Dt were presented in an earlier publication.⁽³⁵⁾ The measured gradients are quite small and higher diffusion coefficients would produce even flatter profiles so the calculated value of D shown by point a in Figure 13 is regarded as a lower limit.

In the second method, tritium was injected into one face of a 0.010 inch thick foil and sections were removed from the back face for tritium measurement. This variation of the preceding method was carried out since Westlake⁽³⁷⁾ observed that electropolishing could force hydrogen into vanadium specimens and produce anomalously flat profiles. Polishing from the back face would prevent anomalously high D's by this process. The annealing time was 1.5 hours at room temperature and the observed tritium profile was essentially flat. It was possible to estimate the lower limit of the diffusion coefficient required to produce an essentially uniform distribution at the back face and this value is shown as point b in Figure 13.

In the third method, the rate of 'lateral' diffusion of tritium within a specimen was measured. Approximately one-half of the injection face of a niobium foil was coated with Li_2CO_3 and irradiated. Levels of tritium were determined subsequently in surface layers on both the front and back faces of the uninjected half of the sample as a function of aging time. From these values it was possible to obtain an estimate of the rate of 'lateral' redistribution of tritium as a

function of time. Using a solution presented by Crank⁽³⁸⁾ (eq. 217) a lower limit diffusion coefficient value was calculated from these measurements and is shown as point c in Figure 13. Since all three methods yielded diffusion coefficients reasonably consistent with Hickman's values, it appears that the tritium is diffusing rapidly within the specimens and the flat profiles obtained by the first method are not an anomaly produced by the polishing method.

3.1.2.2.2. Tritium Release Results

Tritium release rates from niobium were significantly lower than the rates predicted from the bulk diffusion coefficients reported by Hickman.⁽³³⁾ Below 600°C the disparity was extremely pronounced. The total tritium released over a four-to-five-day period was less than 10% at temperatures up to 500°C whereas bulk diffusion coefficients would imply essentially complete release after one second at room temperature.

Figure 14 shows a set of experimental release fraction vs $t^{\frac{1}{2}}$ curves along with a curve which shows the predicted release fractions at 25°C from the reported 'bulk' diffusion coefficient value.⁽³³⁾ A linear dependence with $t^{\frac{1}{2}}$ was observed over the very low release fractions measured. The data for 400°C and 500°C were obtained from samples which were preoxidized at 200°C for 1 hour in air prior to tritium implantation. The data for temperatures 25°C and 200°C were obtained from samples which were not subjected to any additional treatment following annealing.

Figure 15 shows tritium release curves at higher temperatures and release fractions. The $(t)^{\frac{1}{2}}$ dependence observed for low release fractions disappeared and the fraction was linear with time for all the temperatures up to release fractions of 0.4 or 0.5. The data at 900°C show a decrease in release rate with time but the decrease was most apparent above $f = 0.5$ where the depletion of the tritium in the specimen would be expected to show such an effect. A calculated

curve at 300°C derived from bulk diffusion coefficients is included in Figure 15 to illustrate the disparity between observed and predicted release fractions.

If the tritium release rate decreased in proportion to the average concentration of tritium remaining in the specimen, the fractional release curve would be of the form:

$$f(t) = 1 - e^{-kt} \quad (26)$$

where

k = a constant

A plot of $\ln(1 - f)$ versus t would then give a straight line for all release fractions. Figure 16 shows the higher temperature data plotted in this fashion. Up to release fractions of approximately 0.9, linear behavior was obtained. No data above release fractions of 0.9 were included as there was some uncertainty associated with the determination of total tritium in the specimens which accentuated the error in $(1 - f)$ at high fractions.

Figures 14, 15, and 16 illustrate a release pattern in which the tritium release fraction is proportional to $t^{\frac{1}{2}}$ for very low fractions and then stabilizes at an essentially constant release rate which decreases in proportion to the total tritium remaining in the specimen. This pattern is not consistent with a single-region bulk diffusion solution but can be explained by surface controlled release as might result from the presence of a surface oxide film. The following section describes one model which can be used to represent the experimental results.

3.1.2.2.3. Tritium Release Model

All of the experimental results can be qualitatively explained on the basis of classical diffusion in niobium cylinders with a 1-2 μm thick surface region that controls the tritium release rate. This model is depicted schematically in

Figure 17. Tritium concentrations in the two regions are described by the equations

$$\text{Region I: } D_1 \nabla^2 C_1(r, t) = \frac{\partial C_1}{\partial t} \quad , \quad a < r < b \quad (27a)$$

$$\text{Region II: } D_2 \nabla^2 C_2(r, t) = \frac{\partial C_2}{\partial t} \quad , \quad 0 < r < a \quad (27b)$$

with the boundary and initial conditions,

$$C_1(b, t) = 0 \quad , \quad t > 0 \quad (28)$$

$$\left. \frac{\partial C_2}{\partial r} \right]_{r=0} = 0 \quad , \quad t > 0 \quad (29)$$

$$C_1(a, t) = C_2(a, t) \quad (30)$$

$$D_1 \left. \frac{\partial C_1}{\partial r} \right]_{r=a} = D_2 \left. \frac{\partial C_2}{\partial r} \right]_{r=a} \quad (31)$$

$$C_1(r, 0) = C_0 \left[1 - \frac{b-r}{b-R} \right] \quad , \quad a \leq r \leq b \quad (32)$$

$$C_2(r, 0) = C_0 \left[1 - \frac{b-r}{b-R} \right] \quad , \quad R \leq r \leq a \quad (33)$$

$$C_2(r, 0) = 0 \quad , \quad 0 \leq r \leq R \quad (34)$$

where D_1 = the diffusion coefficient in the surface region and D_2 = the bulk diffusion coefficient.

The initial conditions assume that the recoiled tritium is distributed linearly with a surface concentration C_0 at $r = b$ and zero concentration at $r = R$. The quantity $(b - R)$ is the recoil range of tritium in niobium. This initial distribution is shown to be appropriate for recoil-implanted diffusant atoms by DiCola and Matzke. (13)

The above set of equations can be solved by eigenfunction expansion method as outlined by Ozisik⁽³⁹⁾ but numerical computation using this solution is generally inefficient. Furthermore, a two-region slab approximation for the cylinder would be sufficiently accurate since the radius of the niobium samples is about 0.25". In this case the thickness of the slab will be equal to the radius 'b' of the cylinder and all of the equations (26)-(34) with independent variable 'r' changed to x would apply. Such a set of equations was solved numerically using standard finite-difference approximations. A second-order correct finite-difference analog was used to compute the concentration profile as a function of reduced time variable $\tau = D_1 t / (b - a)^2$ for the following values of the reduced parameters: $D_2/D_1 = 10^4$, $(b - R)/(b - a) = 21$, and $b/(b - a) = 6.35 \times 10^3$. Figure 18 shows the concentration profile for five different values of τ . After a sufficiently long time, the concentration profile in the bulk region becomes essentially uniform and the profile in the surface layer is nearly linear. The release rate for this case must be approximately constant with time until the bulk concentration becomes depleted and the gradient across the surface layer gets smaller.

From the finite-difference program, it was possible to calculate the fractional release as a function of reduced time τ , using Fick's first law. Figure 19 shows the results for $10^{-2} < \tau < 2 \times 10^3$. The surface film initially contained about 10% of the total tritium. The 5-6% release obtained up to $\tau = 2$ is primarily release of this tritium present initially in the surface layer. For $\tau > 10^3$, the release rate appears to be essentially constant implying that a quasi-steady state has been reached. For surface layers that are thinner than the 1 μm assumed in this calculation, the steady-release rate would be reached at smaller values of τ than 10^3 . After this quasi-steady state has been reached, the release rate is controlled by the gradient of the concentration in the surface region which is $-C_2/(b - a)$, i.e.,

$$-D_1 \left. \frac{\partial C_1}{\partial x} \right]_{x=b} = D_1 \left(\frac{C_2}{b-a} \right) = hC_2 \quad (35)$$

where h is the mass transfer coefficient at the surface of the bulk region and $h = D_1/(b - a)$.

The above formulation implies that at long times the release fractions may be computed from a one-region model with a mass transfer boundary condition. Using the same notations as in the case of the two-region slab model, the equivalent one-region slab model is represented by

$$D_2 \frac{\partial^2 C_2(x, t)}{\partial x^2} = \frac{\partial C_2}{\partial t}, \quad 0 < x < a \quad (36)$$

$$\left. \frac{\partial C_2}{\partial x} \right]_{x=a} = 0, \quad t > 0 \quad (37)$$

$$D_2 \frac{\partial C_2}{\partial x} - hC_2 = 0, \quad x = 0 \quad t > 0 \quad (38)$$

$$C_2(x, 0) = C_0 \left(1 - \frac{x}{R} \right), \quad 0 \leq x \leq R \quad (39)$$

$$C_2(x, 0) = 0, \quad R \leq x \leq a \quad (40)$$

The solution to this problem is easily obtained by the integral transform technique discussed by Ozisik⁽³⁹⁾ and the fractional release as a function of time is given by

$$f(t) = 1 - \frac{2}{R} \sum_m A_m \sin \beta_m a e^{-D_2 \beta_m^2 t} \quad (41)$$

where β_m are calculated from

$$\beta_m \tan \beta_m a = \frac{h}{D_2} \quad (42)$$

$$A_m = \frac{2S}{\beta_m} \left[\sin \beta_m a + (1/\beta_m R) \{ \cos(\beta_m a) - \cos[\beta_m (a - R)] \} \right] \quad (43)$$

and

$$S = (\beta_m^2 + h^2/D_2^2) / [a(\beta_m^2 + h^2/D_2^2) + (h/D_2)] \quad (44)$$

The dotted line in Figure 19 represents the results of this model for the range $10^1 < \tau < 10^4$. The initial amount released from the surface film (approximately 5.5% as shown by the two-region model) has been added to the values obtained from the above one-region model, since the latter does not take that into account. The two-region model results and the one-region model results appear to converge for τ of the order of 5×10^3 . Unfortunately, the finite-difference computations could not be extended beyond $\tau = 2 \times 10^3$ because of computational restrictions. Figure 19 also shows the fit of results predicted by the model of DiCola and Matzke⁽¹³⁾ according to which the initial fractional release is given by

$$f(t) = \frac{4}{R} \sqrt{\frac{Dt}{\pi}} \quad (45)$$

It is clear that the initial release from the oxide film in the two-region model essentially coincides with the release calculated by the above equation (45).

A further simplification can be made for computing release rates at long times by ignoring the diffusional resistance within the bulk. Since the surface film resistance is several orders of magnitude higher than the bulk diffusional resistance, this seems justifiable. In that case the release rate would decrease in proportion to the average concentration of tritium remaining in the specimen, i.e.,

$$v \frac{dC_2}{dt} = -h \cdot A \cdot C_2 \quad (46)$$

where v and A are the sample volume and surface area respectively. This equation can be rewritten as

$$\frac{df}{dt} = \frac{hA}{v} (1 - f) \quad (47)$$

where f is the fraction released. The solution to this problem has been given earlier by equation (25). In this case

$$k = \frac{hA}{v} \quad (48)$$

The results using this formula [equation (26)] are shown as circled points on Figure 19. The long time release is well represented by this simple expression. Furthermore, as pointed out earlier, $\ln(1 - f)$ is a linear function of time which agrees with the experimental observations in the temperature range 600°C - 900°C (Figure 16). For $kt \ll 1$, $f(t) \approx kt$ which shows that at relatively short times, the fractional release is proportional to time (Figure 15).

Log h values are plotted versus $\frac{1}{T}$ for each individual sample in Figure 20. The lines connect results for identical samples. For all the samples a distinct break is observed in the plots at about 600°C . Below this point, the activation energy characterizing a least-squares fit to the data was 5.3 kcal/gm mole . The activation energy values for the least-squares fit obtained above 600°C was $23.2 \text{ kcal/gm mole}$.

The least-squares, best-fit values of h from Figure 20 are given by:

$$h(\text{cm sec}^{-1}) = 6.39 \times 10^{-6} + \frac{8.69 \times 10^{-6}}{3.69 \times 10^{-6}} \exp[-(5260 \pm 1170 \text{ Cal})/RT] \quad ,$$

$$200^{\circ}\text{C} \leq T < 600^{\circ}\text{C} \quad (49)$$

$$h(\text{cm sec}^{-1}) = 0.277 + \frac{0.442}{0.150} \exp[-(23180 \pm 2150 \text{ Cal})/RT] \quad ,$$

$$600^{\circ}\text{C} < T \leq 900^{\circ}\text{C} \quad (50)$$

The sample to sample variation in the h values in Figure 20 are considerable. Since $h = D_1/(b - a)$ where $b - a$ is the thickness of the surface film, the most plausible explanation seems to be a change in surface film thickness values. For two of the samples an unexpected decrease in the release rate was observed when

heated from 300°C to 400°C (Figure 20). Accidental oxidation of the surface (thus a change in b - a) is believed to be responsible.

3.1.2.2.4. Temperature Cycling

Specimens were heated through various temperature cycles and the tritium release rates measured at each temperature. These experiments showed that tritium release rates at a given temperature could be influenced by the specimen-temperature history, presumably as a result of changes in the surface films during heating.

Tritium release rates at temperatures above 600°C were unaffected by cycling specimens to lower or higher temperatures. This fact is illustrated in Figure 21A where the 600°C and 700°C release curves for a sample heated through the sequence 400°C, 600°C, 700°C (marked I); 400°C, 600°C, 700°C (marked II) are plotted. The tritium release properties of the surface film were apparently unchanged for the two 600°C, and the two 700°C heatings. It was similarly observed that a sample could be cycled through any temperature sequence between 100°C and 500°C without changing the release rate at any given temperature. Figure 21B shows the results from a typical experiment with a heating sequence 300°C, 400°C, 500°C (marked I); 400°C, 300°C (marked II). However, the reproducibility of low temperature (< 500°C) release rates disappeared if the temperature exceeded 600°C during a cycle. For example, in Figure 21A the release rate at 400°C during the second heating (marked as II) was virtually zero. The total fraction of tritium released was far below the total contained in the specimen so the result reflects changes in the properties of the surface film rather than tritium depletion.

Thermally stressing a specimen produced changes in the surface film. A specimen giving low tritium release rates at 400°C following heating to temperatures > 600°C, would again begin releasing tritium when the sample was suddenly cooled

to room temperature or lower and heated back to 400°C. Curve II in Figure 21C shows the new release rate at 400°C after sudden cooling to room temperature for a sample initially giving no release at 400°C (marked I).

When a sample containing tritium was electropolished to remove 4-5 μm of metal from the surface, release rates at all temperatures reached values higher than those obtained for a freshly implanted annealed sample. The behavior described above during temperature cycling could then again be reproduced.

A possible explanation for this behavior is the existence of channels, cracks, or other defects in the surface film which control tritium release at temperatures below 600°C for the annealed and freshly implanted samples. The low activation energy observed for tritium release below 600°C (Figure 20) supports this interpretation. The activation energy in this temperature region is close to the values reported for bulk diffusion of hydrogen in niobium.^(33,59) This would be observed if the tritium release at low temperatures was controlled by bulk diffusion while the effective sample surface area was constrained to some low value by a network of cracks. Strehlow and Savage⁽⁴⁰⁾ have proposed a similar model to explain their hydrogen permeation results for oxidized steel specimens. Exposure to high temperature ($> 600^\circ\text{C}$) presumably results in 'healing' of these cracks and the tritium release is then controlled by diffusion or solubility of the tritium in the oxide film. Oxygen diffusion rates in niobium become significant above 600°C which could promote crack healing. This interpretation is consistent with the cycling results.

3.1.2.2.5. Film Thickness Effects

The tritium released from specimens at room temperature gave initially linear f versus $t^{1/2}$ plots which then dropped to a negligible release rate at very low release fractions. A release fraction linear in $(\text{time})^{1/2}$ is characteristic of a one-region diffusion solution which has the following form for a recoil-injected slab:

$$f(t) = \frac{4}{R} \sqrt{\frac{Dt}{\pi}} \quad \text{for} \quad \frac{Dt}{R^2} \ll 1 \quad (51)$$

where

R = tritium recoil range (cm)

D = diffusion coefficient (cm^2/sec)

t = annealing time (seconds)

From Figure 19, it is apparent that the release drops significantly when 50% of the tritium in the oxide film is released (the remaining 50% diffuses into the metal). The release fraction associated with a rapidly decreasing release rate at low temperatures was assumed to correspond with 50% of the initial tritium in the oxide and the oxide thickness was calculated accordingly.

Film thicknesses calculated by this approach are subject to a number of assumptions and uncertainties, not the least of which is the assumption that a specific film thickness exists. Oxygen profiles taken with an Auger spectrometer show an oxygen gradient in the specimen surface layers but not a discontinuity which could mark a metal-oxide interface (Figure 22). The film thickness calculated above identifies only a surface layer from which tritium release is rapid and which may or may not correspond to a physical oxide barrier on the specimen surface. The thicknesses calculated are believed to represent lower limits since some tritium release occurred during irradiation (believed to be less than 15%) and some small additional amount of tritium could be removed from the surface layers by heating above room temperature.

The film thicknesses calculated from the room temperature release studies were used as 'b-a' to obtain values of D_1 from the plot of $\ln h$ in Figure 20. since $h = \frac{D_1}{b-a}$. These D_1 's are plotted in Figure 23 as $\ln D_{\text{thru}}$ vs $1/T$ and represent effective diffusion coefficients for tritium transport through the surface film as represented by equation (35). It should be noted that the spread in results is considerably diminished from that presented in Figure 20 which suggests

that tritium release rate decreases with increasing oxide thickness over the measured range of film thickness from $\sim 200\text{\AA}^{\circ}$ to 3000\AA° . Values of D_{thru} are given by:

$$D_{\text{thru}}(\text{cm}^2 \text{sec}^{-1}) = 9.02 \times 10^{-11} \frac{+2.51 \times 10^{-11}}{-1.96 \times 10^{-11}} \exp[-(6060 \pm 320 \text{ Cal})/RT] \quad ,$$

$$200^{\circ}\text{C} \leq T < 600^{\circ}\text{C} \quad (52)$$

$$D_{\text{thru}}(\text{cm}^2 \text{sec}^{-1}) = 2.59 \times 10^{-6} \frac{+0.89 \times 10^{-6}}{-0.66 \times 10^{-6}} \exp[-(23630 \pm 600 \text{ Cal})/RT] \quad ,$$

$$600^{\circ}\text{C} < T \leq 900^{\circ}\text{C} \quad (53)$$

The activation energy in equation (52) differs slightly from that in equation (49) because several specimens with thick oxide films were not used in the least-squares calculation of D_{thru} . The D 's identified as D_s in Figure 23 represent diffusion coefficients for release of tritium from the surface film and were calculated from the initial slope of the release curves and equation (51). These values are represented by:

$$D_s(\text{cm}^2 \text{sec}^{-1}) = 1.38 \times 10^{-15} \exp(-1300 \text{ Cal}/RT) \quad (54)$$

It was possible to measure these low values of D_s without significant interference from tritium diffusing through the film because the tritium in the bulk metal was uniformly dispersed prior to the release experiment whereas the surface film tritium remained concentrated near the surface. Tritium release rates from the surface film therefore exceeded the release rates through the film during the initial stages of an experiment even though the diffusion coefficients for transport through the film were much larger than the surface-layer D 's.

The observation of different oxide diffusion coefficients for the tritium initially at rest in the oxide (D_s) and the tritium diffusing through the oxide from the substrate (D_{thru}) is at variance with the model in Section C which

assumes a single diffusion coefficient (D_1) for transport through the surface film. This difference is not unexpected physically since the diffusion rate of tritium within the surface film crystallites could be lower than the diffusion rate between the crystallites. Also the model assumes that the tritium concentration is continuous across the oxide-metal interface which is not necessarily true in the real case. A partition coefficient other than unity would produce different apparent diffusion coefficients for transport through the film and release from the film.

Because of the difficulties in determining an effective oxide film thickness and the actual tritium concentration in the oxide at the interface, the quantity h in equations (49) and (50) and in Figure 20 is a less ambiguous representation of the effect of oxide surface films than the values D expressed in equations (52) and (53).

Thick oxide films tended to spall from the metal surface and were no more effective than thinner films in retarding tritium. The tritium release rates from the oxide were complex and appeared to represent several different release rates. A typical release curve from a highly oxidized specimen is shown in Figure 24 which illustrates the several components to the release curve. The results suggest that it is thin, adherent oxide films of several hundred to several thousand Angstroms thickness which are most effective in retarding tritium release.

Oxide film thicknesses from Auger spectra were estimated by arbitrarily assuming that the film terminated when oxygen concentrations dropped to 20% of the surface concentration (Figure 22). Auger spectroscopy, direct observation and surface-film tritium release showed the same trends for film thickness changes from specimen to specimen but agreement between the absolute values was poor. Table 3.1 presents measured thicknesses for the three methods for different specimen treatments.

The results show that it was possible to modify tritium release rates somewhat by controlling specimen oxidation but it was not possible to obtain

Table 3.1. Sample Film Thicknesses As Determined By Various Methods

Techniques Employed	Sample Pretreatment: As annealed	Sample Pretreatment: As annealed and electropolished	Sample Pretreatment: As annealed, exposed to He at >700°C and cooled to room temper- ature	Sample Pretreatment: Oxidized in air (1 hour at 400°C)
Surface film release method	1730 ± 760 Å ^o	282 ± 52 Å ^o	Not determinable	6,000 Å ^o
Auger Analysis	183 ± 125 Å ^o	32.5 ± 3.5 Å ^o	27.5 ± 3.5 Å ^o	180 Å ^o
Direct Observation	10,000 Å ^o	2500 - 5000 Å ^o		20,000 Å ^o

sufficiently clean surfaces by electropolishing or vacuum annealing to significantly increase tritium release.

3.1.2.2.6. Effects of Reducing Atmospheres

Attempts were made to lower the oxygen potential during tritium release by adding hydrogen to the flow gas or wrapping specimens with lithium metal ribbon. The purpose was to determine if the surface oxide film could be sufficiently altered by the reducing environment to increase tritium release rates from the specimens.

Heating in 22% H₂, 78% P-10 (mixture of 10% methane in Argon) gave tritium release fractions below 500°C which were unchanged from earlier values but release fractions at 700°C and 800°C were increased dramatically and were consistent with the release fractions expected for bulk diffusion controlled release. Experiments between 500°C and 700°C showed a transitional behavior and gave release fractions higher than those observed with a P-10 gas flow but lower than the values predicted from bulk diffusion coefficients. The release rate at 500°C increased steadily with time and reached a maximum value 15 to 16 hours after the initial heating, implying kinetic effects on film removal.

Lithium metal is more reducing than hydrogen and would maintain a lower oxygen potential than hydrogen at equilibrium. Release experiments at 200°C, 400°C, and 500°C in the presence of lithium metal and hydrogen P-10 gas flow gave tritium release fractions which were increased substantially from the values obtained with hydrogen only, showing further destruction of the oxide film.

The experimental release results are presented in Figure 25 as a semilog plot of tritium fractional release rate (R) versus (Temperature)⁻¹.

In the low temperature hydrogen experiments where release was still controlled by the surface film the release rate is proportional to $D_1/(b-a)$ (or more appropriately $\frac{D_{thru}}{(b-a)}$) and tritium concentration, as given in equation (35).

The release rates were observed to drop slowly as bulk concentrations decreased and it is the initial release rates which have been tabulated in the figure. The data band shown in Figure 25 indicates the initial release rates obtained from the data in Figure 20 which were obtained with a P-10 gas flow. It is apparent that release results below 500°C were unchanged by H₂ flow but were significantly increased by the addition of lithium.

The pronounced increase in release rate at higher temperatures was believed to reflect removal of the oxide film. The release rate for a uniform distribution of diffusing gas is strongly time dependent with R dropping as $t^{-\frac{1}{2}}$ for short time periods. The release rate tabulated is therefore an average value for the first 1 to 5 minutes of heating and a similar average was taken for the upper dotted curve which presents the predicted release rates determined from the bulk diffusion coefficients proposed by Hickman⁽³³⁾. The use of an averaged release rate for the high temperature data is not a completely satisfactory method of presentation but is one way of representing the transition from bulk-controlled to film-controlled release on a single plot.

Figure 26 shows that the high temperature tritium release in hydrogen was consistent with published diffusion coefficients and one-region bulk diffusion at all release fractions. All data points consistent with these D's will lie on the heavy black line since the bulk diffusion D's were used in the calculation of the abscissa values (see Crank⁽³⁸⁾). Agreement of the 800°C and 900°C data is excellent, the 700°C results lie somewhat below the line, and the 500°C data begin to show a significant surface film effect.

The stability of the surface oxide film in hydrogen at temperatures below 500°C may be due to trace moisture impurities in the hydrogen. Five different types of oxides can form on the niobium sample:⁽⁴¹⁾ two suboxides — NbO_x and NbO₂, the exact composition for which are not known, and the three oxides — NbO, Nb₂O₄ (or NbO₂) and Nb₂O₅. Thermodynamic data for the suboxides are unavailable

so the following discussion is limited to the three known oxides. The oxide reduction reaction in H_2 may be written:



where K_1 and K_2 are the equilibrium constants.

Assuming the solids have an activity of unity, the product $K_1 K_2$ gives the equilibrium pressure of water vapor divided by the pressure of hydrogen, $P(H_2O)/p(H_2)$. This ratio is plotted in Figure 27 for the three known niobium oxides using values of K_1 and K_2 from Schick.⁽⁴²⁾ The presence of as little as .01 ppm H_2O as an impurity in the hydrogen is seen to be sufficient to stabilize all oxides at temperatures below approximately $450^\circ C$. Alternatively, at $800^\circ C$ all oxides are reduced even if the moisture concentration is allowed to go as high as 1 ppm. In spite of efforts to reduce moisture concentrations by cold-trapping, it seemed unlikely that values below .01 ppm were obtained with the equipment used and the apparent stability of the oxide film below $500^\circ C$ can be explained by the presence of a small amount of moisture in the flow gas. This interpretation is supported by the experiments with lithium which can maintain a much lower equilibrium oxygen potential than hydrogen and which exhibited higher tritium release rates. The tritium release rates in the presence of lithium were lower than the values expected if the oxide had been completely removed. However, post-heating analysis of the lithium metal showed sufficient tritium in the lithium for the specimen release to have occurred at rates characteristic of the metal with no surface oxide. The lithium metal results in Figure 26 should therefore be regarded as lower limits.

In view of the difficulty in maintaining known, low oxygen potentials in flow systems, no further experiments were carried out on film stability. From

the earlier results, it seems reasonable to infer that no oxide film effects on tritium release from niobium will be observed if the oxygen potential can be maintained at a value below the equilibrium potential for the known oxides.

An apparent effect of oxide films and oxygen potentials is evident in the literature on hydrogen permeation of niobium. Results have been reported by Steigerwald,⁽⁴³⁾ Stickney,⁽⁴⁴⁾ and by Rudd, Vose, and Johnson.⁽⁴⁵⁾ The permeability coefficient data reported for the temperature ranges between $\sim 400^{\circ}\text{C}$ - 750°C show a strong temperature dependence with an apparent activation energy of ~ 51 kcal/gm mole. However, above 700°C - 750°C , the activation energy characterizing the permeability data,^(43,45) falls to ~ 3 kcal/gm mole. Figure 28 shows the permeability data reported by Steigerwald⁽⁴³⁾ and Rudd, Vose, and Johnson⁽⁴⁵⁾ along with the data in the present study from Figure 25. The change observed with temperature is similar for the two sets of data. The permeability data, therefore, appears to reflect an oxide film effect within the temperature range $\sim 500^{\circ}\text{C}$ - 750°C . Any experiment carried out with commercially pure hydrogen (~ 1 ppm H_2O) would not remove the surface oxides in this temperature range and would be suspect.

3.1.2.3. Conclusions

1. The several diffusion coefficients estimated for tritium in bulk niobium by sectioning experiments are consistent with the Arrhenius relationship proposed by Hickman.

2. Tritium release from niobium specimens in nonreducing atmospheres is controlled by the surface oxide film. A two-region diffusion model which assumes lower diffusion coefficients in the surface layers than in bulk can fit the experimental results.

3. Tritium release rates from the niobium specimens which had been electro-polished, stored in a room atmosphere, and injected with tritium are given by:

$$R = \frac{df}{dt} = \frac{hA}{v} (1 - f) \quad (57)$$

where

$$h(\text{cm sec}^{-1}) = 6.39 \times 10^{-6} \frac{+8.69 \times 10^{-6}}{-3.69 \times 10^{-6}} \exp[-(5260 \pm 1170 \text{ Cal})/RT] ,$$

$$200^{\circ}\text{C} \leq T < 600^{\circ}\text{C} \quad (58)$$

$$h(\text{cm sec}^{-1}) = 0.277 \frac{+0.442}{-0.150} \exp[-(23180 \pm 2150 \text{ Cal})/RT] ,$$

$$600^{\circ}\text{C} < T \leq 900^{\circ}\text{C} \quad (59)$$

The uncertainty in the above expressions includes the variation which was observed for specimens with different oxide film thicknesses.

4. Tritium release above 600°C is characterized by a different activation energy than release at lower temperatures. Tritium release appears to occur through cracks or defects in the oxide film below 600°C with transport through an intact film at higher temperatures. Subjecting specimens to stress increased tritium release rates below 600°C , presumably through the introduction of film defects.

5. Tritium release fractions at short heating times were proportional to $t^{1/2}$ and are attributed to tritium release from the surface films. Release fractions at longer times were due to tritium transport through the surface films and were proportional to t , the release rate eventually dropping in proportion to the bulk tritium concentration within the specimen.

6. Increasing the oxide film thickness decreased tritium release rates over a limited thickness range (200°A to 3000°A), the maximum reduction being a factor of ten. The D 's for tritium diffusion through the oxide film are given by:

$$D_{\text{thru}}(\text{cm}^2 \text{sec}^{-1}) = 9.02 \times 10^{-11} \exp[-6060 \text{ Cal}/RT] ,$$

$$200^{\circ}\text{C} \leq T < 600^{\circ}\text{C} \quad (60)$$

$$D_{\text{thru}} (\text{cm}^2 \text{sec}^{-1}) = 2.59 \times 10^{-6} \exp[-23630 \text{ Cal/RT}] ,$$

$$600^\circ\text{C} < T \leq 900^\circ\text{C} \quad (61)$$

when film thickness is calculated from the initial tritium release fraction.

The diffusion coefficient for tritium initially at rest in the surface oxide is given by:

$$D_s = 1.38 \times 10^{-15} \exp(-1300 \text{ Cal/RT}) , \quad 200^\circ\text{C} \leq T \leq 500^\circ\text{C} \quad (62)$$

7. The oxide films could be removed with a reducing hydrogen atmosphere to give tritium release consistent with bulk diffusion coefficients at temperature above 700°C . Problems in obtaining a sufficiently low oxygen potential resulted in persistence of oxide surface film effects below this temperature.

8. Apparent anomalies in permeation results cited in the literature appear to be explainable in terms of oxide surface film effects and the results exhibit the same general trends as the present study.

3.2. Tritium in Fusion Reactor Blankets

Two potential problems with fusion reactors concern the possible diffusion release of tritium to the environment and the possible buildup of undesirably large tritium inventories within structural components. Many metals have a relatively high hydrogen permeability so diffusion release must be considered for the reactor blanket, recovery, and injection systems. Acceptable tritium release rates to the environment have been estimated as about 3 Ci/d,⁽⁴⁶⁾ and a typical plant inventory may be 10^7 - 10^8 Ci so the allowable fractional release rate is quite low. Also, since the tritium worth is high, it will be highly desirable to maintain the inventory of dissolved tritium in the system as low as possible.

Calculations of tritium permeation rates or inventories are speculative at best since there are many uncertainties in the tritium transport process and the

system designs are in an early stage. Nevertheless, it is useful to evaluate tritium release rates from reference systems as a guide to establishing the critical system parameters and approximate values for tritium distributions.

The present section gives results for calculated equilibrium tritium permeation rates and inventories for the reactor blanket of the Los Alamos Theta-Pinch fusion reactor. (47,48) This reactor was selected simply as a reference system for the calculations. Steady-state conditions were assumed so the values presented represent upper limits. The purpose of the study was to assess the steady-state transport rate of tritium to different regions of the blanket and to determine the effect of different system parameters in influencing the tritium concentration distribution or release rates.

3.2.1. The Model

3.2.1.1. Equilibrium Diffusion

The reactor blanket was assumed to be approximated by a series of concentric cylinders with uniform materials and thermal properties. The temperature within each region was assumed constant to allow a constant value for the tritium diffusion coefficient. Temperature gradients within the blanket were accommodated by step temperature changes at the interface between regions.

The time independent, Fick's Law diffusion equation for multiple regions assuming linear tritium trapping rate is given by:

$$D_i \nabla^2 C_i(r) - \alpha_i C_i(r) + S_i = 0 \quad (63)$$

D_i = tritium diffusion coefficient in the i^{th} region

$C_i(r)$ = position dependent tritium concentration in the i^{th} region

α_i = trapping coefficient for the i^{th} region (assumed constant for a given region)

S_i = tritium source term for the i^{th} region (assumed constant over that region)

Solutions to this equation have been programmed for a reactor blanket involving n regions, subject to the limitations described.

The trapping coefficients are intended to represent hydrogen precipitation at defects within a region or chemical combination. There is no present sound basis for assigning values to these coefficients so they were included only to provide maximum flexibility to the model and to allow assessment of the effect of arbitrary values of α on the results.

Tritium source terms occur for the beryllium layer, the natural lithium coolant, and the enriched lithium breeding layers. Tritium diffusing from the plasma was accommodated by specifying a given tritium concentration at the plasma-first wall interface. Values of S_i were either obtained directly from Los Alamos design reports on the theta-pinch concept^(47,48) or else were calculated from the average neutron fluxes reported.⁽⁴⁷⁻⁴⁹⁾ A tritium source was assumed to be uniformly distributed in any given region. The tritium partial pressure above the coolant in a given region was also assumed to be uniform over the entire region surface.

Tritium diffusion coefficients were determined from literature values of hydrogen diffusion coefficients or by extrapolation of results for similar systems when data were unavailable.^(33,35,50-52) The solubilities and diffusion coefficients employed for the principal materials in the blanket are tabulated in Table 3.2.

The sequence of materials in the blanket and their approximate dimensions were taken directly from Los Alamos design reports for the Reference Theta Pinch Reactor.⁽⁴⁷⁾ A representation of the blanket layers shows as many as 34 separate regions in moving from the plasma to the outer shield (Figure 29). It quickly became apparent that most of these layers did not influence the tritium distributions and that six or seven critical layers were controlling. Most calculations were performed using just the critical regions after first verifying for representative cases that the results were identical to those obtained using all regions.

Table 3.2. Diffusion and Solubility Data¹

Material	D_o^2 (cm ² /sec)	ϕ_D (Kcal/mole)	S_o (Stdcc/ mole/atm)	ϕ_s (Kcal/mole)
Al ₂ O ₃ (upper value)	1.82×10^{-2}	21.0	1.32×10^4	-35.1
Al ₂ O ₃ (most probable value)	0.183	34.8	1.32×10^4	-35.1
Al ₂ O ₃ (lower value)	1.08×10^2	63.3	1.32×10^4	-35.1
Niobium	5.77×10^{-4}	3.0	0.956	8.44
Beryllium	2.95×10^{-7}	4.42	1.40×10^{-2}	4.33×10^{-4}
Copper	1.32×10^{-2}	11.3	5.20×10^{-2}	8.70

¹The expressions for the diffusion coefficient, D, and solubility, S are $D = D_o \exp(-\phi_D/RT)$, $S = S_o \exp(\phi_s/RT)$ where R = the universal gas constant.

²Graham's Law is used to convert data given for hydrogen for application to tritium.

Two temperature distributions were considered. One assumed a "conventional" low temperature Li-Na-steam system while the second was based upon a high-temperature advanced system with a potassium topping cycle. The radii for the critical regions and the assumed region temperatures for the two concepts are listed in Table 3.3.

Tritium diffusion through the graphite moderator is highly uncertain, but considering its porosity, instantaneous tritium redistribution in this region was assumed. The calculated uniform tritium distribution within the graphite was included in the inventory calculations.

Several boundary conditions at the region interfaces are possible. The expected condition is that the surface tritium concentrations would be in equilibrium with the vapor phase and the tritium concentration distribution across the interface would simply equal the inverse ratio of the Sievert's Law constants. In this case, at an interface at $r = a$ between the i and the $(i + 1)$ regions,

$$C_i(a) = k_i P_i^{1/2}(a) \quad (64)$$

If $P_i(a) = P_{i+1}(a)$ then

$$\frac{C_i(a)}{C_{i+1}(a)} = \frac{k_{i+1}}{k_i} = \beta_i \quad (65)$$

Values of β_i for the materials and temperatures used were calculated from the pressure-solubility equations in Table 3.2. The special case of uniform concentration across an interface ($\beta = 1$) might be a better approximation for some boundaries and was the usual assumption employed when partition data were unavailable. A third, but little used boundary condition, assumed that the concentration difference across an interface was proportional to the flux. That is,

$$C_{(i+1)} - C_i = h_i \theta_i \quad (66)$$

Table 3.3. Temperature Estimates for the Reference Theta-Pinch Reactor Core

Region Title	Layer No. (Material)	Outer Radius (cm)	Temperature °K	
			HTP ¹ Case	LTP ² Case
First Wall	1 (Al ₂ O ₃)	50.0 (0.03 cm thick)	1390	800
	2 (Nb)	50.1	1360	770
Beryllium	1 (Nb)	53.2	1320	730
	2 (Be)	55.7	1500	900
	3 (Nb)	55.8	1350	760
Ca ³	1 (Nb)	67.7 (0.1 cm thick)	1320	760
	2 (Al ₂ O ₃)	62.73	1420	830
Cooling	3 (Nb)	67.83	1500	920
	4 (C)	82.57	1500	920
	5 (Nb)	82.67	1500	920
	6 (Al ₂ O ₃)	82.7	1520	940
	7 (Nb)	82.8	1450	870
Stagnant Lithium	1 (Nb)	0.6 (0.1 cm thick)	1400	780
Magnet Cooling	1 (Nb)	88.95 (0.05 cm thick)	1340	760
	2 (Al ₂ O ₃)	89.5	800 ⁴	520 ⁴

¹HTP = High Temperature Plant

²LTP = Low Temperature Plant

³Temperature in the inner graphite region are considered the same

⁴These represent an estimate based upon the assumption that the implosion coil temperatures will be the same as for the compression coil.

Such a boundary condition might apply when an oxide film was present on one surface and transport was controlled by permeation through the film. Fick's first law of diffusion for a slab is

$$\phi = -D \frac{\partial c}{\partial x} \quad (67)$$

where ϕ is the flux of diffusing atoms at the plane where $\frac{\partial c}{\partial x}$ is measured. The difference in tritium concentration between either side of a surface film of thickness ΔX would be given by

$$C_{(i+1)} - C_i = \left(\frac{\Delta X}{D}\right)_i \phi_i \quad (68)$$

which is identical to the boundary condition in equation (66) when $h_i = \left(\frac{\Delta X}{D}\right)_i$. The parameter "h" in equation (66) may therefore be viewed as analagous to a film thickness divided by a diffusion coefficient for tritium in the surface film.

The remaining boundary condition which was always used with the above three options specified continuity of flux at each interface:

$$D_i \frac{\partial C_i}{\partial r} \Big|_{r_i} = D_{i+1} \frac{\partial C_{i+1}}{\partial r} \Big|_{r_i} \quad (69)$$

Analytical solutions to equation (63) for the three types of interface conditions were programmed to provide values of tritium flux at each interface and tritium inventory in each region for selected values of D_i , α_i , S_i , β_i (or h_i) for N concentric regions ($n < 10$). These calculations were performed separately for each composite region separated by sinks.

Figure 30 represents a partial cross section of the RTPR (Reference Theta Pinch Reactor) core as simplified for the mathematical analysis.

3.2.1.2. Equilibration Times

The equilibrium diffusion solution may grossly overestimate the actual tritium release rate if the time to attain equilibrium greatly exceeds the

projected life of the reactor. Equilibrium conditions have been used because time dependent solutions for multi-region diffusion problems become excessively complex. However, it is desirable to have some measure of the time required to attain approximate diffusion equilibrium as a guide to the amount of conservatism inherent in the steady-state solutions.

A gas diffusing through a slab will approach a constant release rate with time if the concentration of gas at the entering face is maintained constant. A plot of total released gas versus time will linearly extrapolate to a positive time value identified as a "breakthrough" or "lag" time which marks a time at which the diffusing gas begins to be released at the exit face in significant quantities. Ash, et al.⁽⁵³⁾ have derived general expressions for the diffusion lag time in multiple layers for slab, cylindrical, and spherical geometries. These expressions involve computational problems for large numbers of regions but they are satisfactorily approximated by the one-region solution if there exists one region for which $X^2/D[(\text{thickness})^2(\text{diffusion coefficient})]$ significantly exceeds the comparable value for any other region. The one-region lag time for a cylinder is given by:

$$t_{\ell} = [R_1^2 + R_0^2] \ln \frac{R_1}{R_0} - (R_1^2 - R_0^2) / 4D \ln \frac{R_1}{R_0} \quad (70)$$

where R_1 and R_0 are respectively the outside and inside cylinder radii for the region and D is the tritium diffusion coefficient in the region. Values of t_{ℓ} were calculated for each region in the system as a rough guide to the time required for tritium to reach each sink in the system.

3.2.2. Results

A series of standard conditions were adopted as reference when the effect of any given parameter was being investigated. These standard conditions assumed $\beta_1 = 1$ for all regions and the values for the most probable diffusion coefficients for Al_2O_3 in Table 3.2. The tritium partial pressure on the plasma side of the first wall was assumed to be 10^{-2} torr based upon the design condition of 45 mtorr

neutral gas pressure (50% D, 50% T) for 2/3 of the cycle and 10 mtorr for the remaining 1/3 of the cycle.⁽⁴⁷⁾

The tritium production rates in the stagnant lithium and in the beryllium blanket were taken as 1.67×10^{-11} moles $\text{cm}^{-3} \text{sec}^{-1}$ and 8.89×10^{-13} moles $\text{cm}^{-3} \text{sec}^{-1}$ respectively. These numbers were based upon a proposed tritium consumption rate of 484 moles of tritium per day (12,000 Mw thermal power) and the breeding ratios and region volumes outlined by Dudziak.⁽⁴⁾ The tritium vapor pressure in the flowing lithium coolant was taken as 10^{-10} atmospheres based upon calculations by Maroni⁽⁵⁴⁾ related to tritium extraction. When tritium production rates were the defined primary quantities, concentrations were obtained by equating total tritium production in a region to the tritium fluence from the region. When vapor pressures were specified, Sievert's Law relationships were used to calculate surface tritium concentrations. Both the high temperature and low temperature options in Table 3.3 were considered as standard and calculation were generally conducted for each option.

A typical plot of the equilibrium tritium concentrations for high and low temperature cycles is presented in Figure 31.

3.2.2.1. Insulator Effects

The alumina insulator exerted a significant effect on tritium transport because of the low postulated diffusion coefficient for tritium in Al_2O_3 . Figure 32 presents the tritium flux in Curies/yr from the plasma to the first wall, into the inner coolant channel from the static lithium, and into the magnet coolant channels for the assumed high, low and "most probable" expression for the alumina diffusion coefficients. The calculated flux varies by several orders of magnitude over the range of possible D's. Tritium release to the magnet cooling channel could constitute a possible path for the release of tritium to the environment. It is noteworthy that the tritium flux to the magnet coolant channels can be significant (2×10^5 Ci/yr for the worst case tabulated in Figure 32).

Fowler, et al.⁽⁵⁵⁾ have reported preliminary results for tritium diffusion coefficients in Al_2O_3 as well as other ceramic materials of potential interest to the fusion program — Y_2O_3 , BeO , SiC , and pyrolytic carbon. Tritium was injected into specimens and the diffusion coefficients measured from the time rate of tritium release during heating. The diffusion coefficients for both single crystal and sintered Al_2O_3 specimens were closer to the values represented by $D_{(\text{low})}$ rather than $D_{(\text{most probable})}$ in Table 3.2. Below 700°C , the measured D 's were even lower than the assumed expression for $D_{(\text{low})}$ so the insulator would be expected to exert a major influence on tritium permeation. Diffusion coefficients for other ceramic materials have also been observed to be quite low so the insulator may control tritium transport, irregardless of the particular material selected.

It is also of interest that the tritium leakage rate out of the plasma becomes at least a visible fraction of the total fueling rate for some conditions. For the high temperature plant and high diffusion coefficients for alumina, the leakage becomes 4×10^7 Ci/yr or about .1% of the fueling rate.

Use of the β_i boundary condition derived from Sievert's Law coefficients produces little change in tritium flux from the plasma for the high temperature plant but results in considerably lowered values for the tritium release to the magnet cooling channels and the tritium flux from the plasma for the low temperature plant (items 1 and 7 in Table 3.4).

3.2.2.2. Effect of Oxide Films

Chandra, et al.⁽⁵⁸⁾ have reported that tritium release from niobium under inert atmospheres is controlled by oxide films on the specimen surfaces which significantly lower tritium release rates. The values of (D/X) [equations (49) and (50)] determined from these studies were used as values of "h" for the film controlled boundary condition in the present study to simulate the effect of oxide films on the niobium components. The films produced some change in permeation rates (items 11 and 12 in Table 3.4) principally an increased tritium release to

the flowing lithium and the magnet coolant as a consequence of slightly increased equilibrium tritium pressures in the static lithium.

Selectively allowing the oxide film to occur on only certain niobium surfaces produced pronounced changes in tritium flow patterns and inventories. For example, making the unlikely assumption that the oxide film occurred only on the niobium faces adjacent to the stagnant lithium resulted in increases of several orders of magnitude in the tritium permeation rate to the flowing coolant and magnet cooling channels (items 13 and 14 in Table 3.4) plus an increase of about a factor of 10 in the total tritium inventory. The niobium surface films have not been observed to persist in the presence of lithium⁽⁵⁶⁾ which is consistent with thermodynamic considerations. It is not apparent that oxygen potentials will be sufficiently high anywhere in the blanket region to sustain oxide films. Nevertheless, the results show that oxide films could play a significant role in controlling tritium flow and inventories if conditions favored their formation. Oxide films or other non-metallic barriers may even be used to advantage to restrict tritium permeation to certain portions of the system.

3.2.2.3. Tritium Inventories

The total tritium inventory in the blanket ranged from slightly over 600 grams to as much as 7300 grams for the different conditions investigated. The inventory calculation was confined to the fixed structural components and excluded tritium in the static or flowing lithium. Over 90% of the tritium in each case resided in the beryllium layer. While differences could be obtained for the tritium in the Al_2O_3 or Nb layers, these differences were not significant when compared with the total tritium in the blanket. Table 3.4 presents typical tritium inventories for some of the conditions evaluated. An inventory of 7 kg represents a rather substantial investment in unused fuel. The inventory could likely be lowered by fabricating the beryllium layer in a manner to allow more rapid release and recovery of the transmutation produced tritium.

Table 3.4. Calculated Tritium Permeation Rates and Lag Times

Run No.	Conditions	Remarks	First Wall To Plasma		Beryllium To Coolant		Stagnant Li To Inner Coolant Channel		To Magnet Cooling Channel	
			ϕ (Ci/yr)	t_1 (yr)	ϕ (Ci/yr)	t_1 (yr)	ϕ (Ci/yr)	t_1 (yr)	ϕ (Ci/yr)	t_1 (yr)
1	LTP ⁽¹⁾ D(O) $\beta=1$		-159	.076	2.5×10^7	.63	3.9×10^4	.019	6.5×10^3	3.2×10^6
2	HTP D(O) $\beta=1$		2.7×10^6	7.5×10^6	2.5×10^7	.25	4.9×10^7	1.1×10^5	300	28
3	LTP D(+) $\beta=1$		-9.1×10^4	1.3×10^4	2.5×10^7	.63	7.4×10^6	1.0×10^4	390	54
4	HTP D(+) $\beta=1$		4.2×10^7	5.1×10^7	2.5×10^7	1.1×10^5	3.5×10^8	3.2×10^6	1.6×10^5	.048
5	LTP ⁽¹⁾ D(-) $\beta=1$		-1.6×10^3	760	2.5×10^7	.63	3.9	197	~ 0	$>10^6$ yrs
6	HTP D(-) $\beta=1$		5.4×10^4	3.8×10^4	2.5×10^7	.25	2.2×10^6	2.6×10^4	2.5×10^3	$>10^6$ yrs
7	LTP D(O) β_i		2.5×10^2	.076	2.5×10^7	.63	2.6×10^2	.019	~ 0	$>10^6$ yrs
8	HTP D(O) β_i		2.9×10^6	7.6×10^6	2.5×10^7	.25	3.5×10^5	1.1×10^5	3.5×10^5	28

Table 3.4. Continued

Run No.	Conditions	Remarks	First Wall To Plasma		Beryllium To Coolant		Stagnant Li To Inner Coolant Channel		To Magnet Cooling Channel	
			ϕ (Ci/yr)	t_1 (yr)	ϕ (Ci/yr)	t_1 (yr)	ϕ (Ci/yr)	t_1 (yr)	ϕ (Ci/yr)	t_1 (yr)
9	LTP ⁽¹⁾ D(+) β_i		15	5.4×10^{-4}	2.5×10^7	.63	5.0	1.0×10^{-4}	~0	54
10	HTP D(+) β_i		3.4×10^7	5.0×10^{-7}	2.5×10^7	1.1×10^{-9}	3.5×10^6	3.2×10^{-6}	2.6×10^{-3}	.048
11	HTP D(O) $\beta=1$	Oxide Film On Nb	2.7×10^6	7.6×10^{-6}	2.5×10^7	.25	6.1×10^7	1.1×10^{-9}	374	28
12	HTP D(+) $\beta=1$	Oxide Film On Nb	3.1×10^7	5.1×10^{-7}	2.5×10^7	1.1×10^{-9}	5.3×10^8	3.2×10^{-6}	2.2×10^5	.048
13	LTP D(O) $\beta=1$	Oxide- Lithium Side Only	-157	.076	2.5×10^7	.63	1.9×10^6	1.0×10^{-4}	0.34	$>10^6$ yrs
14	LTP D(+) $\beta=1$	Oxide- Lithium Side Only	-1.03×10^4	3.8×10^{-4}	2.5×10^7	.63	1.8×10^7	.019	2.0×10^4	$>10^6$ yrs

- (1) HTP = High Temperature Plant
 LTP - Low Temperature Plant
 D(-), (low); D(O), (Most Probably); D(+), (High) Value for Al_2O_3D
 $\beta = 1$
 $\beta = \beta_i$
 $\beta = h$ } Possible Boundary Conditions Described in Text

The tritium concentration in the beryllium resulting from transmutation exceeds the one atmosphere solubility limit in a matter of several days. Expressed another way, the tritium overpressure required to maintain the tritium in solution in the beryllium at equilibrium is of the order of 70 to 500 atmospheres. It does not seem reasonable that hydrogen partial pressures of this magnitude could be sustained so it is likely that tritium would precipitate as bubbles in the beryllium. The beryllium layer can be subdivided into three regions consisting of two surface regions where the tritium solubility is not exceeded and one central region containing a constant concentration of diffusing tritium maintained at the solubility limit. The tritium precipitation rate in the central region can then be determined from the difference between the total source strength and the sum of the flow rates through the outer layers. If an acceptable hydrogen partial pressure above the beryllium can be established from a knowledge of the physical system, this value can be used to establish a hydrogen solubility and an equilibrium hydrogen precipitation rate in the beryllium can then be determined.

3.2.2.4. Lag Times

Four transport paths for tritium in the blanket would appear to be of greatest interest. These involve tritium transfer between the plasma and the coolant, the beryllium and the coolant, the graphite and the coolant, and the static lithium and the magnetic coolant channels. Calculated values of the lag time for tritium breakthrough along these paths are included in Table 3.5. Lag times for tritium transport to the magnet cooling channels exceed the reactor life in almost every case. The tritium release rates calculated for the magnet cooling channels are therefore upper limits and time dependent diffusion solutions may well project considerably lower tritium release rates over the reactor life. The lag times for the other transport processes are sufficiently low that equilibrium diffusion solutions would appear to provide a satisfactory approximation to the transport process.

Table 3.5. Calculated Tritium Inventory

Run No.	Conditions	Remarks	Inventory				
			Al ₂ O ₃ (g)	Nb (g)	Be (g)	Graphite (g)	All Materials (total) (g)
1	LTP D(O) β=1		2.7	6.8	1641	62	1710
2	HTP D(O) β=1		2.8	1.4	624	43	672
3	LTP D(+) β=1		6.9	2.3	1641	62	1712
4	HTP D(+) β=1		2.6	1.2	624	5.6	633
5	LTP D(-) β=1		3.8	2.4	1641	62	1710
6	HTP D(-) β=1		2.8	.79	624	43	669
7	LTP D(O) β=β _i		8 x 10 ⁻⁷	2.5	1641	1 x 10 ⁻⁵	1644
8	HTP D(O) β _i		8 x 10 ⁻³	.8	1624	0.1	625

Table 3.5. Continued

<u>Run No.</u>	<u>Conditions</u>	<u>Remarks</u>	<u>Inventory</u>				
			<u>Al₂O₃</u> (g)	<u>Nb</u> (g)	<u>Be</u> (g)	<u>Graphite</u> (g)	<u>All Materials</u> (Total) (g)
9	LTP D(+) β _i		8 x 10 ⁻⁷	2.6	1638	1x 10 ⁻⁵	1641
10	HTP D(+) β _i		9 x 10 ⁻³	1.4	624	0.1	626
11	HTP D(O) β=1	Oxide Film On Nb	3.5	1.7	627	54	690
12	HTP D(+) β=1	Oxide Film On Nb	3.4	2.0	627	54	687
13	LTP D(O) β=1	Oxide- Lithium Side Only	351	105	2450	3220	6120
14	LTP D(+) β=1	Oxide- Lithium Side Only	357	104	2450	4450	7360

3.2.2.5. General

The plasma, flowing lithium, or static lithium can be either sources or sinks for tritium. The lithium will always be a tritium source in a functioning reactor but, depending upon the efficiency of the separation system, may appear to be a sink in the blanket in that tritium can diffuse into the lithium from adjacent sources such as the beryllium layer. The directions of flow will be controlled by the selection of tritium partial pressures or concentrations in the various sources. Beryllium always was a tritium source for the parameters investigated whereas the magnet cooling channels were always a sink. No tritium transport through the biological shield could be calculated since no tritium was assumed to pass the magnet cooling channels.

The plasma switches from a source to a sink as the tritium partial pressure above the first wall is decreased. Table 3.6 shows results for six cases in which the plasma tritium partial pressure ranges from 10^{-2} to 10^{-6} torr. The tritium flux through the first wall varies from 4.2×10^7 Ci/yr out of the plasma to 1.5×10^6 Ci/yr into the plasma for the conditions picked.

It should be recognized that the assumption of a constant tritium partial pressure above the first wall may not be a satisfactory approximation. The central cavity will be purged after each pulse to remove impurities so tritium concentrations will change rapidly. Also, energetic tritium atoms escaping the plasma and coming to rest in the first wall constitute an additional tritium source.

The energetic particle flux of total charged particles at the first wall is expected to be approximately $10^{16} \text{ cm}^{-2} \text{ sec}^{-1}$ whereas the above tritium permeation fluxes correspond to fewer than 100 tritium atoms $\text{cm}^{-2} \text{ sec}^{-2}$. Since tritium atoms will constitute an appreciable fraction of the total charged particle flux at the first wall, this flux would appear to constitute the principal tritium source from the plasma.

Table 3.6. Effect of Plasma Side Partial Pressure Variation

<u>T₂ Partial Pressure (Torr)</u>	<u>Permeation to the Plasma</u>	
	<u>Permeation Rate (Ci/yr)</u>	<u>Permeation Rate (Ci/yr)</u>
	<u>CASE: HTP:D(0):β=1</u>	<u>CASE: HTP:D(t):β=1</u>
10 ⁻²	2.70 x 10 ⁶	3.43 x 10 ⁷
10 ⁻⁴	1.35 x 10 ⁵	1.72 x 10 ⁶
10 ⁻⁶	-1.25 x 10 ⁵	-1.54 x 10 ⁶
	<u>CASE: HTP:D(0):β=R_{sc}</u>	<u>CASE: HTP:D(+):β=R_{sc}</u>
10 ⁻²	2.88 x 10 ⁶	4.20 x 10 ⁷
10 ⁻⁴	2.87 x 10 ⁵	4.20 x 10 ⁶
10 ⁻⁶	2.85 x 10 ⁴	4.16 x 10 ⁵
	<u>CASE: LTP:D(+):β=1</u>	<u>CASE: LTP:D(+):β=R_{sc}</u>
10 ⁻²	-9.09 x 10 ⁴	14.5
10 ⁻⁴	-9.09 x 10 ⁴	1.43
10 ⁻⁶	-9.09 x 10 ⁴	0.14

The tritium flux to the magnet cooling channel is a strong function of the assumed temperature at the channel. Figure 33 shows how the calculated tritium flux varies for different assumed values for temperature.

3.2.3. Conclusions

1. Ceramic materials, such as the insulator required for the theta-pinch concept, can strongly influence projected tritium inventories and transport rates in a fusion reactor blanket.
2. The large variation in tritium inventory (greater than a factor of 10) resulting for selected parameters in the blanket suggests that actual tritium inventories are subject to considerable uncertainty.
3. The stabilization of oxide surface films on metal components by high oxygen potentials could strongly influence tritium distributions within the blanket.
4. The lag time for diffusional tritium transport through the blanket layers to a point of potential release to the environment (the magnet cooling channels) is generally greater than the anticipated reactor life. However, the simple geometry employed does not allow assessment of more realistic diffusion release paths which might exist in a constructed reactor.
5. Projected tritium levels in a beryllium metal blanket exceed the solubility limit which could result in tritium precipitation within the metal.
6. Tritium flow both into and out of the plasma is obtained for the different blanket conditions considered.

REFERENCES

1. Hurst, D. G., "Diffusion of Fission Gas: Calculated Diffusion from a Sphere Taking into Account Trapping and Return from the Traps," CRRP-1124, Atomic Energy of Canada, Ltd., Chalk River, Ontario, Canada (1962).
2. Norgett, M. J. and A. B. Lidiard, "The Migration of Inert Gases in Ionic Crystals," *Phil. Mag.*, 18, 1193-1210 (1968).
3. Matzke, Hj., "Rare Gas Mobility in Pure and Doped Potassium Bromide," *Z. Naturforsch.*, 22a, 507-518 (1967).
4. Matzke, Hj., D. Rickers, and G. Sorenson, "Rare Gas Diffusion in NaCl," *Z. Naturforsch.*, 24a, 820-826 (1969).
5. Ong, A. S., "The Diffusion of ^{133}Xe in CsI and CaF_2 Single Crystals," M.S. Thesis, North Carolina State University, Raleigh, North Carolina (1970); Also ORO-3508-3 (1967).
6. Matzke, Hj., "Xenon Migration and Trapping in Doped ThO_2 ," *Jour. Nucl. Mat.*, 21, 190-198 (1967).
7. Matzke, Hj., "Application of 'Channeling' Techniques to Fission Gas Release Studies," *Jour. Nucl. Mat.*, 30, 110-121 (1969).
8. Matzke, Hj. and J. A. Davis, "Location of Inert Gas Atoms in KCl, CaF_2 and UO_2 Crystals by H^+ and He^{2+} Channeling Studies," *Jour. Appl. Phys.*, 238 (2), 805-808 (1967).
9. Elleman, T. S., C. H. Fox, Jr., and L. D. Mears, "Influence of Defects on Rare Gas Diffusion in Solids," *Jour. Nucl. Mat.*, 30, 89-106 (1969).
10. Norgett, M. J. and A. B. Lidiard, "The Migration of Inert Gases in Ionic Crystals," *Phil. Mag.*, 18, 1193-1210 (1968); Also, Harwell Report, TP332 and 370.
11. Matzke, Hj., "Rare Gas Mobility in Pure and Doped Potassium Bromide," *Z. Naturforsch.*, 22a, 507-518 (1967).
12. Ong, A. S. and T. S. Elleman, "Effect of Trapping on the Release of Recoil Injected Gases from Solids," *Nucl. Instr. & Methods*, 86, 117-125 (1970).
13. DiCola, G. and Hj. Matzke, "The Determination of Rare Gas Diffusion Following Recoil Labelling of Plane or Spherical Solids," *Nucl. Instr. & Methods*, 57, 341-345 (1967).
14. Austin, J. H. and T. S. Elleman, "Diffusion of Tritium in Austenitic Stainless Steels," *Jour. Nuc. Mat.*, 43, 119 (1972).
15. Fisher, J. C., "Calculation of Diffusion Penetration Curves for Surface and Grainboundary Diffusion," *Jour. Appl. Phys.*, 22, 74 (1951).
16. Suzouka, T., "Lattice and Grainboundary Diffusion in Polycrystals," *Trans. Japan Inst. Metals*, 2, 25 (1961).

17. Calder, R. D., T. S. Elleman, and K. Verghese, "Grainboundary Diffusion of Tritium in 304- and 316-Stainless Steels," *Jour. Nuc. Mat.*, 46, 46-52 (1973).
18. Austin, J. H., T. S. Elleman, and K. Verghese, "Surface Effects on the Diffusion of Tritium in 304-Stainless Steel and Zircaloy-2," *Jour. Nucl. Mat.*, 48, 307-316 (1973).
19. Levine, H. A. and C. J. MacCallum, "Grainboundary and Lattice Diffusion in Polycrystalline Bodies," *Jour. Appl. Phys.*, 31, 595 (1969).
20. Bellman, R. and R. E. Kalaba, Numerical Inversion of Laplace Transform, American Elsevier Publishing Company, New York, N. Y. (1966).
21. Abramowitz, M. and I. A. Stegun (Eds.), Handbook of Mathematical Functions, National Bureau of Standards, Washington, D. C. (1970).
22. Reed, R. P., "The Spontaneous Martensitic Transformations in 18% Cr, 8% Ni Steels," *Acta Met.*, 10, 865 (1962).
23. Roy, C., "Hydrogen Distribution in Oxidized Zirconium Alloys by Autoradiography," AECL Report-2085, Chalk River Laboratories, Chalk River, Ontario (1964).
24. Louthan, M. R., Jr., et al., "An Autoradiographic Analysis of Microsegregation of Hydrogen in Metals," *Corrosion*, 28, 172 (1972).
25. Kearns, J. J., "Diffusion Coefficient of Hydrogen in Alpha Zirconium, Zircaloy-2 and Zircaloy-4," *Jour. Nuc. Mat.*, 43, 330-338 (1972).
26. Grant, P. J., A. J. Kennedy, D. F. Hallman, E. T. Chulick, and D. L. Uhl, "Oconee Radiochemistry Survey Program," Babcock and Wilcox Technical Paper RDTPL-75-4, May (1975).
27. Abraham, P. M., et al., "Diffusion of Gases in Solids," USAEC Report ORO-3508-8 (1972).
28. Melehan, J. B., "Analysis of Tritium Retention in High Power Saxton and CVTR Fuel," USAEC Report E-IT-71-51 (1971).
29. Laconte, J. and D. D. Malinowski, "Tritium in Pressurized Water Reactors," in Tritium, A. A. Moghissi and M. W. Carter (Eds.), Messenger Graphics, Phoenix, Ariz. (1973).
30. Steele, T. A., "Tritium Generation and Release to In-Plant and Off-Site Environs of the LaCrosse Boiling Water Reactor," in Tritium, A. A. Moghissi and M. W. Carter (Eds.), Messenger Graphics, Phoenix, Ariz. (1973).
31. Goode, J. H. and C. M. Cox, "The Distribution of Fission Product Tritium in a Zircaloy-clad UO_2 Blanket Rod from PWR-1," USAEC Report ORNL-TM-2994 (1970).
32. Birnbaum, H. K. and C. A. Wert, "Diffusion of Hydrogen in Metals," *Berichte der Bunsen-Gesellschaft*, 76(8), 806-816 (1972).
33. Hickman, R. G., "Some Problems Associated with Tritium in Fusion Reactors," USAEC Report UCRL-74057 (1972).

34. Inthoff, W. and K. E. Zimen, "Kinetics of Diffusion of Radioactive Rare Gases from Solid Substances after Irradiation," USAEC Report AEC-tr-3289 (176) (1956).
35. Pennington, C. W., T. S. Elleman, and K. Verghese, "Tritium Release from Niobium," Nucl. Tech., 22, 405-415 (1974).
36. Buehler Corporation: No. 20-8192 AB Edgemet Kit (available as a manual with this number).
37. Westlake, D. G., "Problems in the Preparation of Vanadium-Hydrogen Alloys for Transmission Electron Microscopy," Trans. Met. Soc. AIME, 239, 1106 (1967).
38. Crank, J., Mathematics of Diffusion, Clarendon Press, Oxford (1956).
39. Ozisik, M. N., Boundary Value Problems of Heat Conduction, International Textbook Co., Scranton, Pa. (1968).
40. Strehlow, R. A. and K. C. Savage, "The Permeation of Hydrogen Isotopes through Structural Metals at Low Pressures and through Metals with Oxide Film Barriers," Nuc. Tech., 22, 127 (1974).
41. Kofstad, P., High Temperature Oxidation of Metals, J. Wiley and Sons, New York (1966).
42. Schick, H. S. (Ed.), Thermodynamics of Certain Refractory Compounds, Academic Press, New York (1966).
43. Steigerwald, E. A., TRW Electromechanical Division Report E-5263, NASA, CR-54004, Cleveland, November (1963). Referred to in Reference #44.
44. Stickney, R. E., "Diffusion and Permeation of Hydrogen Isotopes in Fusion Reactors: A Survey," in Chemistry of Fusion Technology, D. M. Gruen (Ed.), Plenum Press, New York (1972).
45. Rudd, D. W., D. W. Vose, and S. Johnson, "Permeability of Niobium to Hydrogen," Jour. Phys. Chem., 66, 351 (1962).
46. Steiner, D. and A. P. Fraas, "Preliminary Observations on the Radiological Implications of Fusion Power," Nuclear Safety, 13, 353 (1972).
47. Krakowski, R. A., et al., "An Engineering Design Study of a Reference Theta Pinch Reactor (RTPR)," USAEC La-5336 (1974).
48. Dudziak, D. J., "Tritium Breeding and Nuclear Heating in a Reference Theta Pinch Reactor (RTPR)," USAEC LA-UR-73-1030 (1973).
49. Dudziak, D. J., "Discrete Ordinates Analysis of a Reference Theta Pinch Reactor (RTPR)," USAEC LA-DC-1427 (1972).
50. Veleckis, E. and R. K. Edwards, "Thermodynamic Properties in the Systems Vanadium - Hydrogen, Niobium - Hydrogen, and Tantalum - Hydrogen," J. Phys. Chem., 73, 683-692 (1969).
51. Jones, P. M. S. and R. Gibson, "Hydrogen in Beryllium," J. Nucl. Mat., 21, 353-354 (1967).

52. Belyakov, Yu. I. and Yu. I. Zveydin, "Temperature Dependence of Hydrogen Permeability Through Cu and its Alloys," Uch. Zap. Leningrad Gos. Univ. Serv. Fiz. Nauk, No. 345, 44-49 (1968).
53. Ash, R., R. M. Barrer, and D. G. Palmer, "Diffusion in Multiple Laminates," Brit. J. Appl. Phys., 16, 873-884 (1965).
54. Maroni, V. A., "An Analysis of Tritium Distribution and Leakage Characteristics of Two Fusion Reactor Reference Designs," 5th Symp. on Eng. Prof. of Fusion Reactors, Princeton, N. J., Nov. (1973).
55. Fowler, J., R. Causey, D. Chandra, T. S. Elleman, and K. Verghese, "Tritium in Fusion Reactors," Gattlinburg, Tenn, Oct. 1-3 (1975).
56. Chandra, D., T. S. Elleman, and K. Verghese, "Tritium Diffusion Through Oxide Surface Films on Niobium," (accepted for publication in J. Nucl. Mat.).
57. Ogurtani, T. O., "The Kinetics of Diffusion of Hydrogen in Niobium," Met. Trans., 2 (H), 3035-3038 (1971).

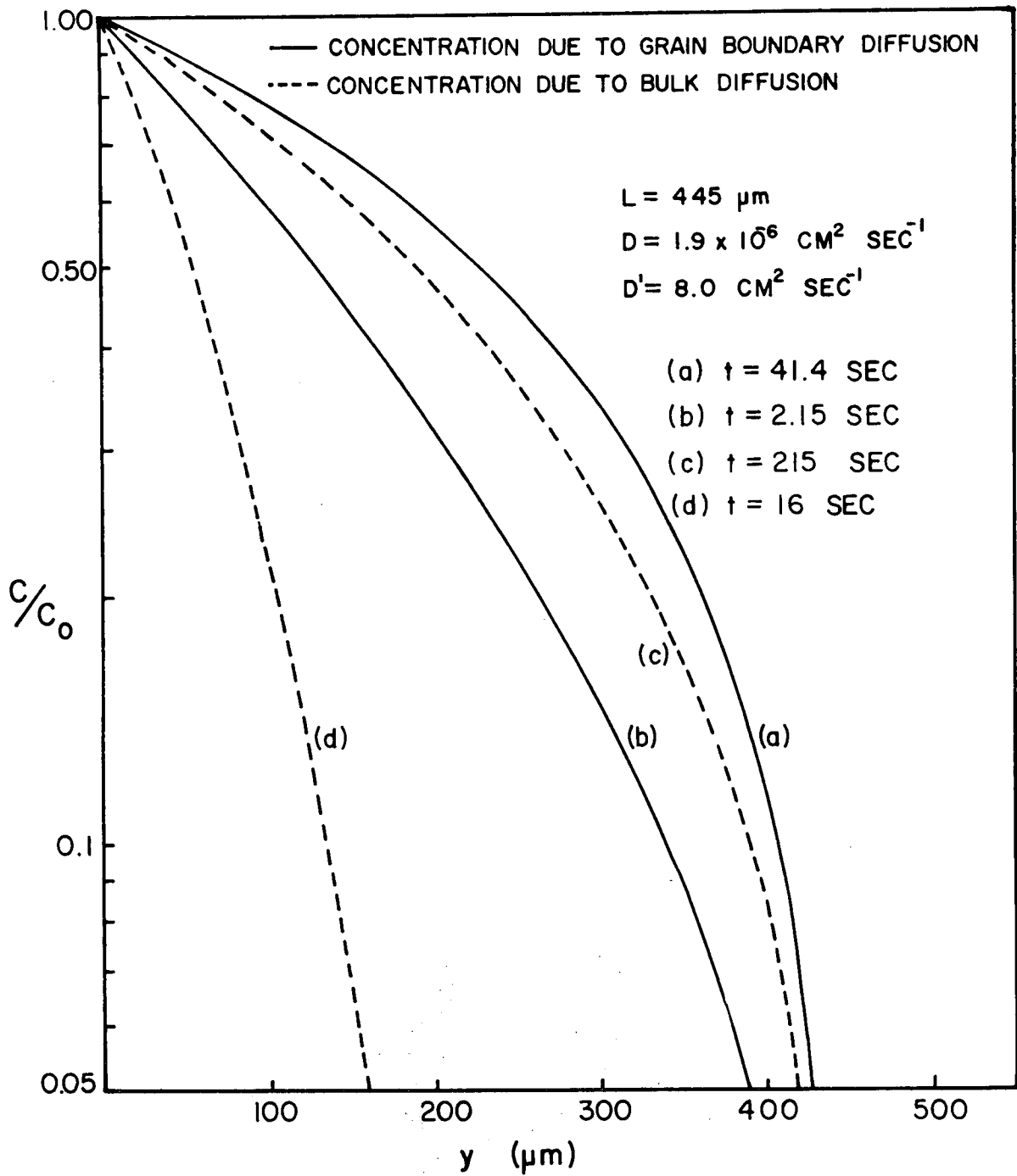


Figure 1. Concentration profiles calculated from grain boundary diffusion model and bulk diffusion model at 500°C

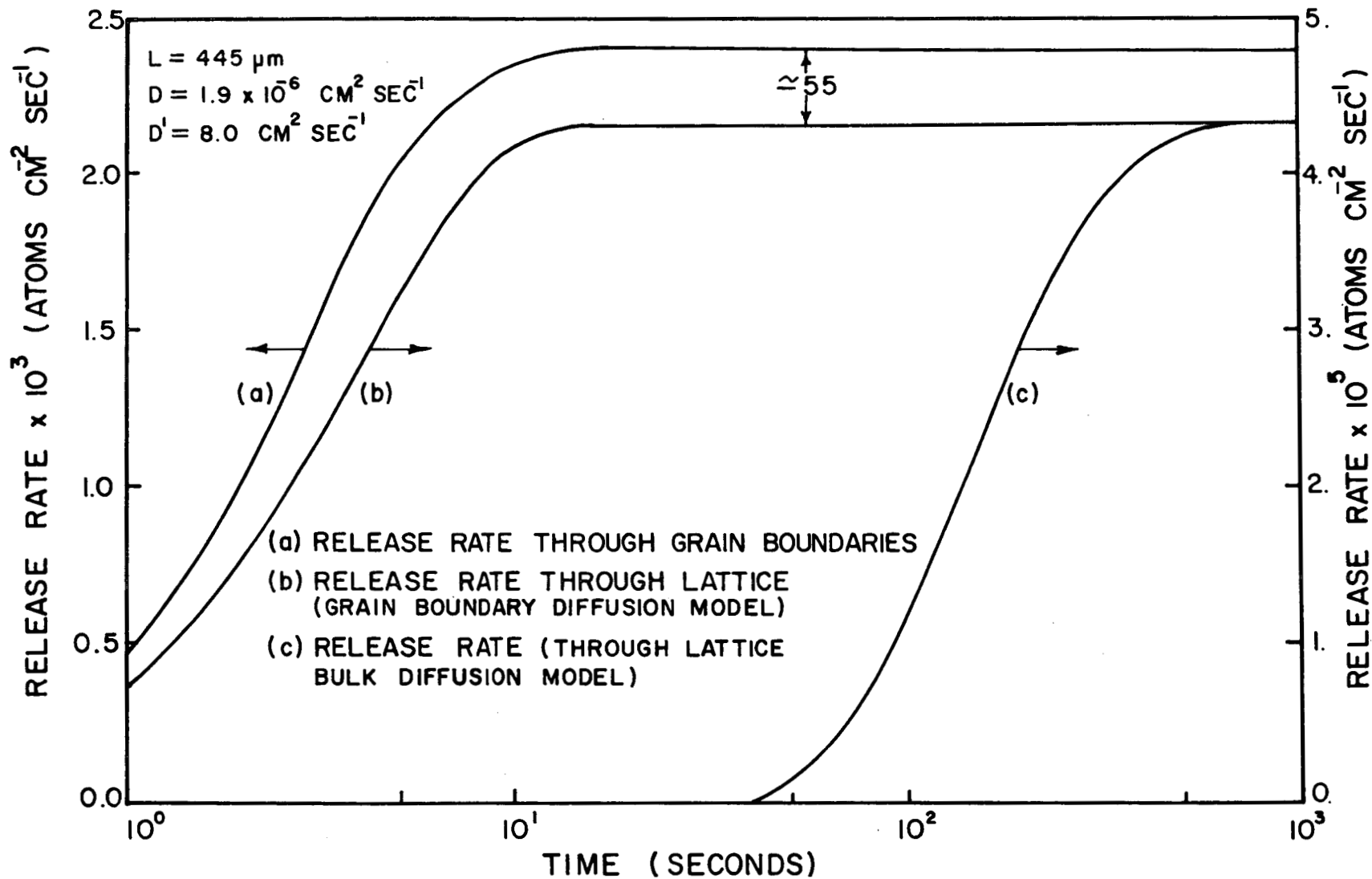


Figure 2. Release rates calculated from grain boundary diffusion model and bulk diffusion model at 500 C



Figure 3. Stripped autoradiograph from unpolished specimen (6 hrs exposure; 406X)

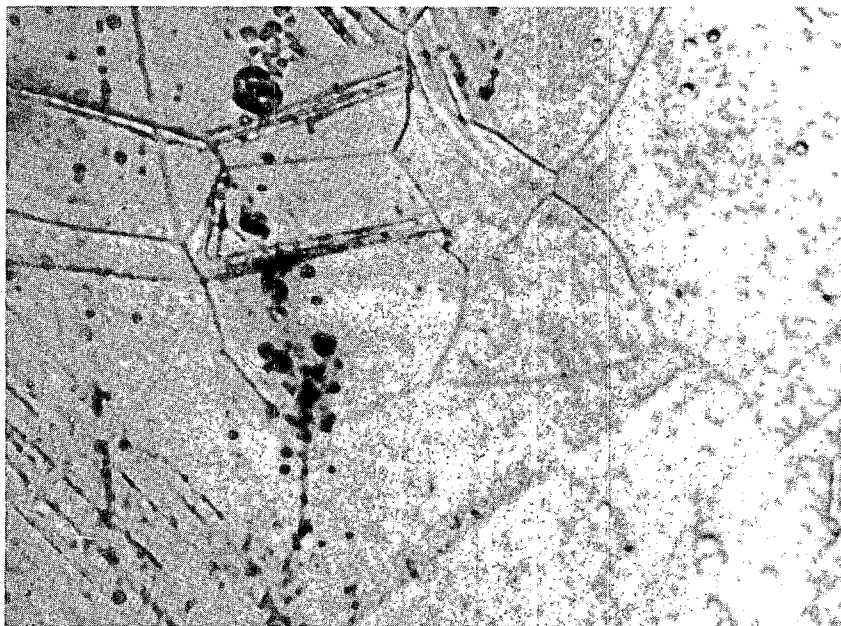


Figure 4. Micrograph corresponding to Figure 3. (750X)

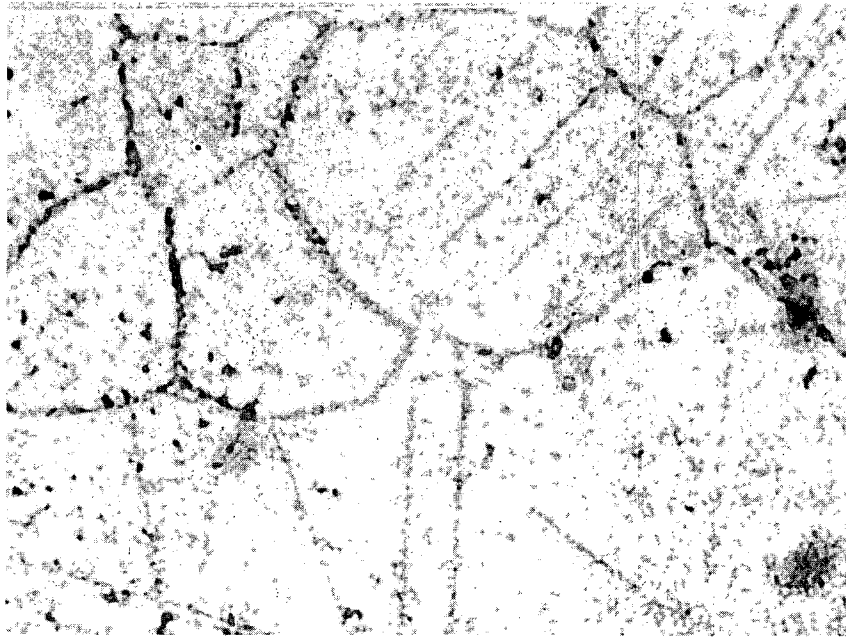


Figure 5. Stripped autoradiograph (3 hrs exposure; 750X)



Figure 6. Autoradiograph of electropolished and etched specimen (3 hrs exposure; 180X)

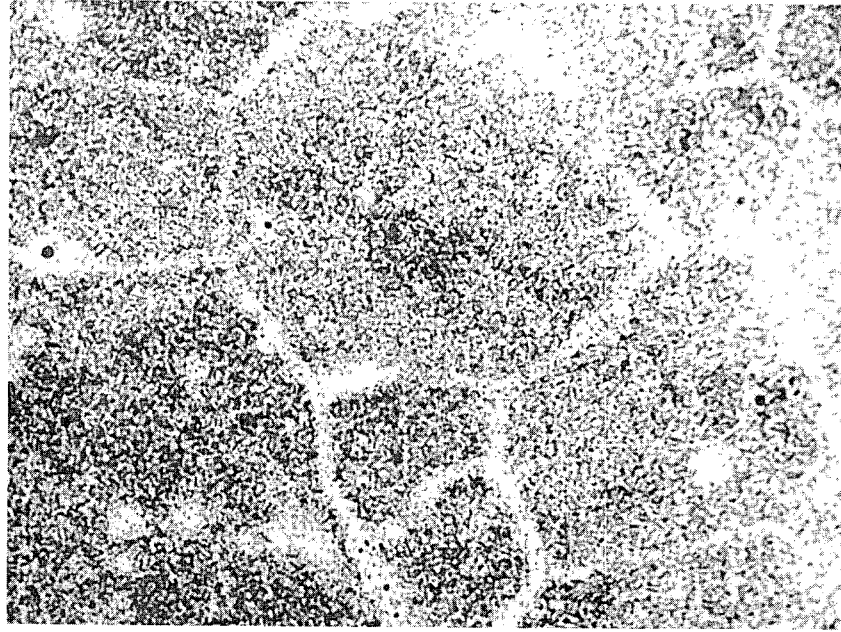


Figure 7. Stripped autoradiograph from etched specimen showing denuded grain boundaries (9 hrs exposure; 810X)

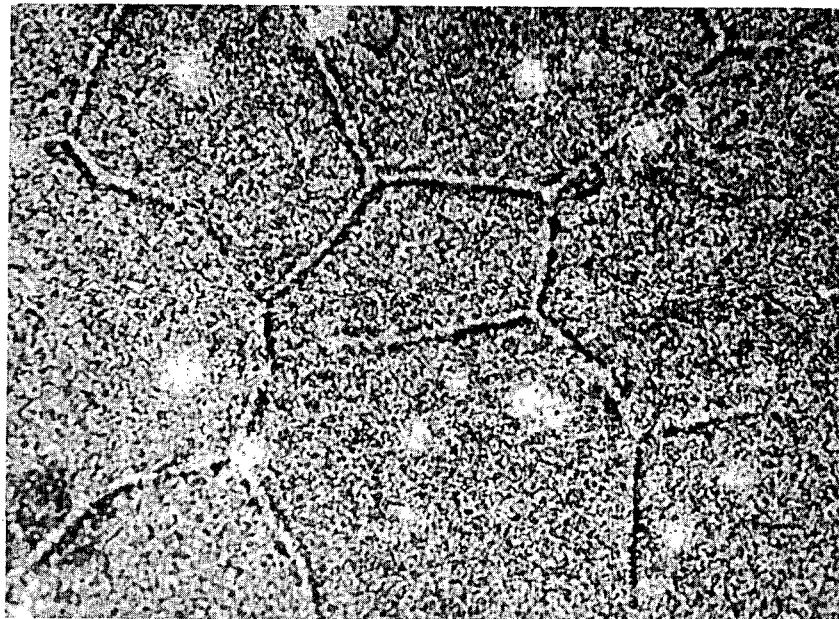


Figure 8. Stripped autoradiograph from etched specimen showing tritium precipitation along the edges of grain boundaries (9 hrs exposure; 810X)

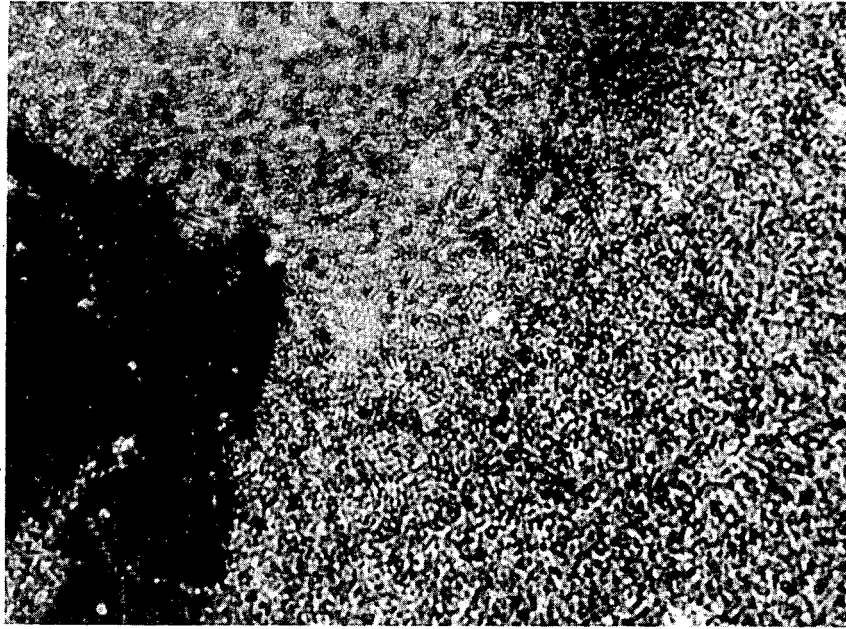


Figure 9. Stripped autoradiograph from an electropolished and etched sample ($7\frac{1}{2}$ hrs exposure; 750X)



Figure 10. Autoradiograph from the same region of the specimen as in Figure 9 but heated at 185°C for 2 hrs (4-day exposure; 750X)

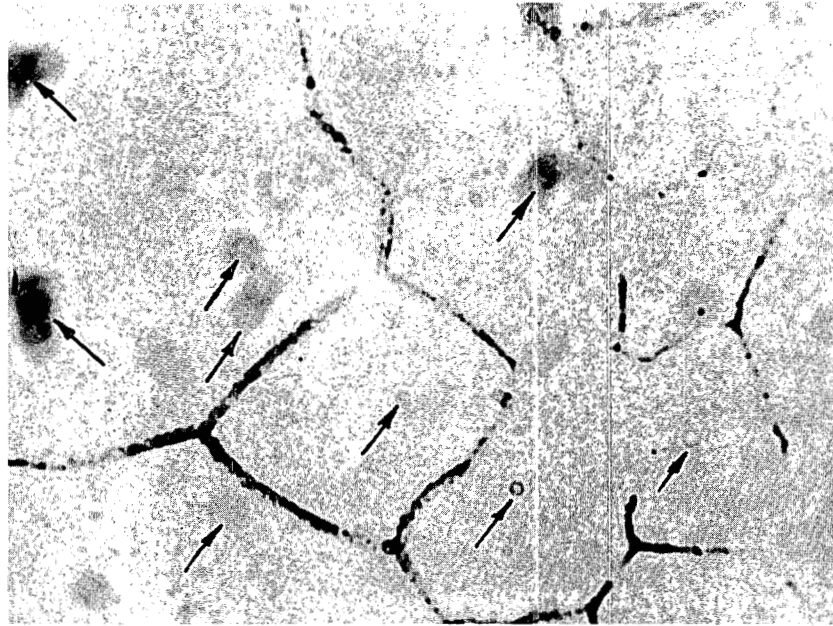


Figure 11. Stripped autoradiograph from an electropolished and etched specimen when surface layer had been removed. (Arrows indicate artifacts; 36 hrs exposure; 750X)

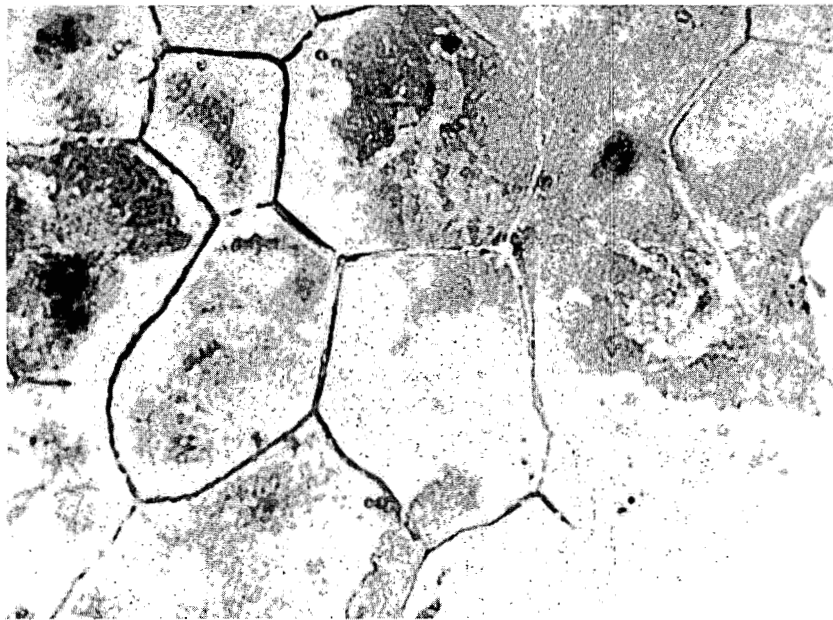


Figure 12. Stripped autoradiograph from back face of a tritium recoil injected specimen (electropolished and etched) (100 hrs exposure; 750X)

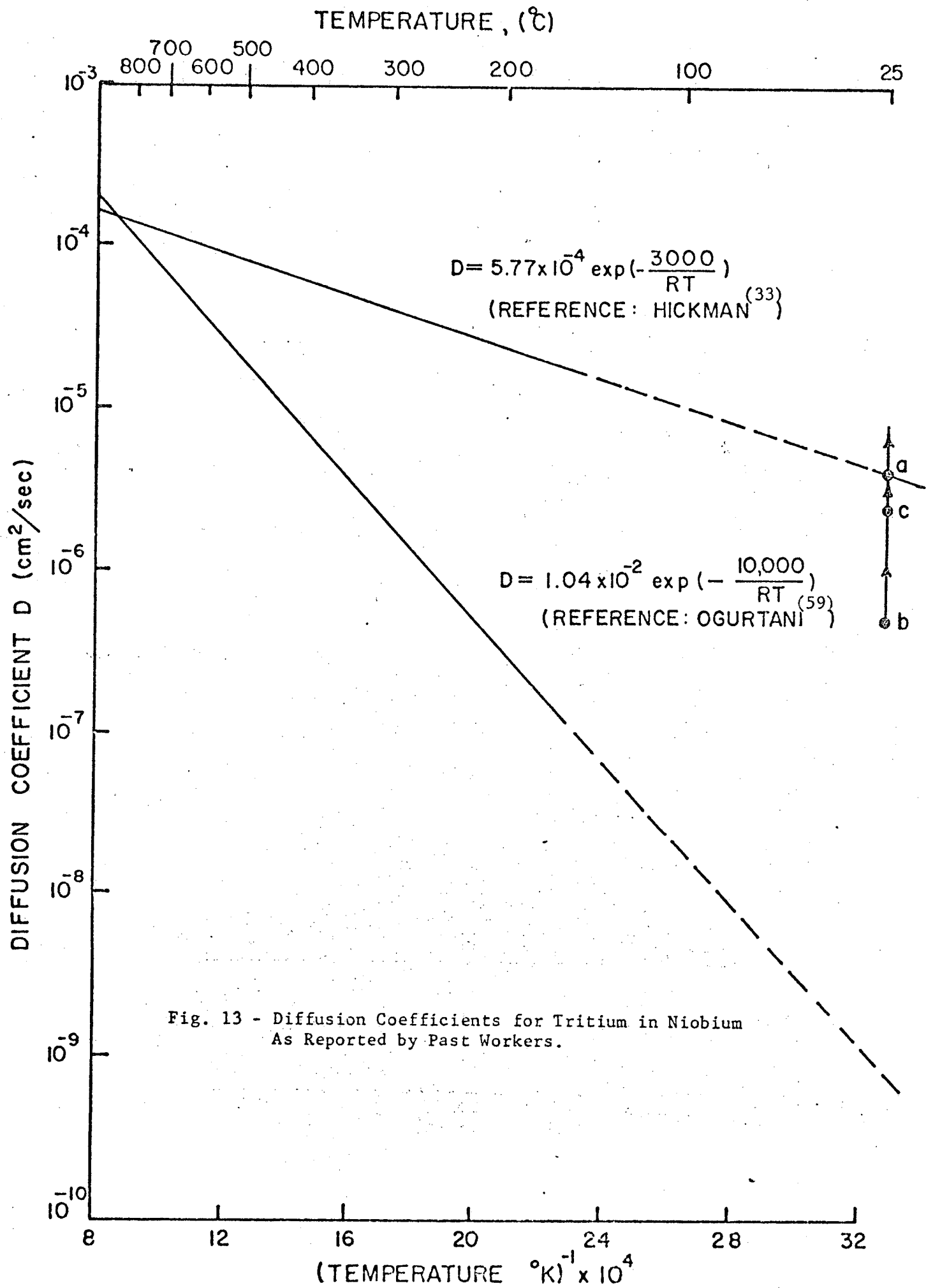
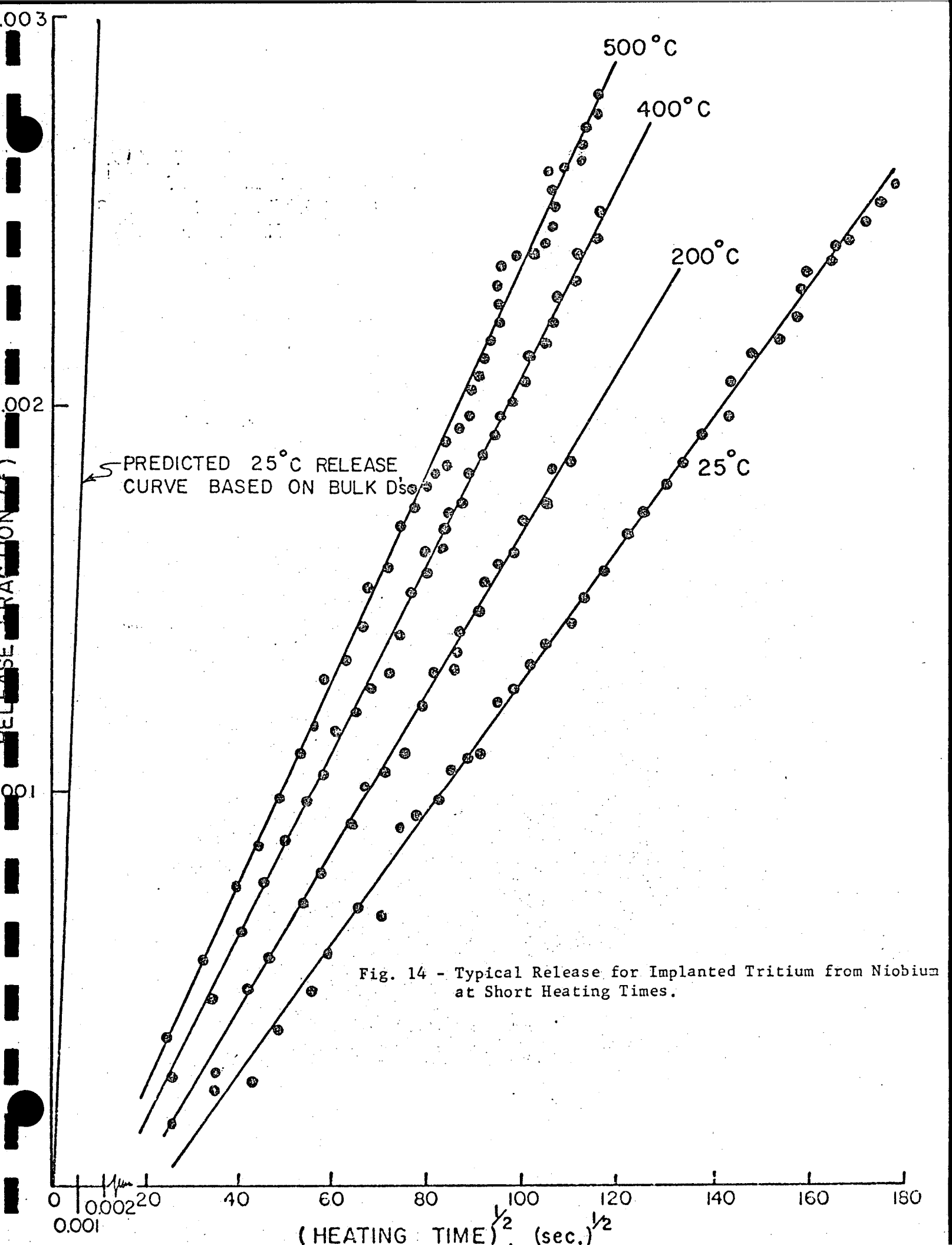
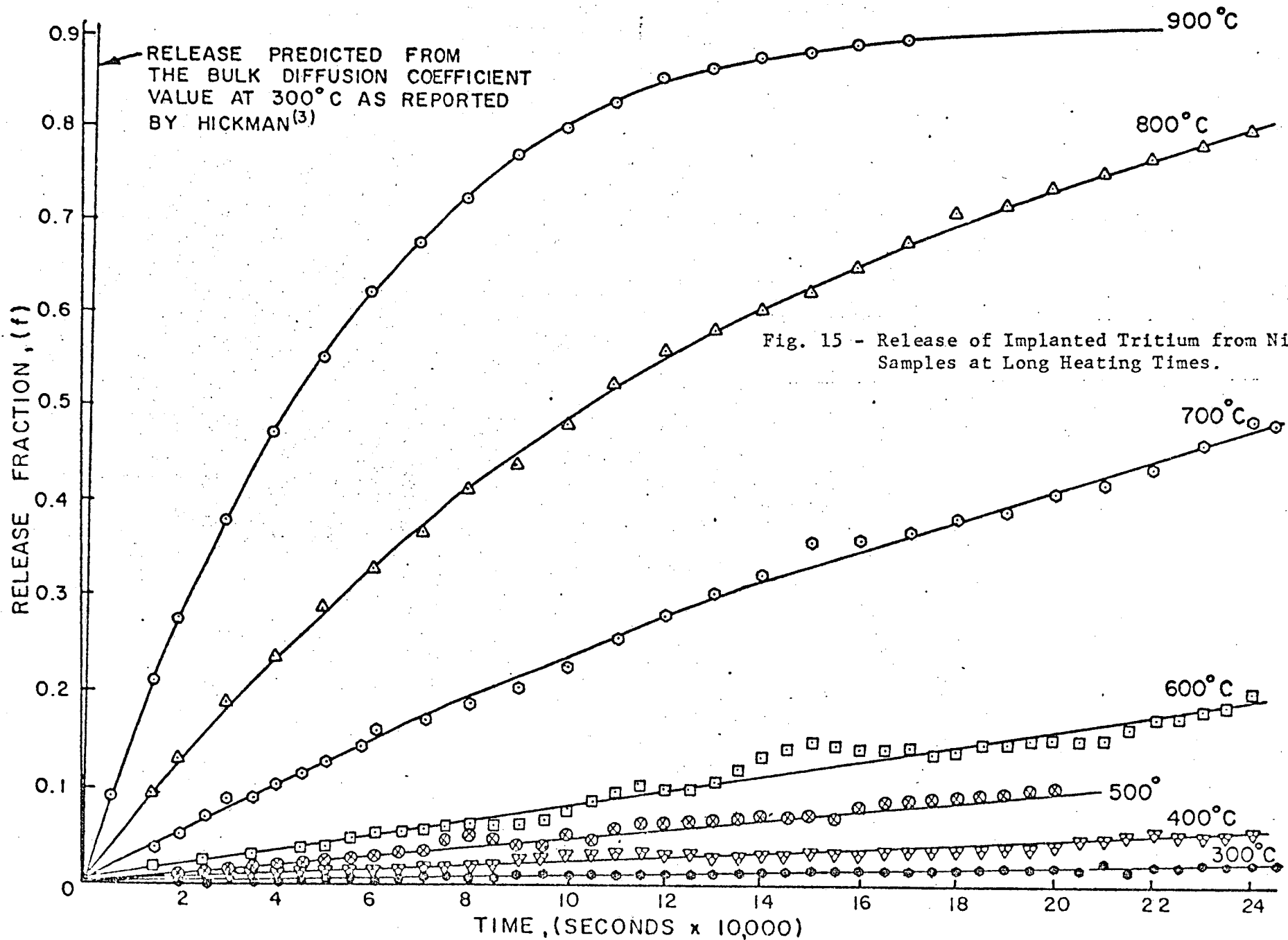


Fig. 13 - Diffusion Coefficients for Tritium in Niobium
As Reported by Past Workers.





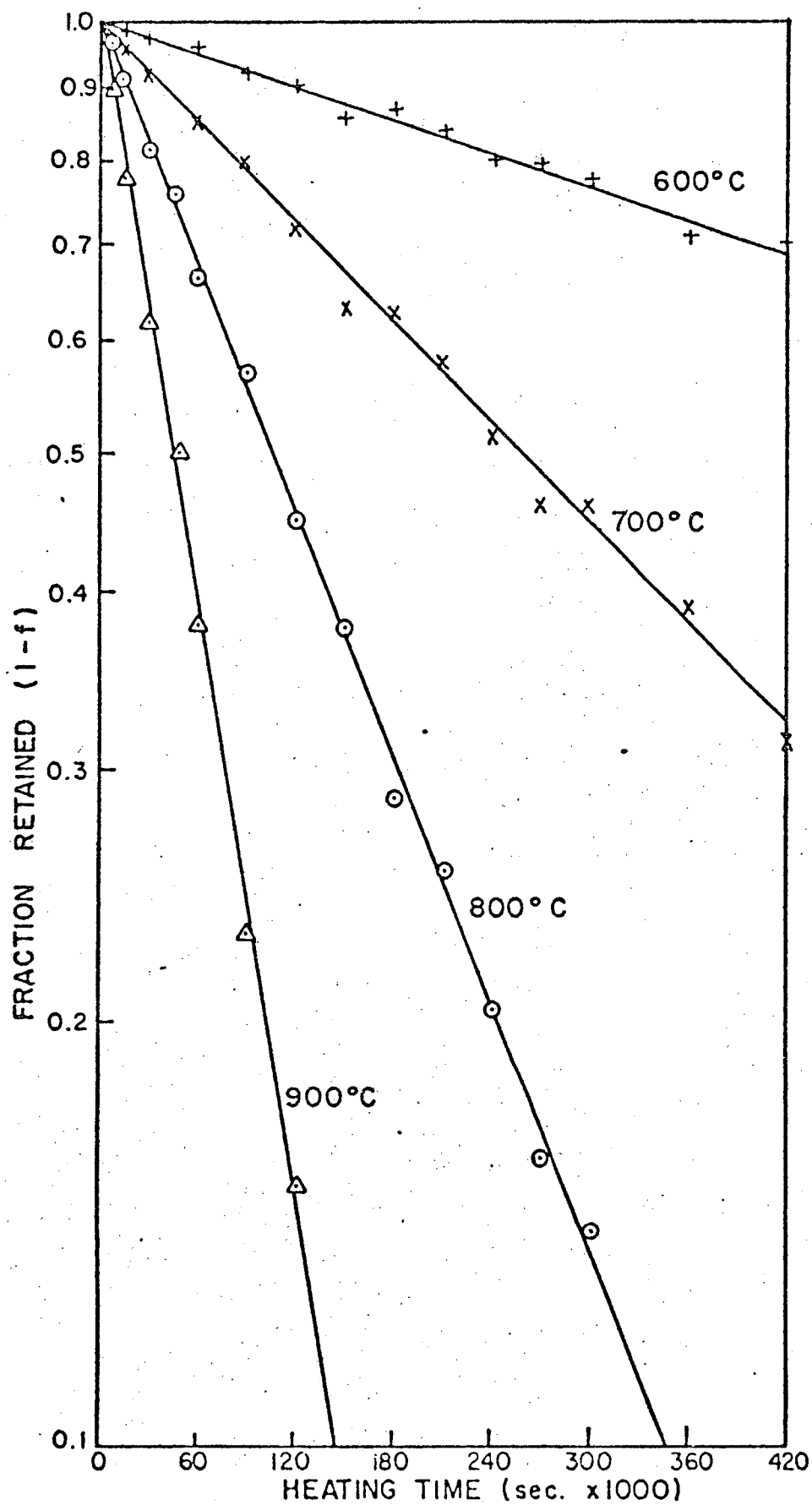


Fig. 16 - Tritium Fraction Retained as a Function of Time for Long Duration Release Experiments.

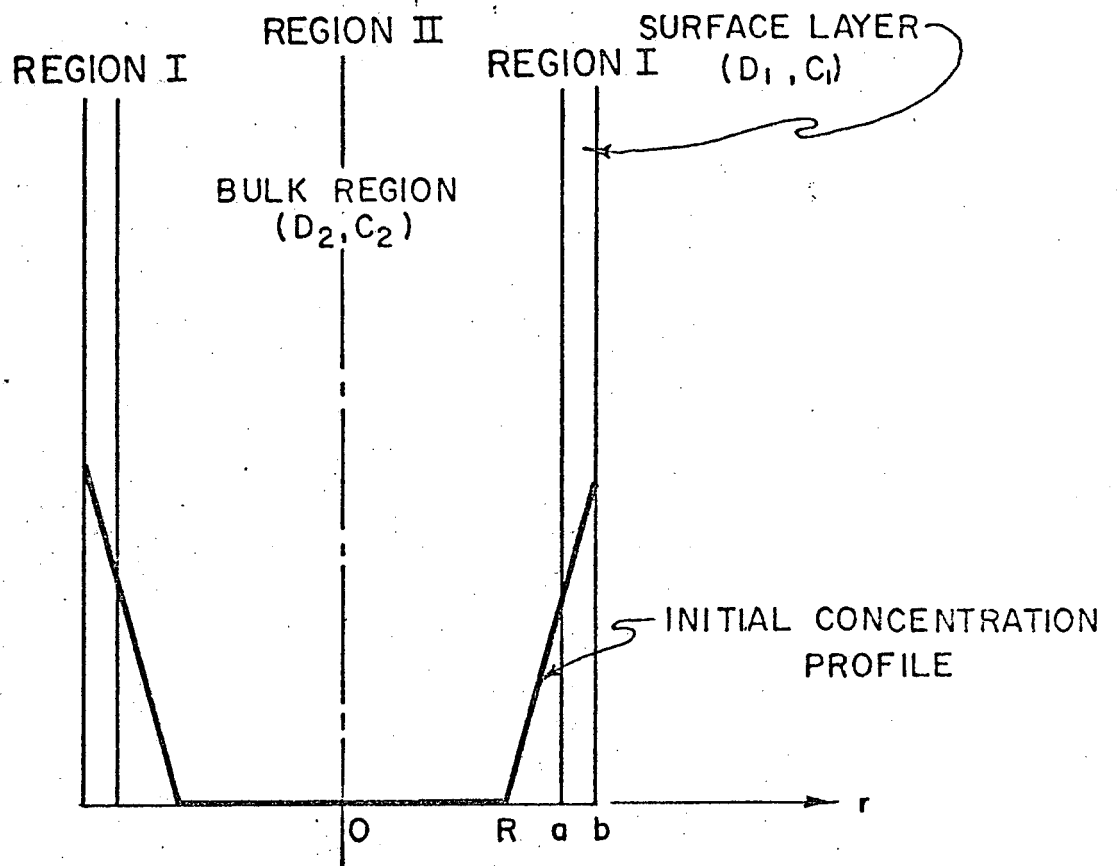


Fig. 17 - Schematic Representation of the Sample Configuration and Notations Used in the Two-Region Diffusion Model.

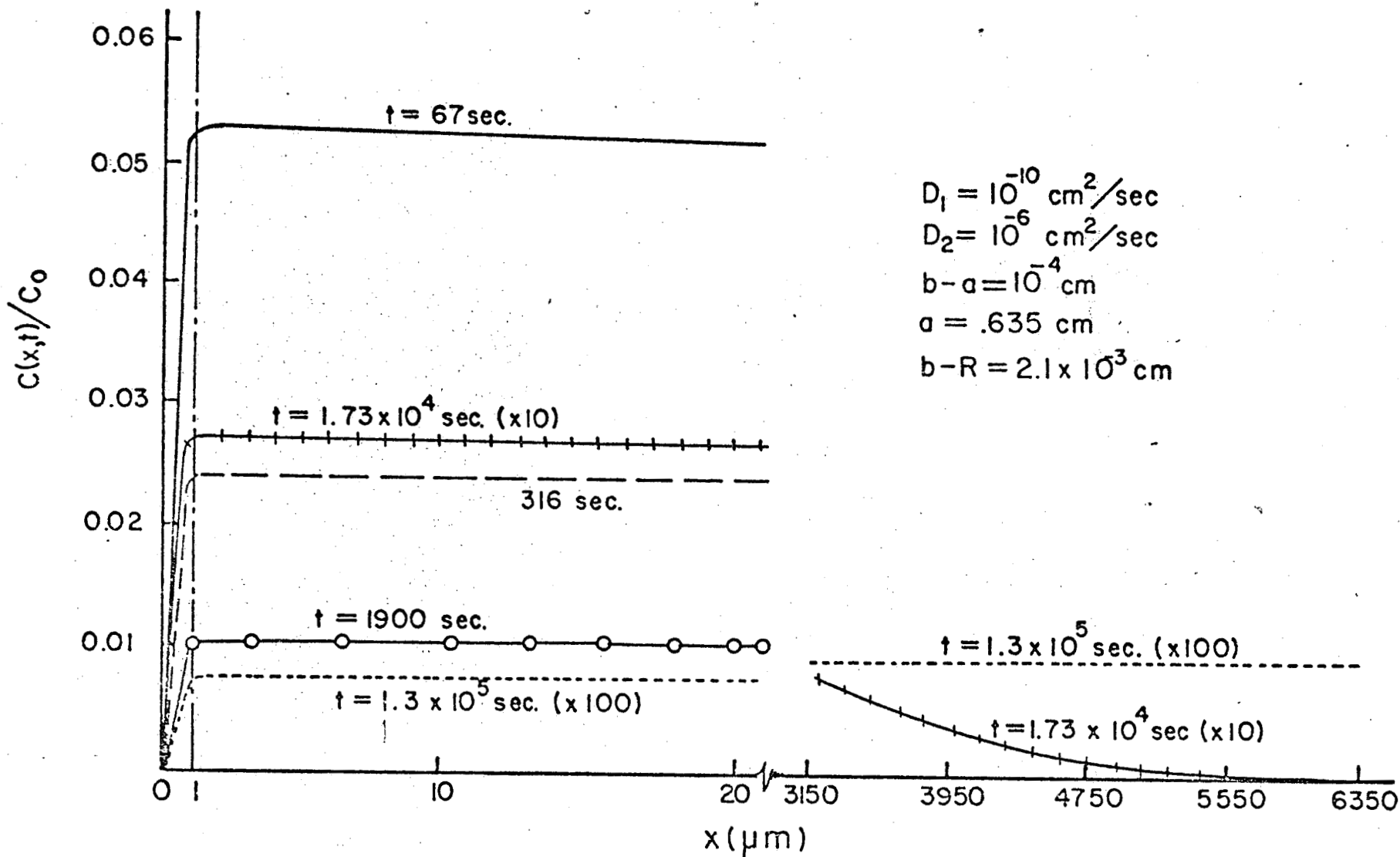


Fig. 18 - Concentration Profiles in a Two-Region Slab at Different Times, as Calculated by the Finite-Difference Method.

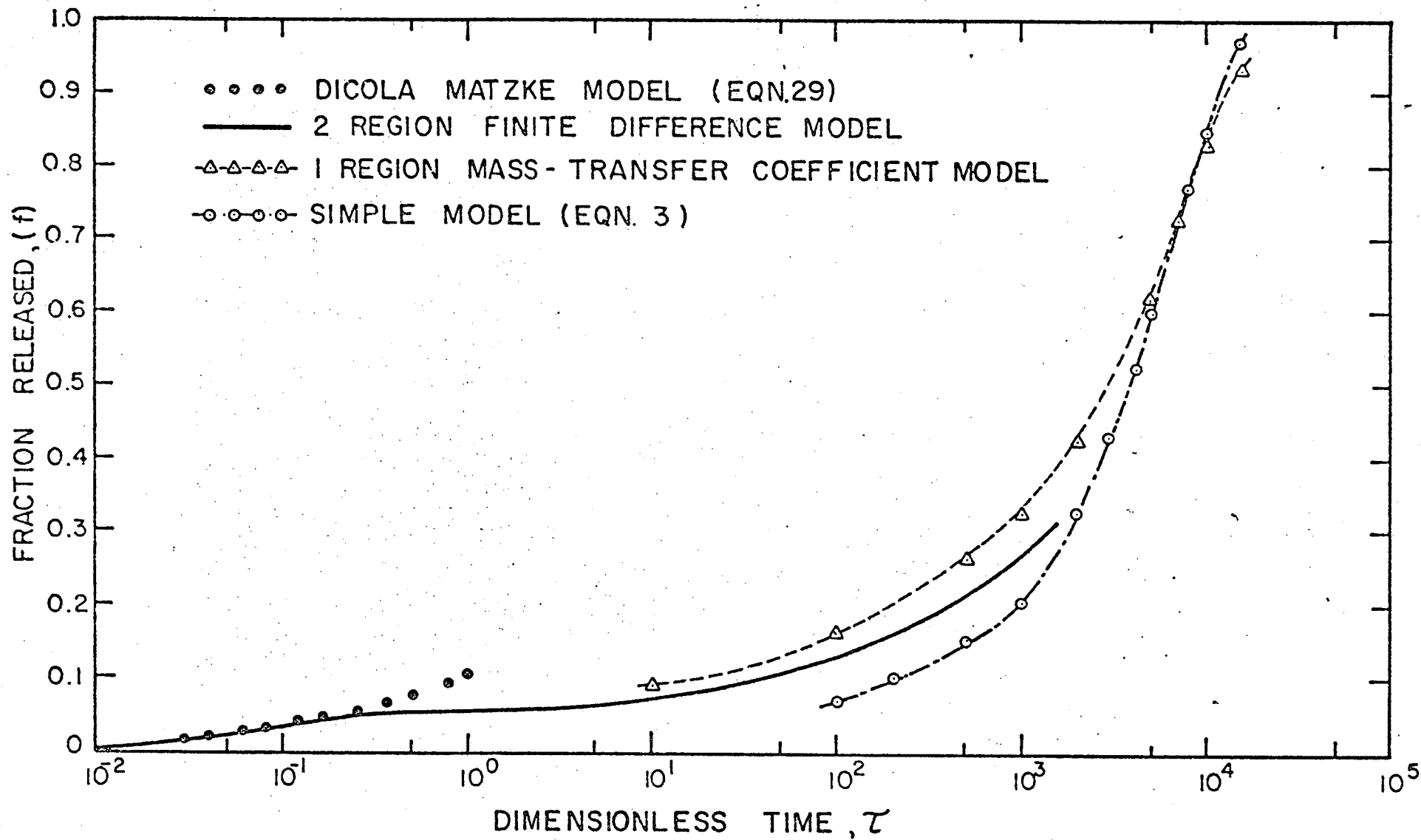


Fig. 19 - Comparison of Release Fractions as Function of Dimensionless Time,
 $\tau = D_1 t / x_1^2$ According to Various Diffusion Models.

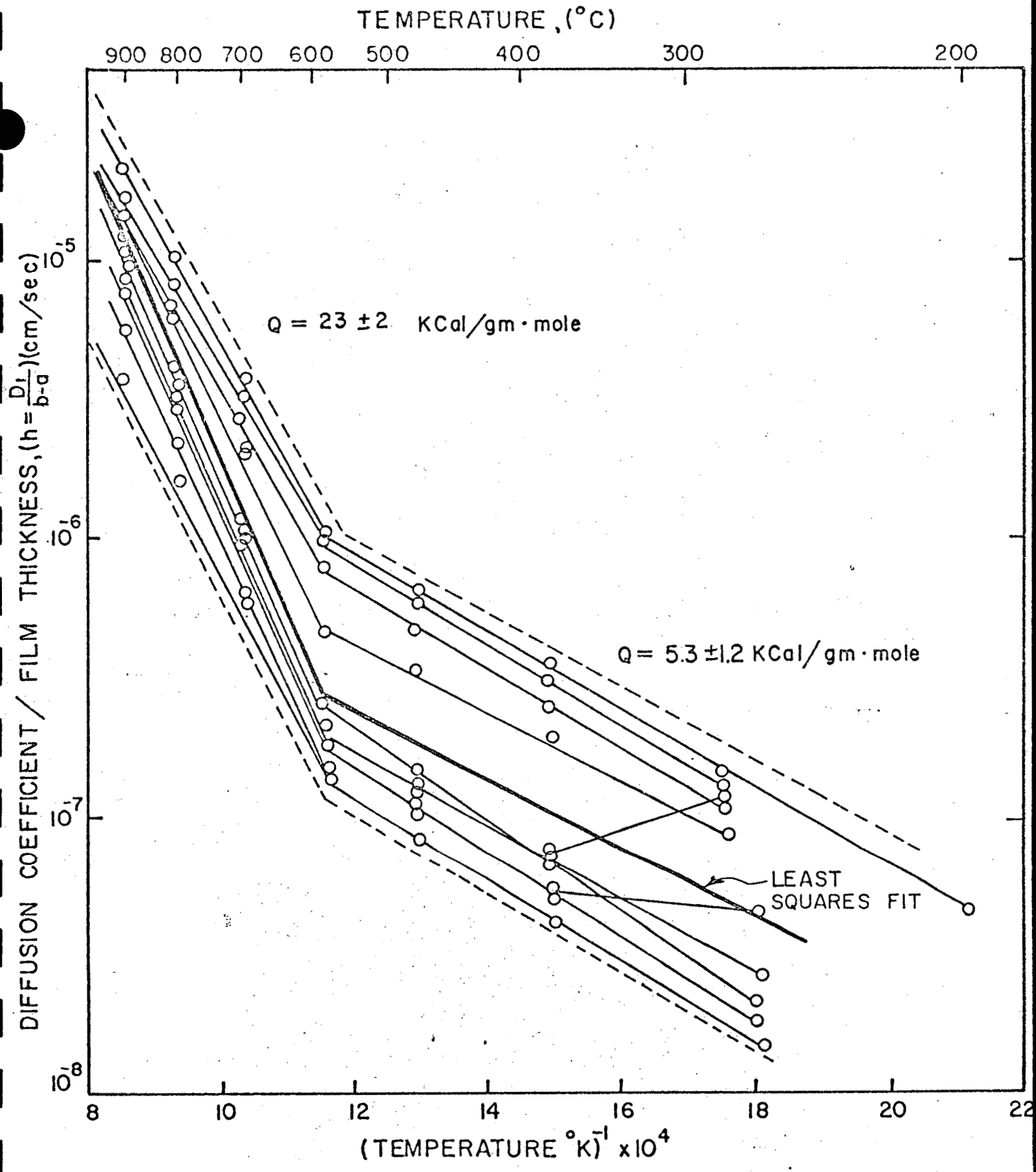


Fig. 20 - Values of the Ratio Diffusion Coefficient/Film Thickness (h) as a Function of Temperature. Dotted Lines Indicate the Envelope within which all Results Fall.

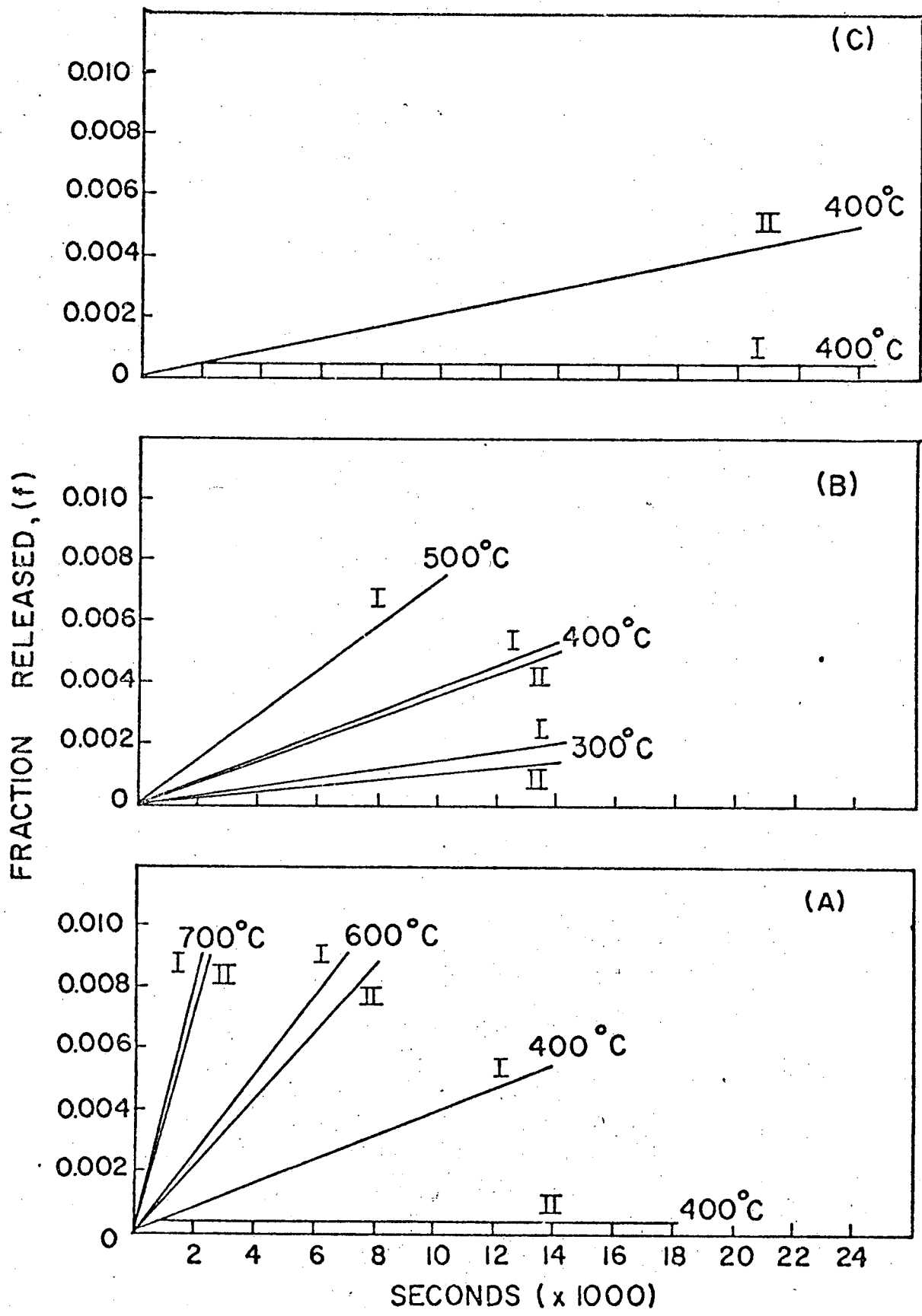


Fig. 21 - Release Behavior for Samples Subjected to Temperature Cycling.

SAMPLE NO.	TREATMENT
------------	-----------

A1	ANNEALED IN VACUUM (AT $\sim 5 \times 10^{-6}$ mm Hg)
----	---

A2, A4	ANNEALED IN HIGH VACUUM ($< 1 \times 10^{-6}$ mm Hg)
--------	---

A3, A5	ELECTROPOLISHED
--------	-----------------

A6, A7	EXPOSED TO H ₂ FLOW AT $> 700^{\circ}\text{C}$ AND THEN COOLED TO ROOM TEMPERATURE
--------	---

A8	ANNEALED IN VACUUM AND THEN OXIDIZED AT 300°C IN AIR FOR 1 HOUR
----	---

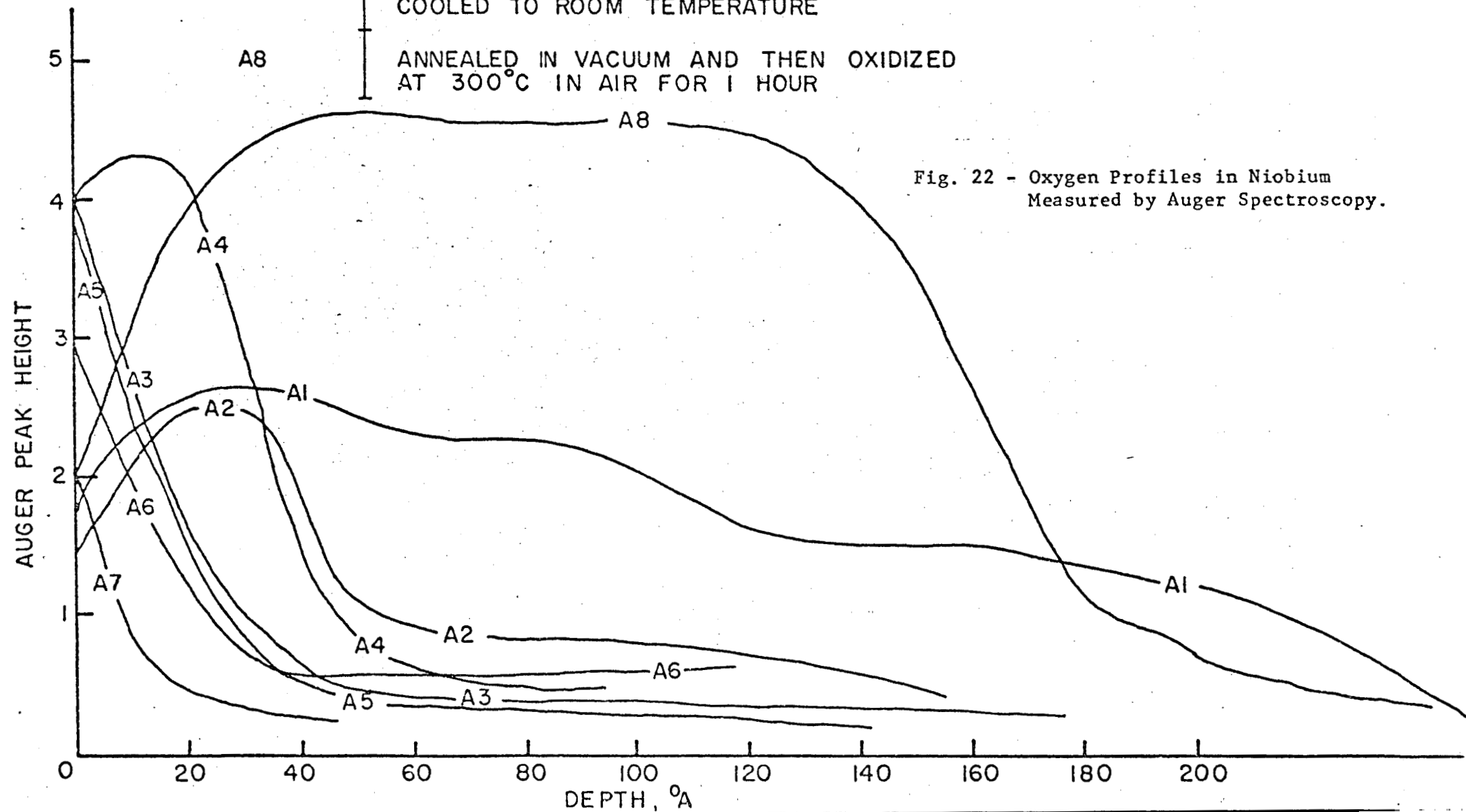


Fig. 22 - Oxygen Profiles in Niobium Measured by Auger Spectroscopy.

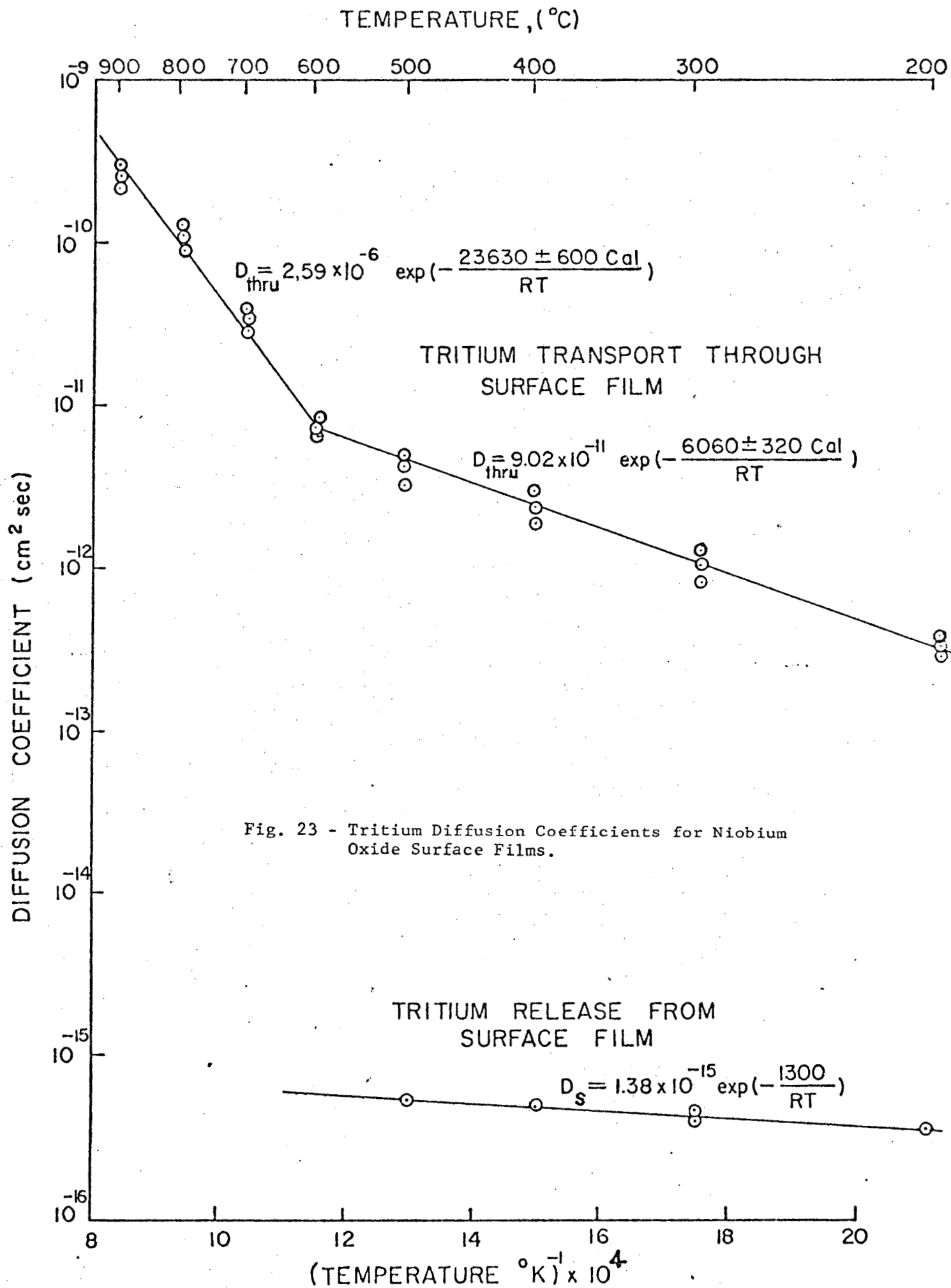


Fig. 23 - Tritium Diffusion Coefficients for Niobium Oxide Surface Films.

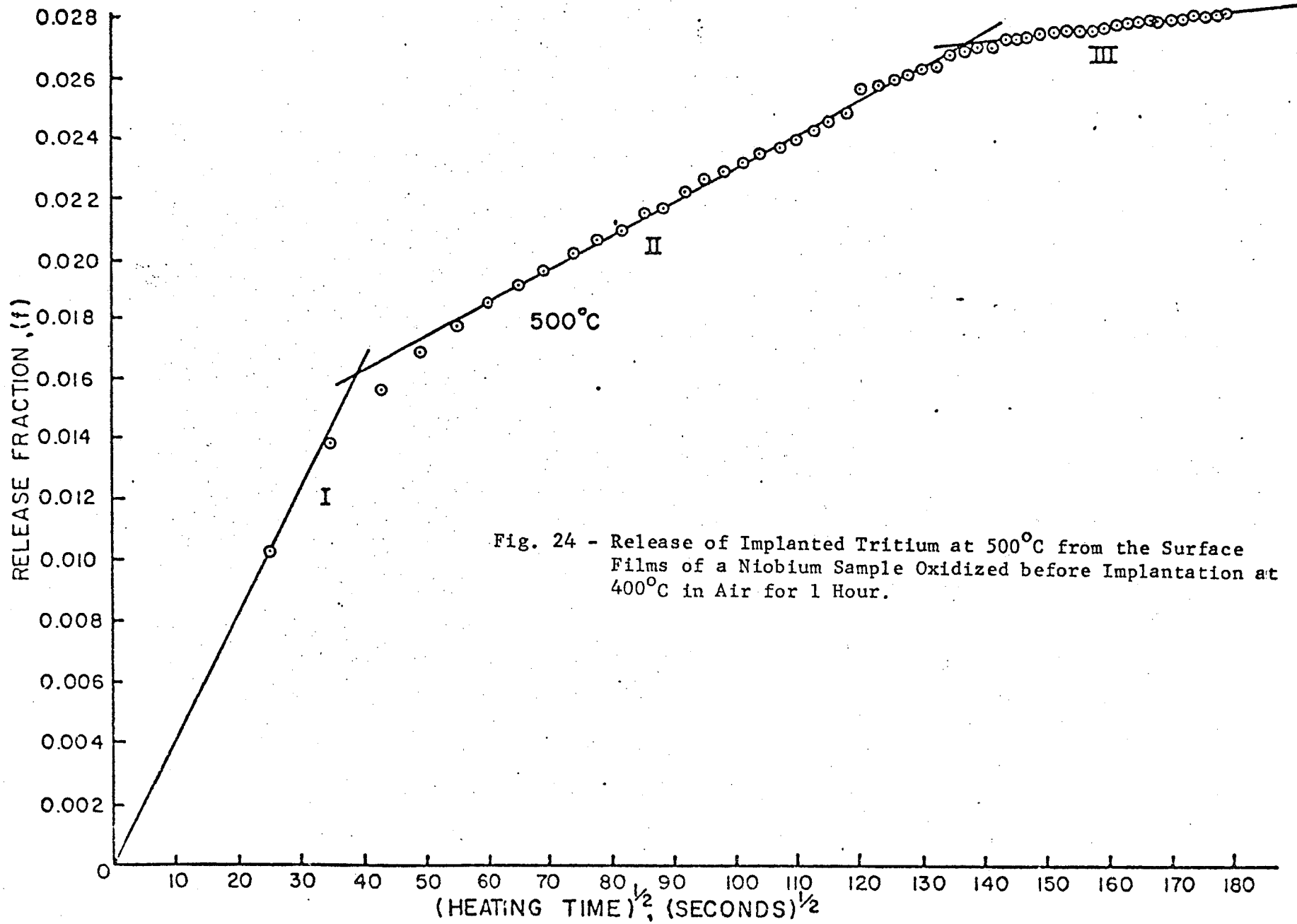


Fig. 24 - Release of Implanted Tritium at 500°C from the Surface Films of a Niobium Sample Oxidized before Implantation at 400°C in Air for 1 Hour.

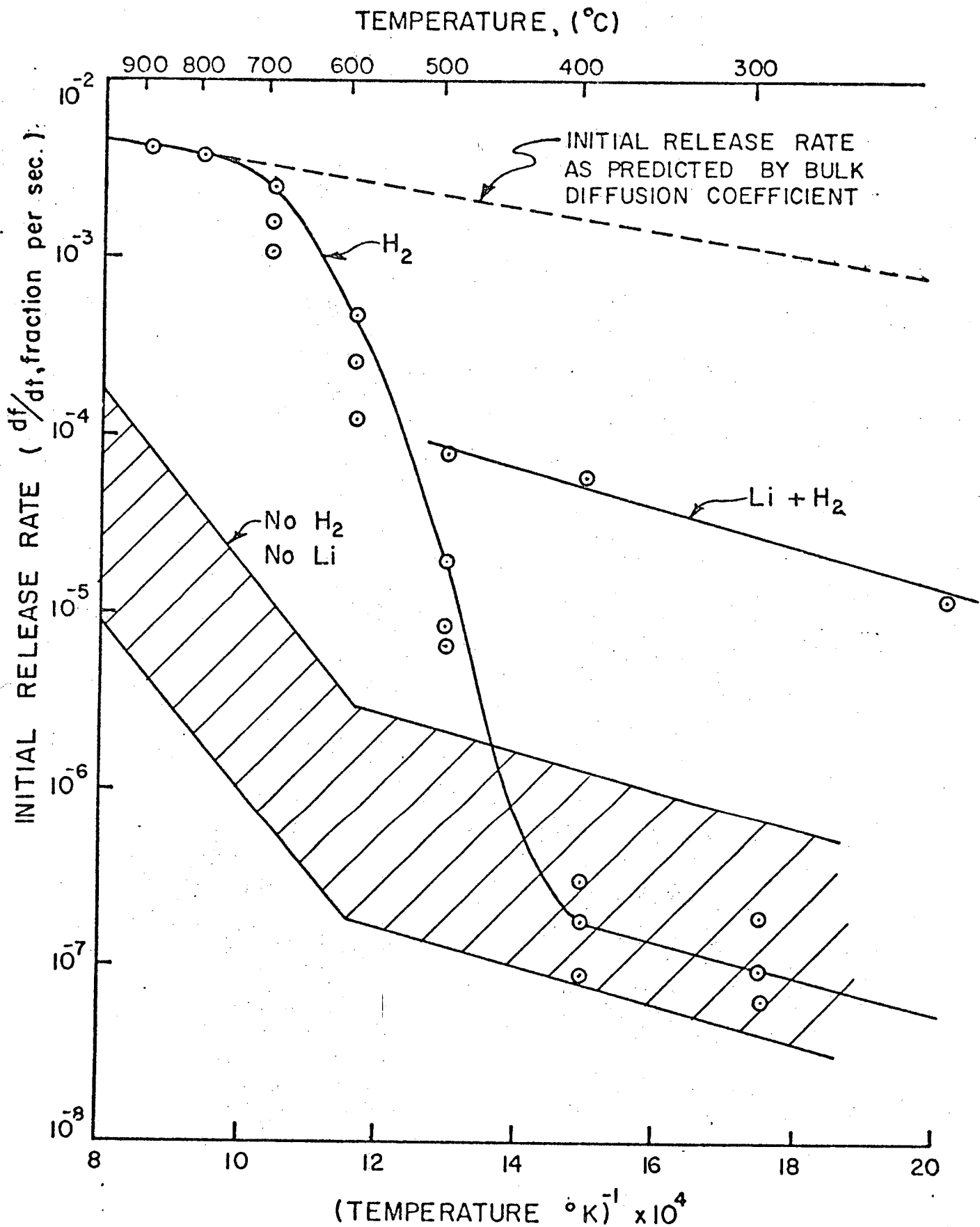


Fig. 25 - Effect of a Reducing Environment on the Initial Release Rate of Tritium from Niobium Samples.

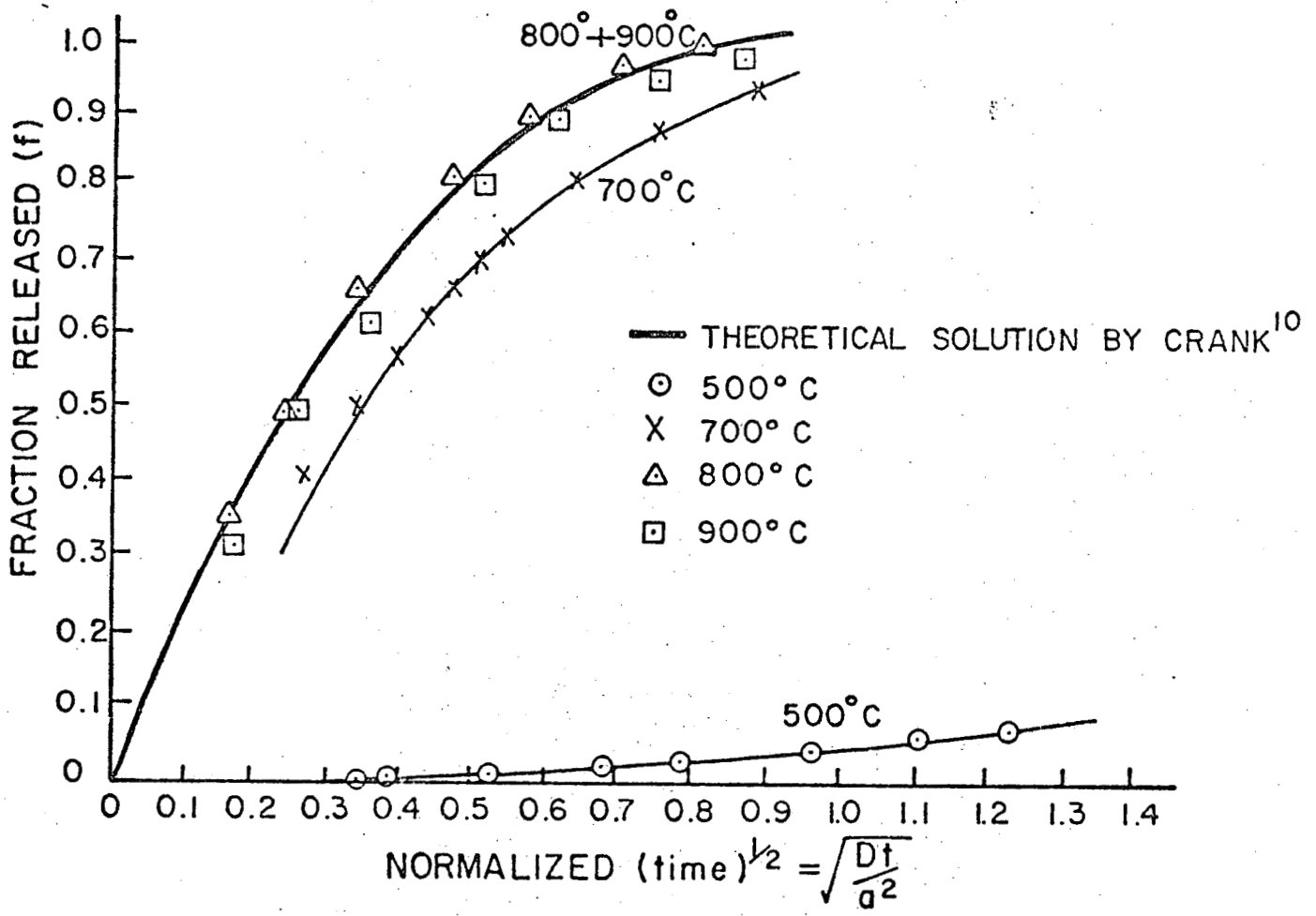


Fig. 26 - Release Behavior under H₂ Flow. Release Fraction Plotted as $\sqrt{Dt/a^2}$ to Verify a Complete Removal of Surface Films (D's Obtained from Hickman's Compiled Data³. a = Specimen Radius)

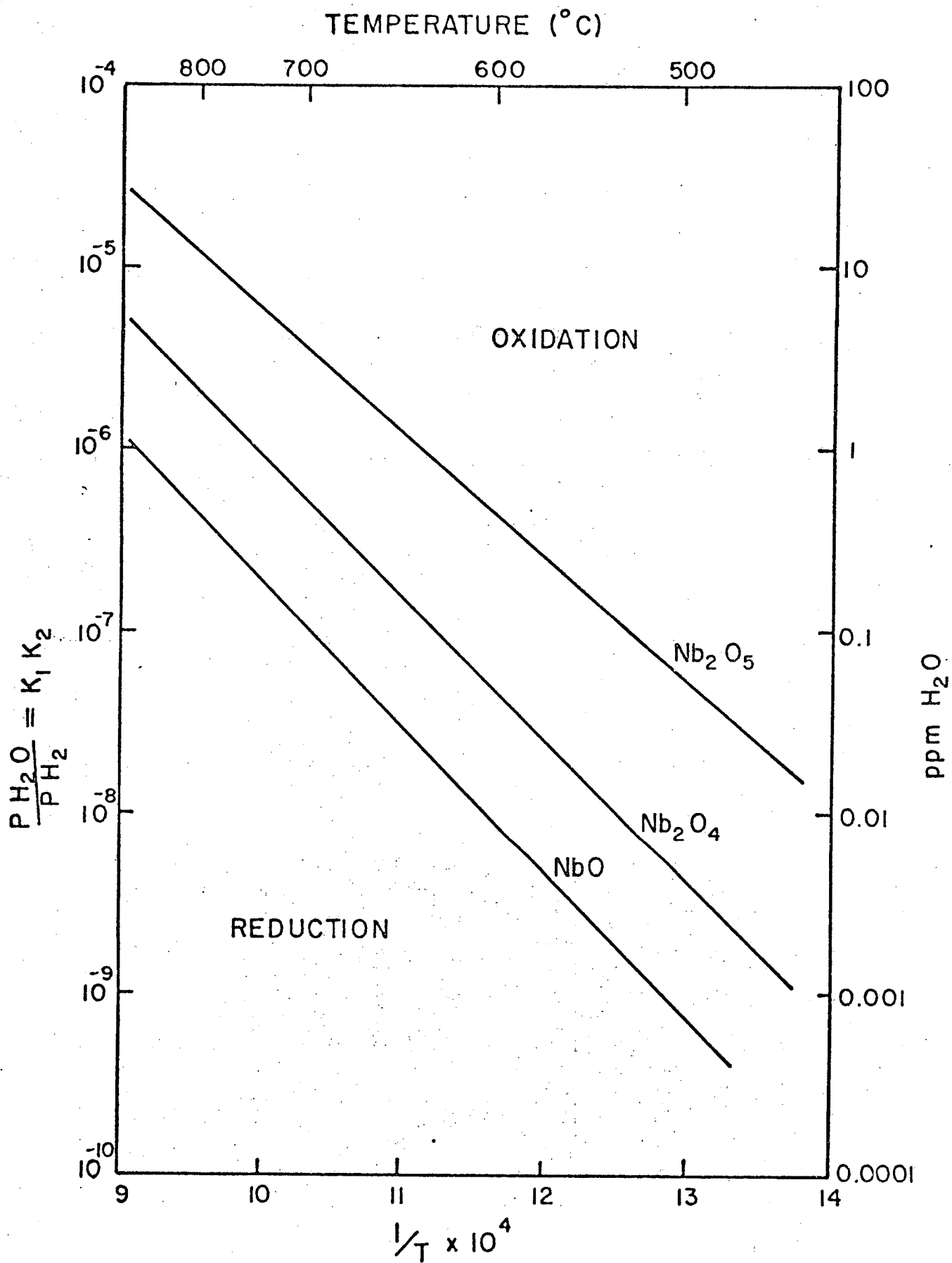


Fig. 27 - Niobium Oxide Stabilities in Contact with Water Vapor.

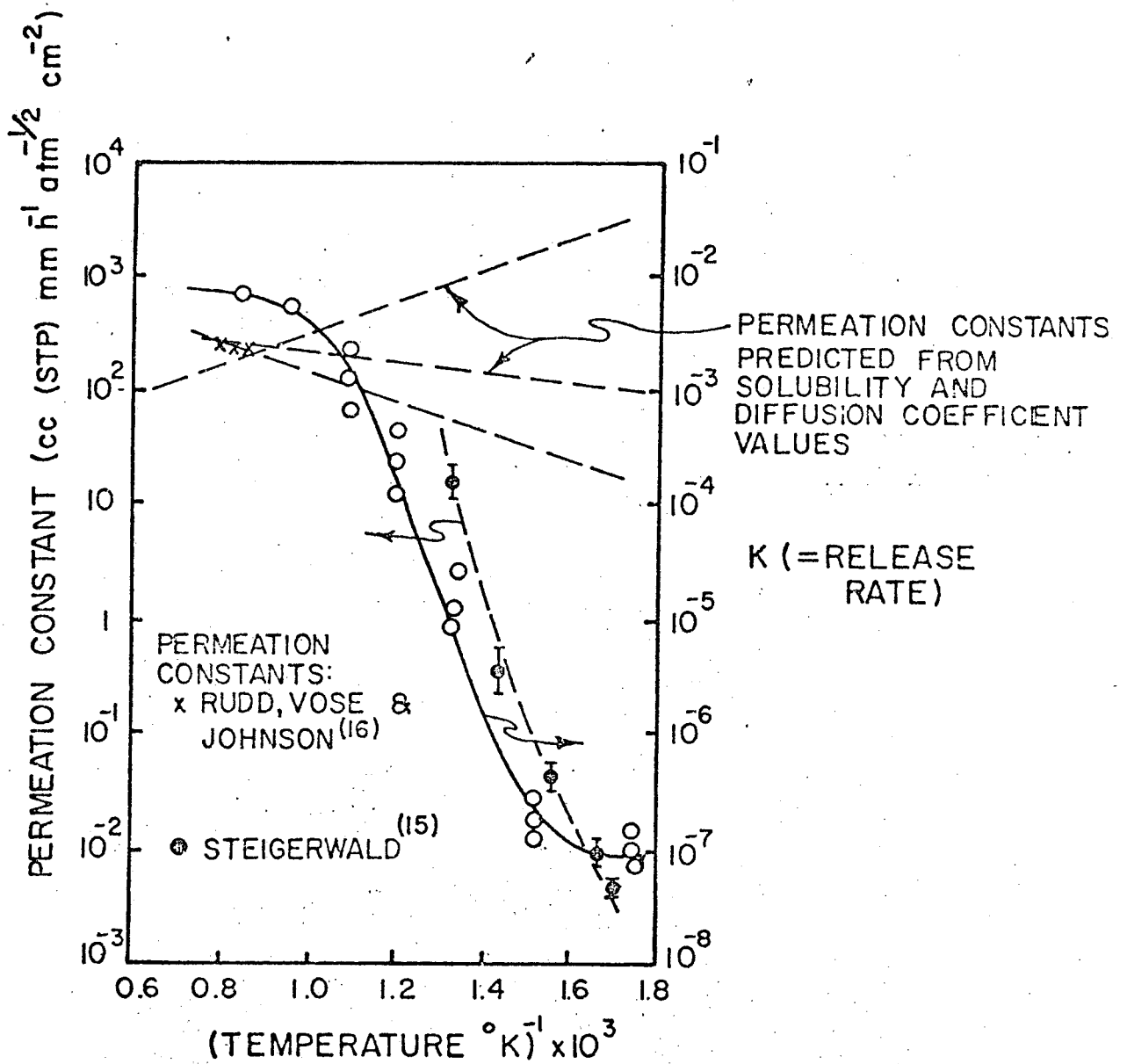


Fig. 28 - Comparison Between Hydrogen Permeation Coefficients and Tritium Release Results.

REGION MATERIAL	NO.	RADIUS (CMS)
PLASMA	1	0.0
VACUUM	2	15.0
ALUMINA LINER	3	49.97
FIRST WALL	4	50.0
Li COOLANT	5	50.1
Nb	6	53.1
Be	7	53.2
Nb	8	55.7
Li COOLANT	9	55.8
Nb	10	60.3
ALUMINA	11	60.4
Nb	12	60.43
GRAPHITE	13	60.53
Nb	14	64.87
ALUMINA	15	64.97
Nb	16	65.0
Li COOLANT	17	65.1
Nb	18	67.6
ALUMINA	19	67.7
Nb	20	67.73
GRAPHITE	21	67.83
Nb	22	82.57
ALUMINA	23	82.67
Nb	24	82.7
ENRICHED ⁶ Li	25	82.8
Nb	26	85.2
Li COOLANT	27	85.3
Nb	28	86.3
ENRICHED ⁶ Li	29	86.4
Nb	30	88.9
ALUMINA	31	88.95
IMPL COIL	32	89.5
ALUMINA	33	92.9
COMP COIL	34	94.9
Ti	35	134.9
ALUMINA	36	140.0
		142.0

Fig. 29 - RTPR Core layers, radii and composition. ⁽¹⁾

¹From Fig. 4.5-3, Reference 46.

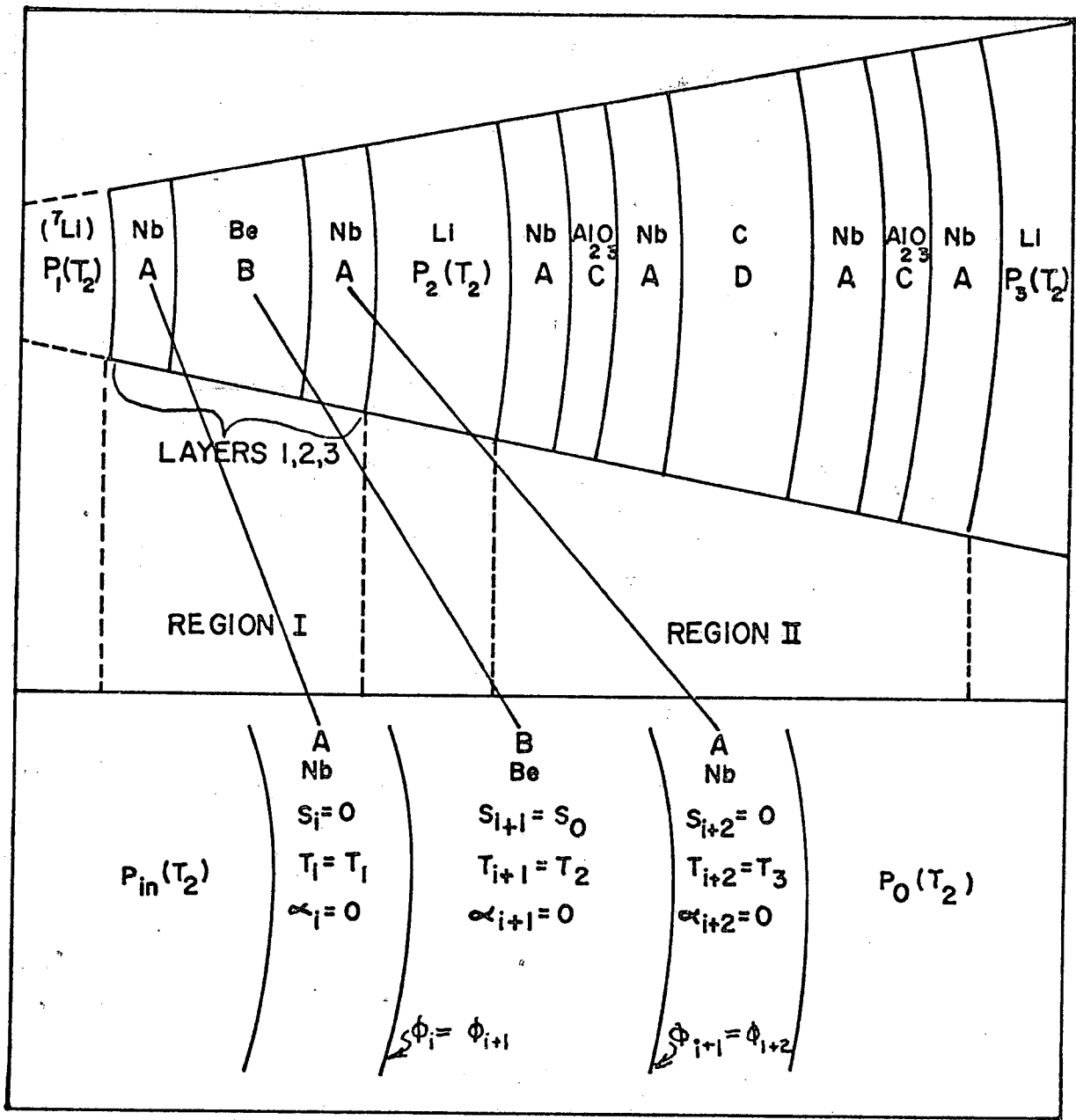


Fig. 30 - Mathematical model of RTPR core.

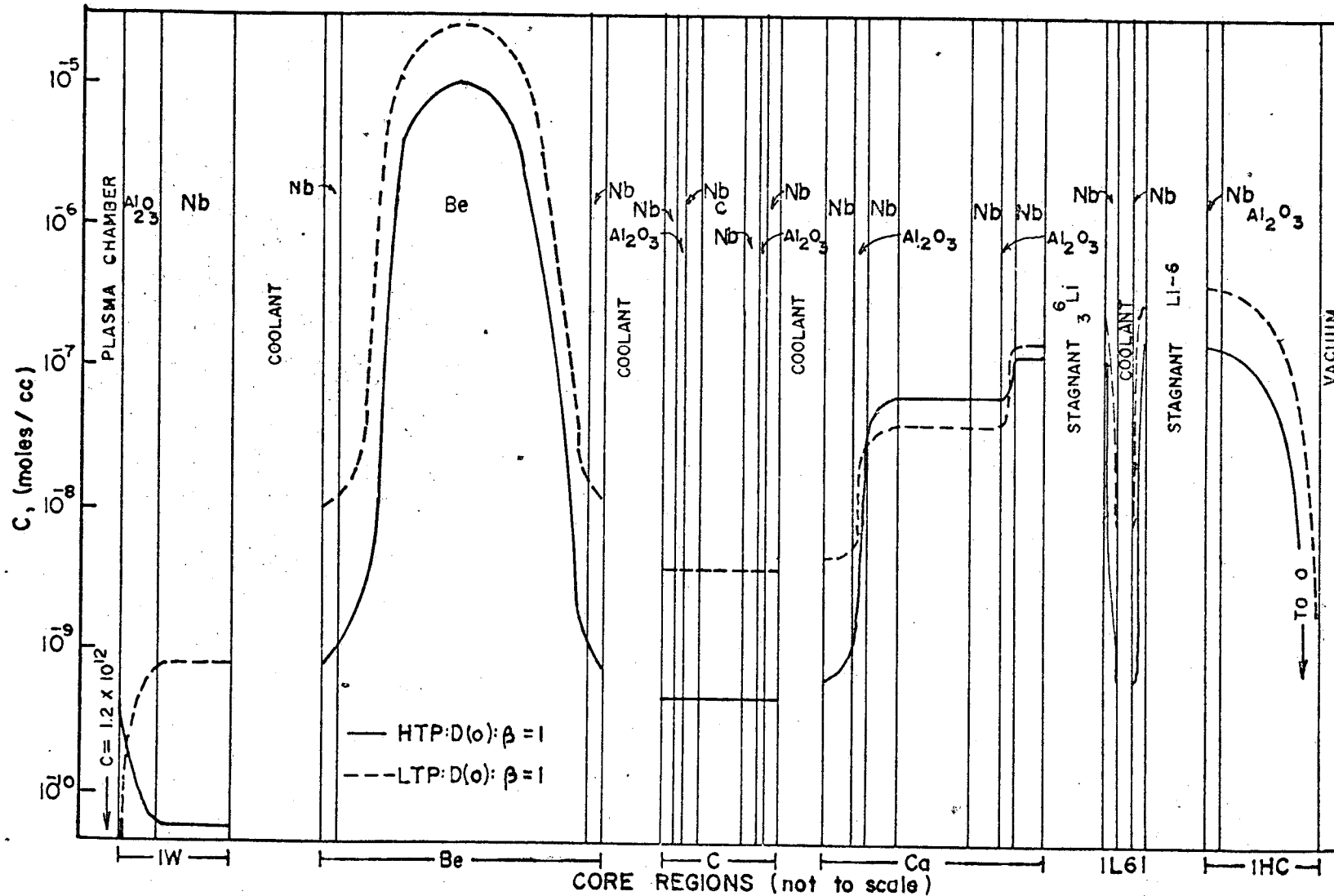


Fig. 31 - Full core concentration profile as a function of plant temperature.

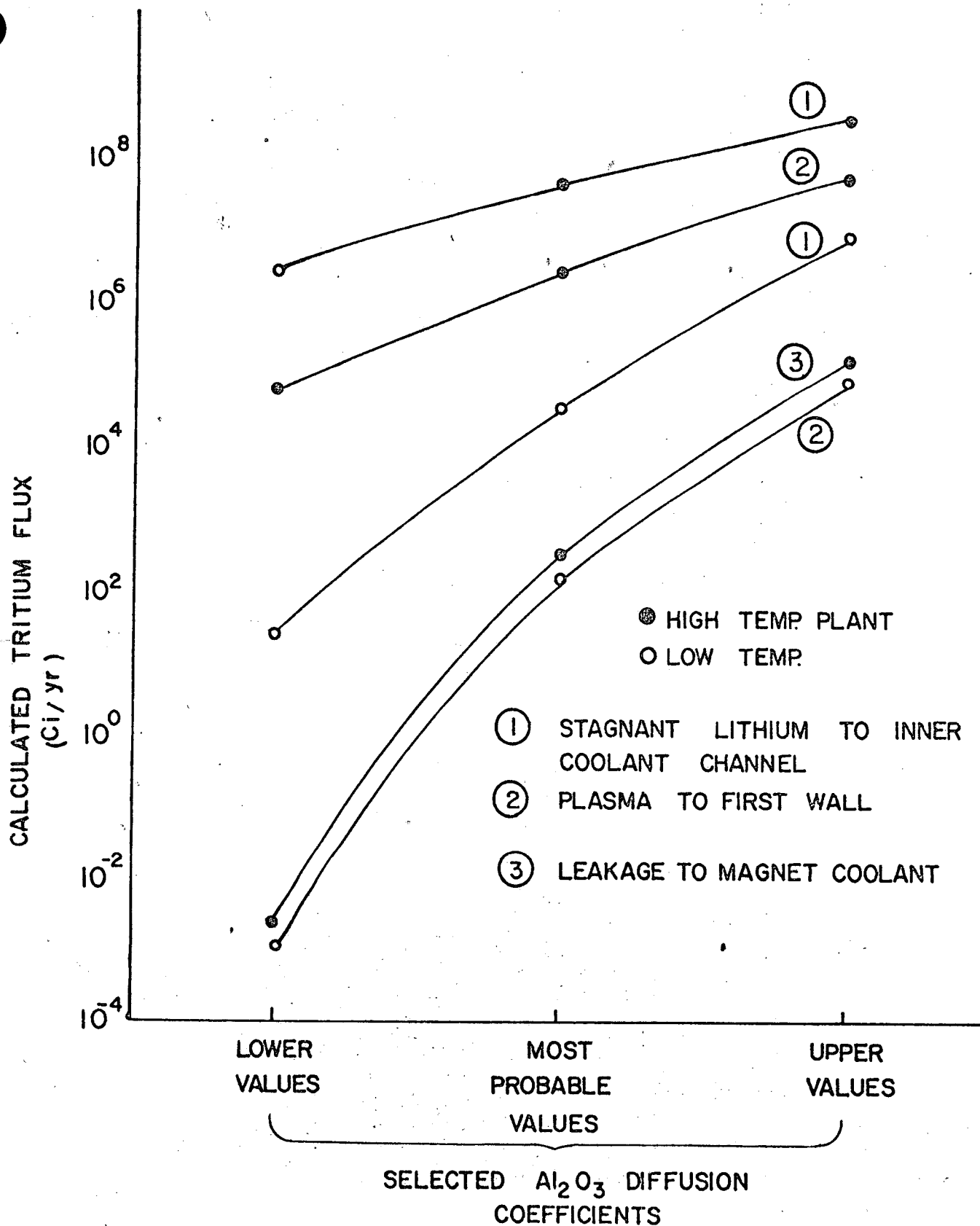


Fig. 32 - Effect of Al_2O_3 insulator on tritium transport in Theta Pinch torus.

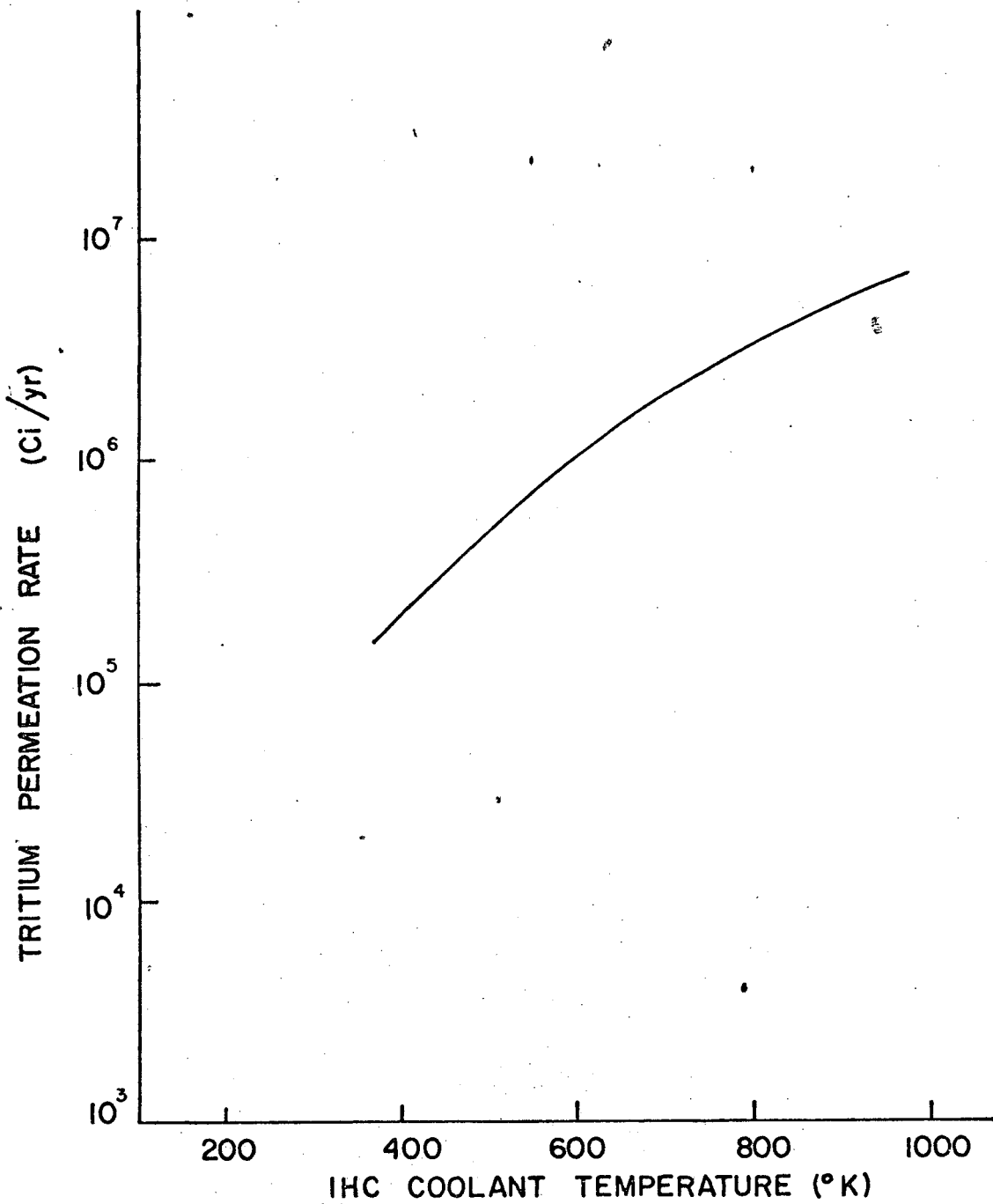


Fig: 33 - Implosion heating coil tritium flux as a function of temperature.

ATTACHMENTS

- I. SUGGESTIONS FOR FUTURE WORK
- II. STUDENTS SUPPORTED
- III. PUBLICATIONS RESULTING FROM CONTRACT
- IV. PRACTICAL BENEFITS

I. SUGGESTIONS FOR FUTURE WORK

A large amount of tritium diffusion data that is pertinent to computing tritium distributions in fission reactors has been determined during the course of this contract. However, in attempting to apply these data to fission reactor systems, several blocks of missing information could be identified.

Among all of the sources of tritium that contribute to activity in the coolant, it appears that the tritium release from boron containing burnable poisons is a very significant source. These poison rods currently consist of either borosilicate glass or boron carbide (B_4C) rods encased in stainless steel tubes. To our knowledge there is little basic data for hydrogen diffusion in B_4C . It would seem desirable to make tritium diffusion measurements in B_4C .

There is little information on tritium partition relationships between fuel pellets and the inner surface of the cladding. In the tritium model mentioned in Section 2.3.2, we have assumed that all of the tritium released from the fuel surface immediately produces a constant distribution at the fuel-clad interface, but it is not clear that this is acceptable. An investigation of tritium partition at ceramic-metal interfaces would also be of interest to controlled thermonuclear reactors.

Of the tritium that builds up in the primary coolant system, it is uncertain how and what fraction of this tritium redistributes itself in the rest of the reactor plant. It is known that tritium levels in the reactor building air can build up to sufficient concentrations to be of concern in maintenance work.

Basic tritium diffusion data is lacking for fusion reactor materials and particularly for ceramics. Furthermore, it is apparent that hydrogen diffusion in ceramics is strongly dependent on trace impurity concentrations. Some studies on ceramics are currently underway at our laboratories.

II. STUDENTS SUPPORTED

One of the less tangible results of this contract has been the large number of graduate students who were financially supported and trained by this program and currently occupy responsible positions within the nuclear industry.

Rare Gas Diffusion:

<u>Name</u>	<u>Degree</u>	<u>Thesis</u>	<u>Current Employment</u>
Ronald Christman	Ph.D.	Yes	Head, Private Consulting Firm
Danny LaBelle	B.S.	No	
Luther D. Mears	M.S. & Ph.D.	Yes	General Atomic Company
Larry Jordan	B.S.	No.	Bechtel Corporation
James Carter	M.S.	Yes	TVA
Andres Sy Ong	Ph.D.	Yes	Institute de Engenharia de Militar, Rio de Janeiro
Donald Kessler	M.S.	Yes	
Charles Fox	M.S.	Yes	Oak Ridge National Laboratory
Eugene Driscoll	M.S.	Yes	U. S. Army

Tritium Diffusion:

John Austin	Ph.D.	Yes	ERDA
Richard Calder	M.S.	Yes	Texas Utilities
Joel Cehn	M.S.	No	Commonwealth Edison
Charles Craft	M.S.	No	Los Alamos Scientific Laboratory
John Davis	M.S.	Yes	Babcock & Wilcox
Kenneth Starr	Prof. Degree	No	U. S. Navy
Charles Pennington	M.S.	Yes	Combustion Engineering
P. M. Abraham	M.S.	Yes	Duke Power Company, N. C.
Mark Mintz	M.S.	Yes	General Atomic Company
Dipankar Chandra	Post Doctoral	-	Brookhaven National Laboratory
James Allen	M.S.	Yes	ERDA

III. PUBLICATIONS RESULTING FROM CONTRACT

I. Rare Gas Diffusion

Papers:

1. T. S. Elleman, L. D. Mears, and R. P. Christman, "Rare Gas Diffusion in CsI - The Use of Fission Recoil Doping Technique," Jour. Amer. Ceram. Soc., 51, 560-564 (1968).
2. T. S. Elleman, L. D. Mears, and R. P. Christman, "Effect of Radiation on Rare Gas Diffusion in Crystals," Trans. Amer. Nucl. Soc., 10, #2, 509 (1967).
3. T. S. Elleman, C. R. Fox, and L. D. Mears, "Influence of Defects on Rare-Gas Diffusion in Solids," Jour. Nucl. Mat., 30, 89-106 (1969).
4. T. S. Elleman and A. Sy Ong, "Surface Effects on Diffusion Release of Rare Gases," Phys. Stat. Sol. (a), 3 (1970).
5. A. Sy Ong and T. S. Elleman, "Effect of Trapping on the Release of Recoil Injected Gases from Solids," Nucl. Instr. & Meth., 86, 117-125 (1970).
6. L. D. Mears and T. S. Elleman, "Rare Gas Diffusion in Alkali Metal Iodides," Phys. Stat. Sol. (a), 7, 509-521 (1971).
7. A. Sy Ong and T. S. Elleman, "Diffusion and Trapping of Rare Gas Xenon in Calcium Fluoride Single Crystals," Jour. Nucl. Mat., 42, 1702-1724 (1972).

Reports:

1. T. S. Elleman, USAEC Report ORO-3508-1 (1967).
2. L. D. Mears and T. S. Elleman, USAEC Report ORO-3508-2 (1967).
3. T. S. Elleman, USAEC Report ORO-3508-3 (1968).
4. T. S. Elleman, USAEC Report ORO-3508-4 (1969).
5. T. S. Elleman, A. Sy Ong, and L. D. Mears, USAEC Report ORO-3508-5 (1970).

II. Tritium Diffusion Work

Papers:

1. J. H. Austin and T. S. Elleman, "Diffusion of Tritium in Austenitic Stainless Steels," Jour. Nucl. Mat., 43, 119 (1972).
2. T. S. Elleman, J. H. Austin, and K. Verghese, "Tritium Diffusion in Zircaloy-2 and Stainless Steels," Trans. Amer. Nucl. Soc., 15, (1) 229 (1972).

3. J. H. Austin, T. S. Elleman, and K. Verghese, "Surface Effects on the Diffusion of Tritium in 304-Stainless Steel and Zircaloy-2," Jour. Nucl. Mat., 48, 307-316 (1973).
4. C. W. Pennington, K. Verghese, and T. S. Elleman, "Tritium Release from Niobium," Trans. Amer. Nucl. Soc., 17, 151 (1973).
5. R. D. Calder, T. S. Elleman, and K. Verghese, "Grainboundary Diffusion of Tritium in 304- and 316-Stainless Steels," Jour. Nucl. Mat, 46, 46-52 (1973).
6. J. H. Austin, T. S. Elleman, and K. Verghese, "Tritium Diffusion in Zircaloy-2 in the Temperature Range -78 to 204°C," Jour. Nucl. Mat., 51, 321-329 (1974).
7. C. W. Pennington, T. S. Elleman, and K. Verghese, "Tritium Release from Niobium," Nucl. Tech., 22, 405-415 (1974).
8. T. S. Elleman and K. Verghese, "Surface Effects on Tritium Diffusion in Niobium, Zirconium and Stainless Steel," Jour. Nucl. Mat., 53, 299-306 (1974).

Reports:

1. T. S. Elleman, et al., USAEC Report ORO-3508-6 (1970).
2. J. H. Austin, et al., USAEC Report ORO-3508-7 (1971).
3. P. M. Abraham, et al., USAEC Report ORO-3508-8 (1972).
4. P. M. Abraham, et al., USAEC Report ORO-3508-9 (1973).

Papers in Preparation:

1. D. Chandra, T. S. Elleman, and K. Verghese, "Tritium Diffusion Through Oxide Surface Films on Niobium," (Submitted to Jour. Nucl. Mat.).
2. P. M. Abraham, T. S. Elleman, and K. Verghese, "Grainboundary Diffusion of Tritium in 304-Stainless Steel," (Submitted to Acta Metallurgica).
3. J. M. Mintz, T. S. Elleman, and K. Verghese, "Tritium Diffusion in Fusion Reactor Blankets."
4. K. Verghese, T. S. Elleman, P. M. Abraham, and A. Kowalczyk, "On the Release of Ternary Fission Tritium in Light Water Reactors."

ATTACHMENT IV

Diffusion of Gases in Solids --

Practical Benefits

The final report on Contract AT-(40-1)-3508 discusses the technical accomplishments of the research. There exists additional evidence that the work produced practical benefits which justify its conduct. This attachment summarizes some of these items.

1. The rare gas trapping studies helped to identify the importance of defects in controlling rare gas release from solids. This work along with a number of other studies at other laboratories, have formed the basis for the current understanding of rare gas release rates from reactor fuels.
2. The results of the xenon diffusion studies in alkali metal halides were used as supporting evidence for rare gas diffusion models developed at other laboratories (1-3). The results for CsI led to a special consideration of diffusion models for b.c.c. alkali halides (3).
3. It was indicated to us that the reported tritium diffusion coefficients in austenitic steels were used as the basis for calculation of diffusional tritium release from FFTF fuel elements.
4. Representatives from Westinghouse and B & W maintained contact on the status of the tritium diffusion studies for application to their own work in this area.
5. Nineteen publications in referred journals resulted from the research.
6. Fourteen graduate students received principal support from the contract prior to receiving graduate degrees. In a number of these cases, graduate study appeared not to have been possible without the contract support. Most of these graduates are currently employed in some phase of the atomic energy field. A number of

additional students working in the contract area received partial assistance from the contract. A larger number of students than those indicated actually conducted their research in the contract subject area as unsupported students. The funded group served as a nucleus to attract additional unsupported students.

7. The faculty salaries charged to the contract were returned to the university as release time funds. These moneys constituted a principal source of support for the teaching assistants needed for the conduct of our educational program.
8. The contract produced collaborative efforts among several department faculty members and productive research in other areas which might not otherwise have occurred.
9. A collaborative program with Carolina Power and Light Company to develop tritium release models for their power reactors has developed as a direct consequence of the funded research.
10. A current contract with the CTR Division of ERDA to study tritium diffusion in nonmetallic solids of interest for fusion reactors has been a direct result of the skills and interests developed under the supported research.

I think it is not too strong a statement to note that the existence of the entire graduate program in nuclear engineering at our university is very strongly dependent upon the existence of research contracts such as the program cited.

References

1. Norgett, M. J. & A. B. Lidiard, "The Migration of Inert Gases in Ionic Crystals" Harwell, T. P. 332 (1968).
2. Muller, M. and M. J. Norgett, "Rare Gas Diffusion in α and β C_{60} " Harwell, T. P. 549 (1973).

3. Muller, M. and M. J. Norgett, "Rare Gas Diffusion in CsI", Harwell T. P. 488 (1972)
4. Personal communication, Dr. Roy Dahl, WAPD.